Next-generation lipidic drug delivery systems for osteoarthritis treatment

Inaugural dissertation

of the Faculty of Science,

University of Bern

presented by

Gregor Bordon

from Slovenia

Supervisor of the doctoral thesis:

Prof. Dr. Paola Luciani

Department of Chemistry, Biochemistry and Pharmaceutical Sciences,

University of Bern

Next-generation lipidic drug delivery systems for osteoarthritis treatment

Inaugural dissertation

of the Faculty of Science,

University of Bern

presented by

Gregor Bordon

from Slovenia

Supervisor of the doctoral thesis:

Prof. Dr. Paola Luciani

Department of Chemistry, Biochemistry and Pharmaceutical Sciences,

University of Bern

Accepted by the Faculty of Science.

Bern, July 21st, 2023 The Dean

Prof. Dr. Marco Herwegh

Table of Contents

Chapter 1.

Background and purpose: Harnessing the multifunctionality of lipid-based drug delivery systems for the local treatment of osteoarthritis

Part of this chapter is to be submitted for publication.

Gregor Bordon, Paola Luciani*

Department of Chemistry, Biochemistry and Pharmaceutical Sciences, University of Bern, Freiestrasse 3, 3012 Bern, Switzerland

*Corresponding author; email: paola.luciani@unibe.ch; office number: +41 (0)31 684 41 60

Author's contribution

G.B. led manuscript writing. P.L. reviewed and edited the manuscript.

1.1 Introduction

1.1.1 A brief overview of osteoarthritis

Prevalence, burden, and risk factors

Osteoarthritis (OA) is a widespread, long-lasting joint condition affecting over 500 million people globally [1]. The rapid growth in its prevalence in recent years can be largely attributed to factors such as increased life expectancy and escalating body weight [1–3]. According to the Global Burden of Disease study, there was a 13.25% surge in OA prevalence between 1990 and 2019 [1,4,5]. By 2019, the highest numbers of OA cases were reported in China, India, and the United States, with a greater prevalence among women and the highest rate among individuals aged 60-64 years [5]. The economic burden of OA is substantial and growing, with OA-related medical costs reaching $460 billion globally in 2019 [6]. Patients with OA face medical costs that are four times greater than those without the condition [7]. Additional indirect expenses, such as job loss and premature retirement, further contribute to the economic burden [1]. OA has emerged as a leading cause of global disability, presenting significant healthcare and socioeconomic challenges [8]. In 2017 alone, OA was responsible for nearly 9.6 million years lived with disability (YLDs), and the age-standardized YLD rate had risen by 9.6% since 1990 [4].

Risk factors for OA include obesity, gender, age, knee injuries, and participation in high-impact sports [9–11]. Aging is considered the most significant risk factor, as age-related biological and molecular changes can disrupt joint structures and contribute to OA development [1,11]. Obesity is another major risk factor, as excess weight increases mechanical stress on joints, leading to cartilage and ligament damage [12,13]. Surprisingly, obesity is also associated with hand OA, suggesting that systemic factors, such as adipokines and cytokines, contribute to OA development [1].

Due to the rising prevalence and economic burden of OA, there is an urgent need for more effective treatments and preventive measures. Current therapies primarily focus on pain relief rather than halting disease progression,

prompting researchers to explore new medications and biological treatments in clinical trials to develop improved OA management strategies.

Current understanding of OA pathology

OA is a complex whole-joint disease involving structural alterations in components like cartilage, subchondral bone, ligaments, and synovium. Its pathogenesis includes mechanical, inflammatory, fibrotic and metabolic factors, ultimately culminating in joint failure [14,15]. Rather than being a mere passive degenerative disease, OA is an active process that arises from an imbalance between joint tissue repair and destruction[14].

As the disease progresses, alterations in the composition of cartilage can cause erosion and heighten its susceptibility to mechanical disruption [11]. This leads to chondrocytes – the only cell type present within the articular cartilage, to generate matrix degradation products and proinflammatory mediators, which are body's attempt to repair the eroded cartilage, as is illustrated in Figure 1. They stimulate proliferative and proinflammatory responses in the adjacent synovial macrophages, which reside inside synovial membrane. Activated macrophages start excreting proinflammatory cytokines, such as IL1β, IL6, and TNFα, as well as profibrotic TGFβ [14,16,17]. This leads to activation of another cell type that resides within synovial membrane – the synovial fibroblasts (SFs). SFs are key drivers of synovial fibrosis, which is manifested by excessive extracellular matrix (ECM) deposition and is associated with joint stiffness and chronic pain in OA patients [15]. In addition to proinflammatory and profibrotic mediators, the activation of SFs is strongly corelated also with the presence of cartilage wear particles that are formed during cartilage erosion [17,18]. The formation of these particles is closely linked with the increased roughness of the cartilage surface in OA, which results in increased friction elevating the mechanical wear. Healthy joints are lubricated by natural biolubricants, including proteoglycan 4, phospholipids, chondroitin sulfate, and hyaluronan, preventing cartilage wear. However, in OA, diminished levels of these biolubricants impair synovial fluid lubrication, leading to increased friction and cartilage degradation [20–22]. Moreover, the remodelling of the subchondral bone, involving hightened bone turnover and vascular invasion into the cartilage, is associated with the development of bone marrow lesions. These lesions are associated with increased severity of the disease and joint pain. Similarly, the formation of

osteophytes, or bone spurs at the joint margins, is strongly influenced by inflammatory factors and abnormal joint movement and contributes to the disease's impact [14,23].

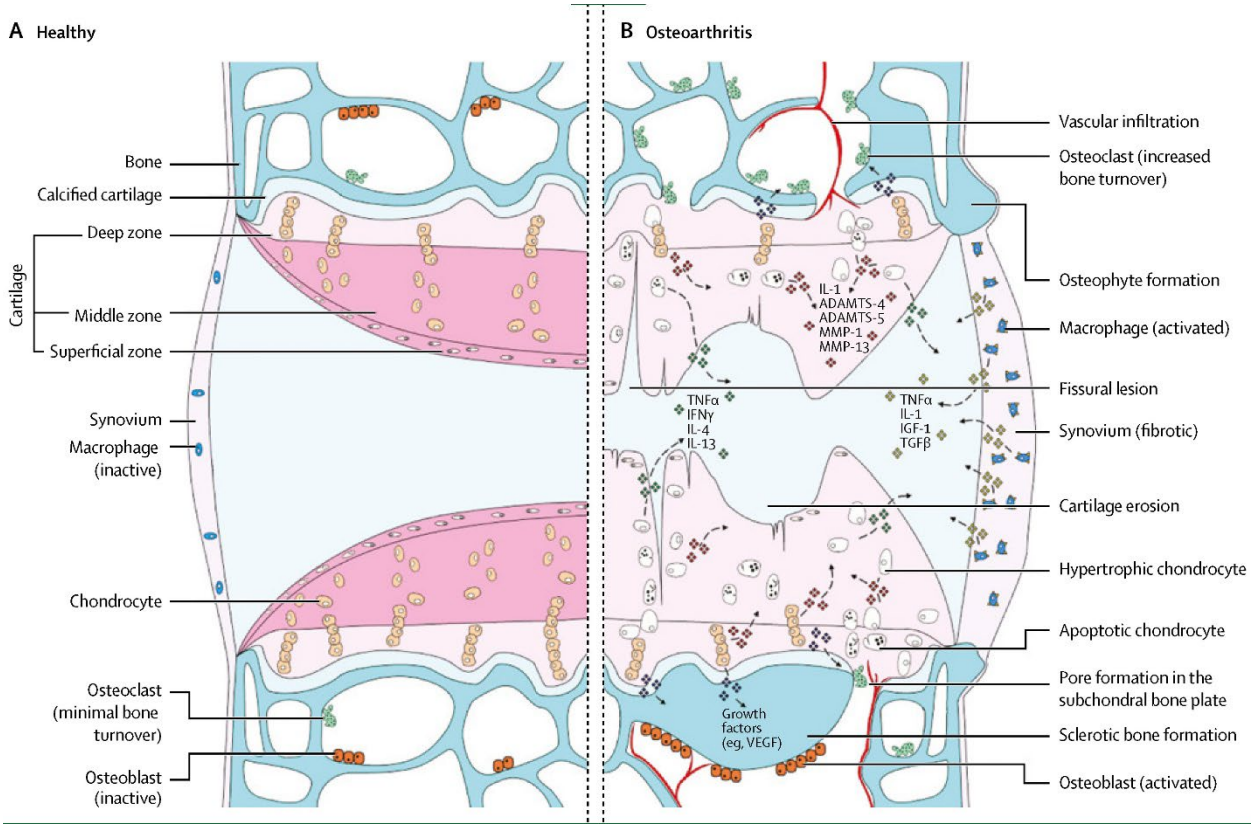

Figure 1: Signalling pathways and structural changes in the development of osteoarthritis. Reproduced from D. J. Hunter and S. Bierma-Zeinstra [14] *with permission.*

To summarize, OA is a multifaceted disease with varying underlying mechanisms that ultimately result in joint damage. It can be seen as a syndrome rather than a single disease, where different risk factors associated with OA can initiate different pathways leading to the disease. This means that the factors that cause OA in older adults may be different from those that cause it in younger adults who have suffered a joint injury or in individuals who are obese [14].

1.1.2 Current OA treatments

Currently, there are no definitive cures for OA, but there are treatment options that help with the management of the disease and can be classified into five distinct categories: lifestyle changes, small-molecule pain medication, large-molecule viscosupplementation, cell therapy, and surgical procedures [24]. As a widely recommended initial approach, patients are directed toward nonpharmacological methods, such as exercise, weight loss, and walking aids, which are considered first-line treatments. Over the past decade, research has demonstrated that exercise therapy partnered with patient education effectively reduces pain and enhances joint mobility. Consequently, exercise has emerged as a crucial aspect of OA management [25–27]. The subsequent treatment strategy is pharmacological pain relief, where non-steroid anti-inflammatory drugs (NSAIDs) are commonly used as well as corticosteroids and paracetamol [24]. Additionally, large molecules such as HA have been used for improving lubrication of the cartilage and consecutive pain relief, however, the clinical results about HA's benefits are inconclusive [28]. The third emerging pillar of OA management is cell therapy, which includes intra-articular (IA) injections of cell concentrates (mainly platelet-rich plasma and bone marrow aspirate concentrate), adipose tissue, and mesenchymal stem cells. While there are some reports supporting the use of platelet-rich plasma, the use of cell concentrates is not well supported by clinical data and their use is mostly limited off-label. Initial clinical data with stem cell therapy showed promise, but better quality large-scale clinical trials are needed [28,29]. When OA progresses to the end stage, joint replacement surgery is the most relevant procedure. It is also considered the most cost-effective procedure for severely affected patients with better functional improvements than non-surgical treatments. However, the procedure is also associated with more serious adverse events, which limits its use for some segments of patient population [30]. In summary, given the absence of approved disease-modifying therapies and considerable side effects associated with long-term pharmacological treatments, the development of superior therapeutic options is crucial for enhancing patients' quality of life.

1.1.3 Latest drug treatments

Lately, drug testing of molecules already approved for other conditions has showed promise in slowing the progression of OA and protecting cartilage from further degradation, which is hinting to the potential development of disease-modifying OA drugs (DMOADs). One of promising strategies is interfering with mammalian target of rapamycin (mTOR) pathway, whose upregulation is known to dampen the autophagy. mTOR inhibition with rapamycin (RAPA) has been found to lower chondrocyte apoptosis and inflammation, thereby safeguarding the cartilage from further deterioration [31,32]. Multiple studies conducted in live animals have validated these outcomes, indicating that RAPA can meaningfully alleviate the severity of OA and mitigate damage to the articular cartilage [33–35]. In addition to RAPA, another promising strategy for OA treatment involves boosting the production of all-trans retinoic acid (atRA), which is an endogenous anti-inflammatory molecule in chondrocytes. Researchers found that increasing atRA with talarozole, a retinoic acid metabolism blocking agent (RAMBA), significantly dampened the inflammation in articular cartilage *in vitro* and *in vivo* as well as reduced the cartilage degradation and osteophyte formation [36]. Two recent reviews highlight various additional pathways that have been recently identified in scientific literature as having the potential to be targeted for modifying the progression of the disease [37,38]. While these results offer a hopeful prospect for the future of OA therapy, the potential side effects associated with long-term systemic administration may undermine the therapy's benefits.

In recent years, there has been significant interest in pharmacological therapy through IA administration, because of the reduction of systemic exposure, fewer side effects and increased local bioavailability of the drugs. However, the drugs' residence time in the joint upon the administration is still a major challenge that limits the utility of IA injections [39,40]. The fast clearance of the molecules from the joint leads to higher frequency of administration, which increases the risk of opportunistic infections during injections [41]. Molecules of larger size, such as proteins (>40 kDa), predominantly exit the joint via lymphatic drainage rather than through vasculature, with the clearance rates reducing as the size of these molecules increases [42]. Interestingly, inflammatory conditions, like those seen in arthritis, have been found to amplify these clearance rates [43]. Considering these clearance dynamics, investigators have turned to three main strategies to decrease the drug

clearance rate. The first one is to chemically modify the drugs, where in the case of triamcinolone, increasing the hydrophobicity by forming hexacetonide achieved a significantly slower rate of systemic absorption compared with triamcinolone acetonide [44]. The second strategy involves formulating the drug with amphiphilic excipients such as polysorbate 80, which showed to significantly increase the efficacy of a single injection of triamcinolone acetonide (TA) over a longer time period [45]. However, these two strategies still cannot provide the long-term efficacy at the level of encapsulating the drugs into a drug delivery system (DDS). DDSs can provide several benefits beyond increasing the drug's residence time by avoiding lymphatic and vascular drainage. These advantages include targeting cartilage to improve drug retention inside the joint [40,46], allowing on-demand drug release triggered by disease-associated cues to limit drug exposure when less urgently needed [47,48], and providing lubrication to articulate cartilage, which reduces its wear and tear [21]. DDSs commonly take form of nanoparticles, microparticles and gels. In the case of particulate systems, another pharmacokinetic consideration is important – phagocytosis by immune cells, namely macrophages and dendritic cells [45]. This process can result in the elimination of these particles by resident and recruited cells, causing an inflammatory response and T cell activation. Additionally, particles may undergo surface adsorption of complement proteins found in synovial fluid, leading to their elimination by mast cells through opsonin-dependent phagocytosis. However, by applying neutralizing cationic coatings on nanoparticles and minimizing non-specific interactions between particles and proteins in the synovial fluid, both hydrophobic and hydrophilic, there has been a demonstrated decrease in particle uptake by immune cells [45]. Other research also showed that increasing the particle size beyond 10 μm significantly decreased the uptake by the macrophages, providing avenues to improve the retention inside joints [49,50]. The growing body of work in the field of DDSs for IA administration has explored various therapeutic strategies, including the use of NSAIDs, corticosteroids, DMAODs, and RNA therapeutics. While polymer-based systems (natural and artificial) have been well described elsewhere [51,52], this review will primarily focus on the lipid-based systems developed in the last 3 years for each of these therapeutic categories, as is presented in **Figure 2**.

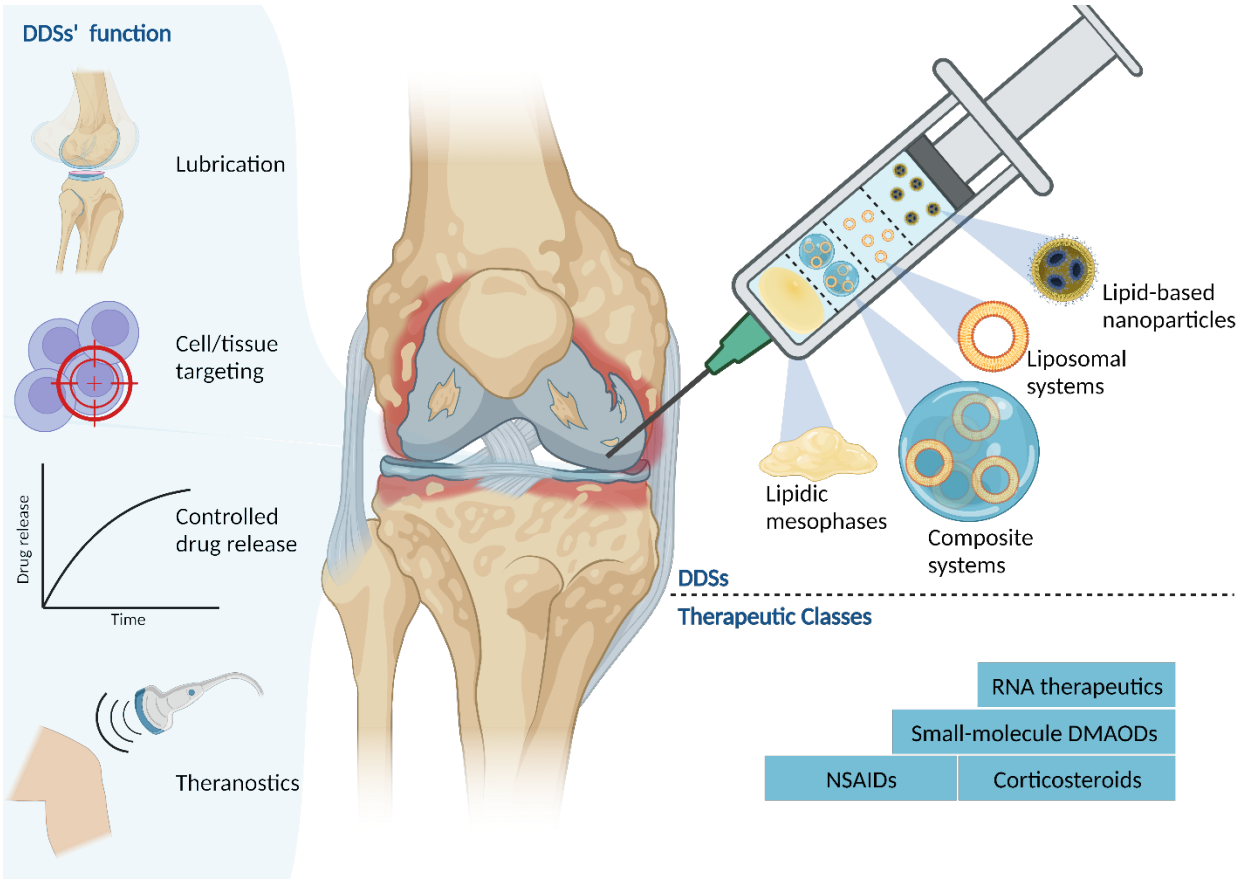

Figure 2: Overview of lipid-based drug delivery systems (DDSs) for IA administration, their functions, and classes of encapsulated therapeutics including RNA therapeutics, small-molecule disease modifying anti-osteoarthritis drugs (DMAODs), non-steroid anti-inflammatory drugs (NSAIDs), and corticosteroids. Image created with BioRender®.

1.2 Therapeutic Strategies with Lipid-Based DDSs

In this chapter, we will discuss the applications of lipid-based DDSs in the context of different drug classes for osteoarthritis treatment via IA route. Table 1 provides a comprehensive overview of the systems and functions associated with each drug class, serving as a reference for the following sections. We will explore each category in detail, highlighting the unique features, challenges, and potential future directions for lipid-based DDSs in OA treatment.

Table 1: Overview of lipid-based DDSs for IA administration of different drug classes for OA treatment. NSAIDs – non-steroid ant-inflammatory drugs, DMAODs – disease-modifying anti-OA drugs, miRNA – micro RNA; siRNA – small interfering RNA; mRNA – messenger RNA; LNPs – lipid-based nanoparticles; SLNs – solid lipid nanoparticles; NLCs – nanostructured lipid nanoparticles.

Drug Class	Drug	DDS type and function
NSAIDs	Lornoxicam [53] meloxicam [54] naproxen [55] celecoxib [56,57]	Liposomes for sustained release and lubrication [53,54] NLCs for sustained release [55] Hydrogel-lipid composites for sustained release [56,57]
Corticosteroids	Dexamethasone [58,59]	Liposomes for prolonged joint retention [58] Nanobubbles for on-demand release and theranostics [59]
Small molecule DMAODs	Kartogenin [60] dasatinib [61] quercetin [61] rhein [62,63] sinomenine hydrochloride [64] MK-8722 [65] liquiritin [66] rapamycin [67–69]	Liposomes for sustained release [61,67,69], cartilage targeting [61], and cartilage lubrication [69] SLNs for sustained release and cartilage targeting [62,63] Lipidic mesophase for sustained release [64] Lipid composite micro-/nanoparticles for sustained release [60,65,66,68] and cartilage lubrication [68]
RNA therapeutics	miRNA [53,70] mRNA [71]	Liposomes for co-delivery of lornoxicam [53] Exosomes for chondrocyte targeting [70] LNPs for chondrocyte targeting [71]

1.2.1 NSAIDs delivery

Oral NSAIDs are commonly prescribed for OA management due to their proven anti-inflammatory and pain-relieving properties. These effects are achieved by reversibly inhibiting cyclooxygenase isoenzymes COX-1 and

COX-2, leading to a reduction in prostanoid synthesis, including prostaglandins [72]. Although their therapeutic advantages and guideline recommendations [73–76] are well-established, NSAIDs carry potential risks for gastrointestinal, cardiovascular, and renal toxicity [72,77,78]. Gastrointestinal complications may involve gastric mucosal damage, nausea, gastric or duodenal ulcers, and in more severe cases, gastrointestinal bleeding [72,77]. Nephrotoxicity is also a concern, potentially causing renal failure or additional complications in patients with pre-existing conditions [72,79]. Furthermore, NSAIDs are linked to an elevated risk of acute cardiovascular events and heart failure [77,78]. Owing to the toxicity issues associated with oral NSAIDs, alternative administration routes that can alleviate these side effects are warranted. Topical NSAIDs are sometimes prescribed in knee and hand OA, as they limit the systemic exposure and adverse effects [72], but their poor solubility can limit their penetration through the skin and therefore their effectiveness [80]. IA administration emerges as a promising option, offering targeted delivery to the diseased site and reduced systemic adverse effects. In this regard, lipid-based DDSs for IA administration have attracted considerable attention, presenting novel therapeutic approaches for OA management while addressing the toxicity concerns related to oral NSAIDs.

Naproxen, a commonly prescribed drug for arthritic disorders, acts as a non-selective COX 1 and 2 inhibitor, which makes it a greater risk for gastrointestinal adverse effects than the COX 2 selective NSAIDs [81]. Due to this, the local IA administration is of great value. The researchers investigated the potential use of a nanostructured lipid carrier (NLC) formulation, a lipid-based nanoparticle (LNP), to deliver naproxen IA for the treatment of inflammation in temporomandibular joints [55]. NLCs, blending solid and liquid lipids, provide enhanced drug loading and stability compared to other LNPs, notably Solid Lipid Nanoparticles (SLNs). The contrasting structures are illustrated in Figure 3 [82,83]. Indeed, the NLC-naproxen formulation showed stable structural properties for 12 months of storage at 25 °C. The drug encapsulation also resulted in a sustained release profile, prolonging its anti-inflammatory effect in rats for over a week [55].

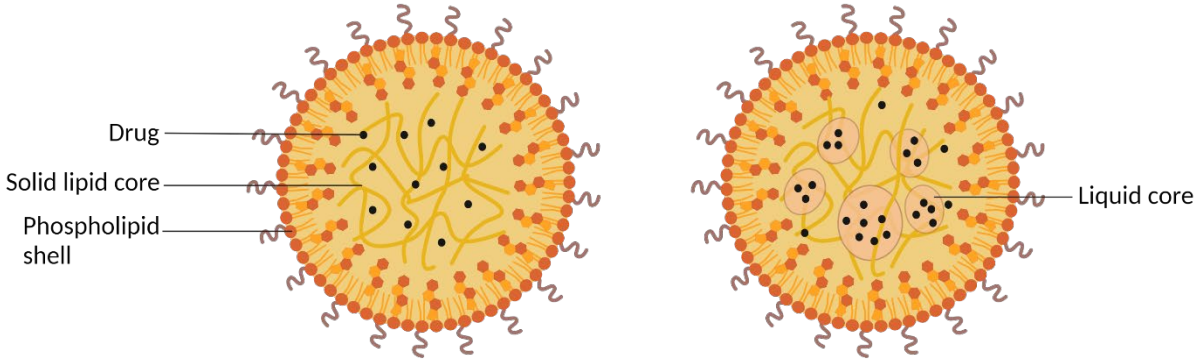

Figure 3: Difference between conventional SLN (left) and NLC (right). Image adapted from R: Tenchov et al [83] *with BioRender®.*

In addition to naproxen, several selective COX 2 inhibitors have also been studied for IA delivery. Lornoxicam, for example, is a potent NSAID used to treat postoperative pain, OA, and RA [53,84]. Recently, it was encapsulated in cationic liposomes together with microRNA-140 (miRNA), and used to achieve simultaneous anti-inflammatory and analgesic effects while promoting the cartilage repair [53]. In the context of lornoxicam delivery, liposomes controlled the drug release over 48 h, although a burst release was apparent with 65% of the drug released after 4 h. Another liposomal formulation was developed for COX 2 selective meloxicam, which is associated with fewer gastrointestinal adverse events, but inferior to equal efficacy to COX 1/2 non-selective inhibitors [37,54]. It is also known for its poor water solubility at 7.15 µg/mL and low bioavailability after oral administration [54]. In the study, meloxicam was actively loaded into PEGylated liposomes made from hydrogenated soybean phosphatidylcholine (HSPC) and cholesterol. To do this, they used a calcium acetate solution as a trapping agent to precipitate the drug inside the vesicle. The precipitated drug was added to the suspension as a meglumine complex, which is highly water-soluble. This process resulted in an encapsulation efficiency of over 98% and achieved a meloxicam concentration of around 1 mg/mL. Actively encapsulated liposomes exhibited a significant decrease in the release rate compared to the passively loaded liposomes, reduced chondrocyte apoptosis, and decreased OA score according to the Osteoarthritis Research Society International (OARSI) grading system in *in vivo* rat model. Additionally, the authors showed that the liposomes were efficient in reducing friction compared to PBS on a nano-tribological level, where atomic force microscopy

(AFM) was employed [54]. Another group developed a hydrogel-lipid composite system with cationic liposomes embedded into HA-based hydrogel and also tested it for its lubricating ability on a macro-tribological scale [57]. The drug that was encapsulated was celecoxib, a COX 2 selective inhibitor, which has been thoroughly studied in clinics for OA-related pain [85]. The composite system retarded the drug release compared to plain liposomes and reduced friction as well as wear compared with a plain hydrogel, as measured on a stainless-steel surface. These encouraging results were also noticeable in an *in vivo* rat model, where the composite system improved the cartilage integrity and reduced the catabolic marker MMP13. Interestingly, a significant improvement was observed even for the system without the drug, which authors ascribe to improved lubrication and reduction in wear that was observed in the tribological study [57]. A different approach to delivering celecoxib was taken by scientists that encapsulated the drug into nanocapsules with a liquid core composed of cationic surfactant and olive oil that is rich in lipids and designed to accommodate hydrophobic drugs [56]. The shell was polymer-based, where HA formed a coating around the oily phase and crosslinked with the cationic surfactant, cetyltrimethylammonium bromide. The system performed better *in vivo* rat model than the IA injection of celecoxib suspension with a lower joint swelling after 3 weeks upon administration. Additionally, both the inflammation and the histopathological evaluation showed better-improved scores after treatment with nanocapsules than with suspension, which was ascribed to the improved joint retention [56]. Although many of the discussed technologies aim to reduce off-target effects, this review has identified a general lack of pharmacokinetic data evaluating the claimed decrease in systemic circulation and off-target effects of NSAIDs. Moreover, not all articles compared the systems with a free drug. Nevertheless, it is apparent that formulating NSAIDs in lipid-based DDSs can improve therapeutic outcomes. These benefits arise not only from the prolonged drug retention in the joint but also from the lubricating ability of the lipids incorporated in DDSs. However, more translational research is needed to evaluate the merit of these systems and to compare them head-to-head with the standard of care in clinical settings.

1.2.2 Corticosteroid delivery

Intra-articular corticosteroids are used for short-term pain alleviation in osteoarthritis patients, with multiple guidelines supporting their use for knee, hip, and occasionally, hand OA [72–74]. Their mechanism of action

involves interaction with nuclear steroid receptors, which influences mRNA and protein synthesis, modulates immune cell activities, and reduces pro-inflammatory cytokine levels [86]. Contemporary corticosteroid formulations increasingly employ nanomaterials or crystalline suspensions to enhance drug retention in the synovium and promote localization within joint tissues [72]. However, the long-term effects of corticosteroid injections on articular cartilage and potential adverse joint outcomes remain unclear [87]. Some *in vivo* studies have demonstrated the cytotoxic nature of corticosteroids on articular cartilage. Furthermore, corticosteroid injections have been linked to systemic side effects, including hormonal imbalances, such as diminished levels of sex hormones like estrogen and androgens [88]. Additionally, infrequent flares or localized reactions may occur post-corticosteroid injection, likely due to the crystalline formulation, but typically resolve spontaneously within three days [72]. The incorporation of DDSs could help mitigate such adverse events by providing localized sustained release and utilizing biocompatible lipid systems. Moreover, the hydrophobic nature of corticosteroids makes this drug class particularly well-suited for lipid-based DDSs, as encapsulation efficiencies of 90% are commonly achieved [43].

A recent double-blinded, placebo-controlled clinical trial involving 75 patients evaluated the effectiveness of a liposomal formulation of dexamethasone (TLC599) in providing sustained pain relief by increasing its residence time in the joint space [58]. In a single injection to the diseased knee, liposomes were able to reduce the Western Ontario and McMaster Universities Arthritis (WOMAC) pain index for up to 24 weeks. Patients who received the liposomal formulation also consumed less paracetamol over a 20-week period compared to those who received a sham injection, indicating less severe pain in the former group. The study showed that liposomes used for intra-articular injection of dexamethasone can provide sustained pain relief for a longer period compared to the typically reported duration of injected solutions (less than 4 weeks) [58]. To validate these findings, a larger phase III trial was conducted (ClinicalTrials.gov identifier: NCT04123561), which included a head-to-head comparison with dexamethasone solution. Although the results of this trial have not been publicly released, they are expected to provide additional insights into the advantages of the liposomal system. Another group encapsulated the same corticosteroid in so-called nanobubbles [59], which are tiny, gas-filled vesicles with a lipid bilayer shell that can encapsulate drugs or imaging contrast agents. These nanobubbles provide a versatile platform for targeted drug delivery and can be triggered to release their contents upon exposure to external

stimuli like ultrasound, enabling precise, localized treatment [89]. This theranostic approach uses an echogenic contrasting agent to detect joint inflammation with ultrasound and trigger on-demand dexamethasone release. The study[59], achieved 70% drug encapsulation and showed burst release triggered by a 30 s ultrasound pulse. They tested the system in a rat model of rheumatoid arthritis (RA), demonstrating improved joint swelling compared to controls. The anti-inflammatory effect was superior in vitro for ultrasound-triggered nanobubbles compared to untriggered ones and free drug. The echogenic effect was comparable to SonoVue® even after 6-month storage [59]. However, it is unclear if diagnostic ultrasound would trigger release, and if theranostic tools can be used for OA.

1.2.3 Delivery of small molecule DMAODs

In recent years, research has focused on the development of novel therapeutic agents for OA that target the underlying disease processes and have the potential to modify the disease course, as opposed to traditional treatments like corticosteroids and NSAIDs that primarily provide symptomatic relief. These emerging therapies include small molecule DMOADs and natural compounds, which have been shown to exhibit different mechanisms of action, such as targeting pro-inflammatory cytokines, proteolytic activities of catabolic enzymes, the Wnt pathway, autophagy, and stimulating the regenerative potential of cartilage. While some of these compounds are still in preclinical or clinical stages of development, they offer promising alternatives for OA treatment, with the potential to address the limitations of current therapeutic options [37,38]. Despite the diverse nature of these chemical compounds, several of them face challenges such as a narrow therapeutic index [90–93] and poor bioavailability [62,94] due to their poor water solubility. Consequently, considerable research efforts have been dedicated to formulating these compounds into DDSs that can mitigate these drawbacks and enhance the therapeutic outcomes.

In recent years, targeting cellular senescence has emerged as a promising treatment strategy for OA. Cellular senescence is a process in which synovial cells lose their ability to divide and become resistant to apoptosis. These senescent cells contribute to the creation of an inflammatory microenvironment that exacerbates the progression of the disease [95]. By focusing on the clearance of senescent cells, recently co-delivered dasatinib

and quercetin using a liposomal formulation in mice [61]. This drug combination is currently under investigation in clinical trials to treat idiopathic pulmonary fibrosis, a life-threatening disease that is related to cellular senescence [96,97]. The liposomes containing the drug combination were engineered with a targeting component specific to synovial fibroblasts, using an aptamer in this instance [61]. Aptamers are single-stranded DNA molecules that possess unique tertiary structures, allowing them to selectively bind to corresponding molecular targets. They are designed and identified through a technique known as systematic evolution of ligands by exponential enrichment (SELEX), which is commonly used to select ligands capable of specifically binding to molecular targets, thereby improving the therapeutic efficacy of the DDS [98]. The system exhibited remarkable selectivity towards synovial fibroblasts, diminished dasatinib-induced toxicity on healthy fibroblasts and chondrocytes and facilitated sustained drug release. *In vivo* studies demonstrated that, following a single IA injection in mice, the targeted liposomes were retained more effectively within the joint space compared to their untargeted counterparts over a 7-day period. This ultimately resulted in a significant attenuation of cartilage degradation [61]. Another DMOAD that is currently studied in a couple of advanced clinical trials (ANZCTR ID: ACTRN12618001656224; clinicaltrials.gov ID NCT04318041) is diacerein, which is a prodrug of the active metabolite rhein, also known as cassic acid [63,99]. Diacerein, which previously showed promise in slowing the progression of OA in animal models [100], is a semisynthetic anthraquinone derivative that blocks IL1β, an important mediator of synovitis in OA that is associated with higher disease severity [99]. However, in 2014 European Medicines Agency (EMA) applied several restrictions on the use of this drug to manage the systemic risks of severe diarrhea and adverse effects on the liver [38,101]. This led to development of DDSs for local IA delivery such as SLNs that are a type of LNP with a solid lipid core. Their architecture enables improved drug encapsulation, shields against degradation, and regulates release kinetics, particularly for lipophilic drugs, but also for hydrophilic ones [102]. In order to improve the solubility of rhein, the active compound of diacerein, and achieve high drug encapsulation, researchers utilized hydrophobic ion pairing with stearylamine. This approach enhanced the lipophilicity of rhein without altering its chemical composition, enabling its dissolution in the lipid phase. As a result, the encapsulation efficiency reached nearly 100% and the drug release was sustained for over 2 weeks. When administered to rats, SLNs were found in the joints for 3 weeks after injection and accumulated in the cartilage due to the targeting ability of the positively charged particles. Rhein

encapsulation showed improved OARSI scores compared to the drug's suspension. Furthermore, the rhein SLNs significantly reduced IL1β levels over 8 weeks upon administration compared to the rhein suspension control. In a different study, the same research group further optimized the drug delivery system by incorporating chondroitin sulfate, an endogenous glycosaminoglycan known to exhibit targeting potential towards cartilage through its interaction with collagen type II [63]. The investigators demonstrated that adopting this active targeting strategy resulted in a decline in the levels of nitric oxide, IL1β, and catabolic MMP3 while augmenting aggrecan levels in rats 5 to 8 weeks post-injection, relative to passive targeting with cationic SLNs. Although the OARSI score showed a reduction in comparison to the drug's suspension, the improvement was not statistically significant compared to the SLNs with passive targeting [63]. Therefore, additional studies are necessary to confirm the improvement in therapeutic outcomes and clinical significance of the active targeting approach using SLNs. Chondroitin sulfate was also recently used to form hydrogel microparticles-microgels, which were embedded with liquiritin-loaded liposomes [66]. Liquiritin is a flavone compound derived from licorice, which was found to have anti-inflammatory and chodroprotective activity with a high potential for modifying the OA [66,103] progression. Authors employed chondroitin sulfate as hydrogel matrix, because of reports of its anti-inflammatory activity and antioxidant potential [104]. The microgels were produced by combining liposomes, alginate, and chondroitin sulfate and utilizing a customized electro-assisted bioprinter to generate droplets that were then deposited into a $CaCl_2$ crosslinking solution and irradiated with UV light. The composite system exhibited a prolonged drug release profile as compared to plain liposomes over 3 weeks, and its retention in the joint space was extended to 4 weeks. The antioxidant activity was demonstrated *in vitro*, while the therapeutic efficacy was observed in rats, as evidenced by the inhibition of cartilage matrix loss, reduction in osteophyte formation, and alleviation of subchondral bone changes [66]. Another composite system utilizing a combination of poly(lactic-co-glycolic acid) (PLGA) polymer core and PEGylated lipid shell was used for encapsulation of MK-8722 [65]. The latter is a potent activator of 5′-adenosine monophosphate-activated protein kinase (AMPK) known to joint homeostasis, limit oxidative stress and the cartilage and alleviate OA severity [105,106]. The integration of lipids into the composite system enabled the functionalization of the nanoparticle surface with targeting moieties, such as a short collagen-binding peptide, allowing the researchers to target cartilage for deeper penetration and enhanced retention in the joint 48 h post-intra-articular injection in mice.

The system exhibited significantly superior cartilage protection compared to nanoparticles lacking the targeting peptide and demonstrated greater efficiency in reducing proinflammatory markers at the endpoint of the 13 day-long animal study, with intra-articular injections administered every other day. Although the results seem promising, the lipid-polymer nanoparticles achieved only modest drug retention, with a complete release at 48 h [65]. This phenomenon may be connected to the small particle size, below 40 nm, which results in an increased surface area and facilitates the swift clearance of the nanoparticles from the joint [49,50]. Consequently, the requirement for frequent administration of the system might present obstacles regarding patient adherence to the therapy. Slightly slower release kinetics were achieved with a liposomal formulation of rapamycin [67], whose mechanism of action was discussed in chapter 1.1.3. The treatment was combined with low-intensity pulsed ultrasound (LIPUS), which has been reported to attenuate the destruction of the cartilage [107]. The findings revealed that the synergistic effect of LIPUS and liposomal formulation played a crucial role in reducing catabolic and inflammatory markers in an in vitro human OA chondrocyte model. In an animal study involving guinea pigs, subjects received intra-articular injections of the formulations every three days and underwent LIPUS treatment on alternate days. This regimen led to a decrease in catabolic markers and an increase in collagen type II [67]. However, concerns regarding patient compliance should be addressed due to the demanding nature of the treatment schedule. Recently, our group developed another liposomal DDS for rapamycin, where liposomes were loaded into anionic unilamellar vesicles with encapsulation efficiency above 90% and aggregated with Zn^{2+} [69]. The aggregation produced irreversible aggregates with nearly 100 μm in diameter, which was previously reported to increase joint retention time [49,50,69]. The irreversible nature of aggregates allowed further purification of excess Zn^{2+} with dialysis and the system produced a sustained release beyond that of plain liposomes. The tribological experiments showed excellent lubrication on a nano-tribological scale and theparticles' ability to protect ex vivo cartilage from friction on macro-tribological scale [69]. A 3-week release of rapamycin was achieved in a hydrogel-lipid composite formulation involving liposome-embedded microgels [68]. The positively charged liposomes were combined with methacrylated HA and extruded through a microfluidic nozzle into paraffin oil, after which the hydrogel was crosslinked using UV irradiation, as depicted in Figure 4. The paraffin was subsequently removed through dialysis. Macro-tribological analyses demonstrated that the microgels reduced friction in comparison to phosphate-buffered saline (PBS),

while the composite liposomal microgels provided even superior lubrication, attributed to the highly hydrated phospholipid headgroups. In OA rats, the lubricating properties of the composite formulation, through minimizing cartilage wear, contributed to the preservation of cartilage structure. This effect was further enhanced by the encapsulated rapamycin. Moreover, significant increases in aggrecan and collagen type II expressions were observed with the liposomal microgels, and the articular space improved after 8 weeks of treatment during which animals received two injections. Notably, in vivo imaging revealed that the liposomes were retained in the joint for nearly two months, highlighting the potential of this approach [68]. For delivery of kartogenin, a similar system was employed, utilizing methacrylated gelatin and liposomes [60]. Kartogenin promotes cartilage regeneration by stimulating chondrogenic differentiation of mesenchymal stem cells and upregulating the expression of type II collagen and aggrecan [37]. However, its poor water solubility limits its efficacy in clinical use due to low drug dose in aqueous solution, leading to reduced intraarticular delivery efficiency. To overcome this limitation, a system was developed using methacrylated gelatin and liposomes, resulting in a composite that exhibited attenuated drug release for over 3 weeks when produced through microfluidics and UV crosslinking, similar to process in Figure 4. In mouse joints, the composite system prolonged the drug retention period from 2 weeks for plain liposomes to 35 days. The therapeutic efficacy of this delivery system was demonstrated in rats, showing a considerable decrease in OARSI score, osteophyte volume, and cartilage lesions, while the expression of collagen type II and aggrecan was increased [60].

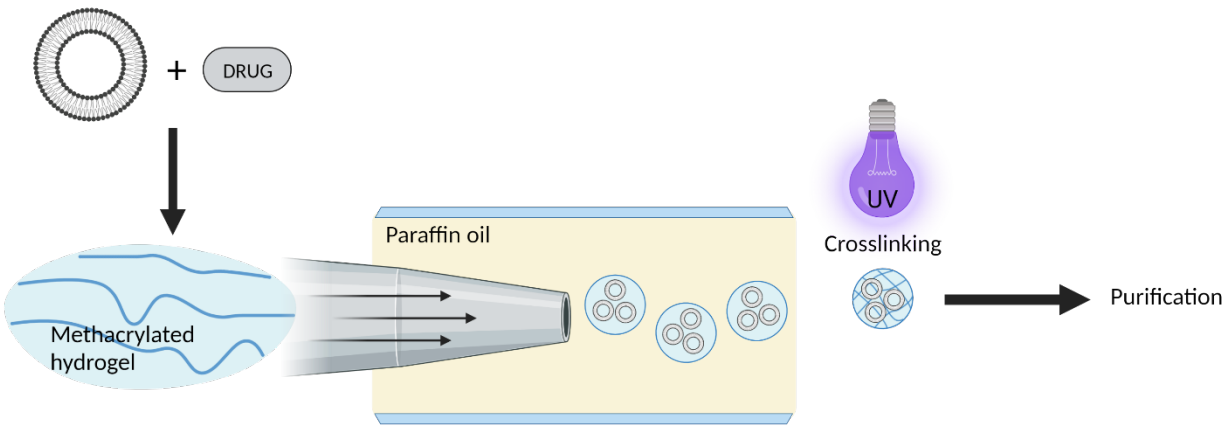

Figure 4: Production of lipid-hydrogel composite microparticles. Image was created with BioRender®.

Another system for sustained drug release was developed for sinomenine hydrochloride, a compound that is a soluble salt of sinomenium, derived from traditional Chinese medicinal herb *Sinomenium acutum*. The compound is known to have protective effects against cartilage degradation, as demonstrated by a reduction in MMP-13 and an increase in collagen type II expression in OA rats [108]. Furthermore, in animal models of sepsis, sinomenium was shown to regulate autophagy, improving survival rates, reducing organ damage, and attenuating the release of inflammatory cytokines [109]. A China-based phase 3 clinical trial (clinicaltrials.gov ID: NCT05764304) is estimated to start recruiting patients soon to evaluate the efficacy of sinomenine compared to corticosteroids for knee OA. On the other hand, the drug's potentially limited potential can be attributed to its short plasma half-life and associated systemic side effects. To address this issue, researchers have formulated the drug within a lipidic mesophase system, consisting of amphiphilic lipids and additives that self-assemble into liquid crystal structures upon contact with water [64]. Depending on the composition, the system can form lamellar, hexagonal, and cubic phases, wherein the lipids create distinct architectures with varying water channel sizes that yield unique rheological and release properties. Phase diagrams delineate the presence of specific phases under certain conditions, with temperature and water content serving as a critical determinants.[110]. The hydrophilic sinomenine hydrochloride was encapsulated in a system composed mainly of amphiphilic phytantriol and vitamin E acetate, which formed a hexagonal phase inside rats' synovial joints. The *in vitro* study showed a prolonged release of over 9 days, which resulted in increased drug concentration in animals' synovial fluid throughout 7 days of the *in vivo* study. The lipidic mesophases successfully decreased the systemic exposure of the drug compared to the drug's solution and reduced IL1β expression in synovium [64].

1.2.4 RNA delivery

Non-coding RNAs (ncRNAs) have recently emerged as a promising alternative to small-molecule and antibody-based therapeutics in the treatment of OA. These RNA-based molecules, including small interfering RNAs (siRNAs), miRNAs, and antisense oligonucleotides (ASOs), offer enhanced versatility in design, allowing for targeted modulation of gene expression while mitigating off-target effects [37]. Each type of RNA molecule differs in its mode of action and target range: siRNAs are designed to exclusively knock down a single target gene, while miRNAs can regulate multiple genes simultaneously, and ASOs can degrade target RNAs that

promote OA [111–113]. Prime targets for RNA-based therapies in OA include key catabolic enzymes such as MMP-13 and ADAMTS-5, which are responsible for the degradation of type II collagen and aggrecan, respectively, as well as the NF-κB pathway, a significant regulatory pathway governing inflammatory responses in OA, and the hypoxia-inducible factor-2α (HIF-2α), a key transcription factor controlling matrix-degrading enzymes during OA development. These targets have been chosen due to their crucial roles in OA pathogenesis and the potential for RNA therapeutics to modulate their expression [37]. Despite their potential, RNA therapeutics face challenges in stability and *in vivo* delivery, which have limited their clinical application. Issues such as rapid degradation, immunogenicity, and inefficient cellular uptake pose significant barriers to their therapeutic efficacy [114]. However, LNP formulations have shown promise in addressing these issues, improving both stability and delivery of RNA molecules [37].

Chapter 1.2.1 touched on the delivery of miRNA-140, which downregulates the expression of ADAMTS-5 with cationic liposomes that were co-loaded with NSAID lornoxicam. The DDS protected miRNA cargo from nuclease degradation and efficient uptake by chondrocytes, which resulted in the upregulated expression of Col2A1 gene. In rats, the liposomal system decreased the histologic Mankin score, which assesses cartilage structure, cellularity, Safranin O staining, and tidemark integrity [53,115]. As miRNA is specifically expressed in chondrocytes, where it exerts its chondroprotective property, the delivery in this cell type is particularly important. However, the specific delivery to chondrocytes is no easy feat, as they reside in densely structured cartilage. One research group has recently employed dendritic cell-derived exosomes that were engineered to actively target chondrocytes [70]. Exosomes, nanoscale vesicles produced by cells, serve as natural communicators between cells, transporting biologically active components like nucleic acids and proteins within their lipid bilayer membrane. These vesicles present advantages over synthetic drug carriers, including reduced cytotoxicity, enhanced tissue and cell permeability, and the capacity for targeted delivery through genetic or chemical modification [116]. In this study, active targeting was achieved by genetically engineering dendritic cells to express a chondrocyte-specific targeting peptide, as in **Figure 5**. After cell culture, supernatants were collected, exosomes isolated and miRNA-140 was loaded with electroporation. The resulting DDS demonstrated preferential uptake into chondrocytes *in vitro*, as opposed to synovial mesenchymal stem cells, leading to decreased IL1β and MMP13 expression levels. The targeted exosomes exhibited increased retention in the joint

24 h post IA injection compared to untargeted vesicles, which were found in other body parts, including the kidneys. MMP13 expression in cartilage was significantly reduced, while detected miRNA levels increased with targeted exosomes. Furthermore, the OARSI score improved four weeks post-injection of the miRNA system, indicating the potential of targeted RNA interference (RNAi) therapy for OA treatment [70].

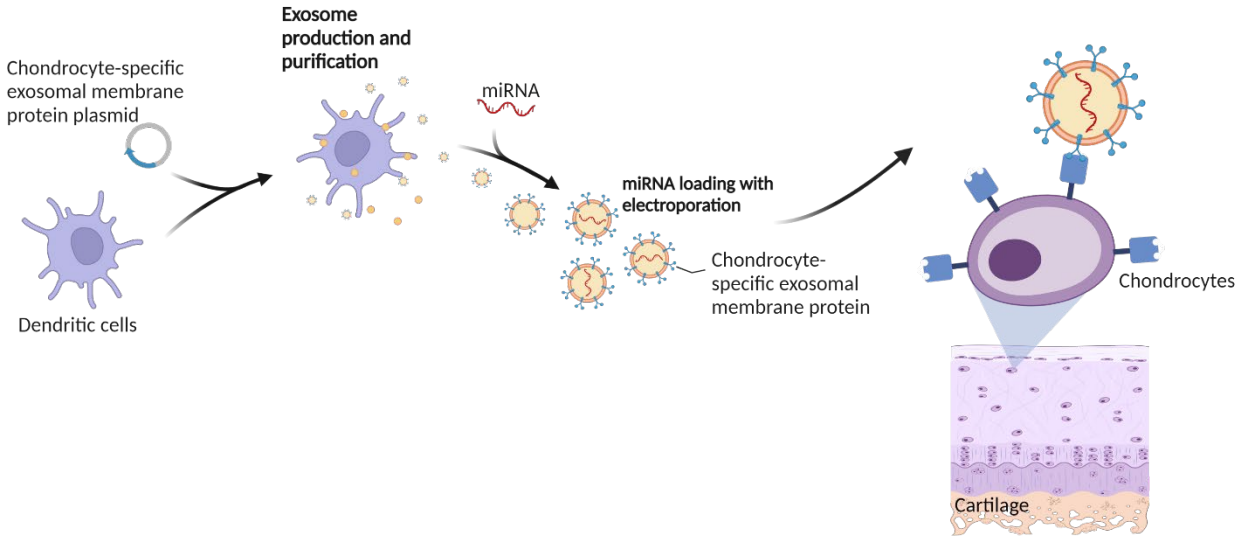

Figure 5: Production of miRNA-loaded exosomes for chondrocyte targeting. Image created with BioRender®.

Apart from RNAi approaches, messenger RNA (mRNA) delivery, which gained traction during the COVID-19 pandemic, has also recently been employed for OA treatment through delivering relevant large-molecule DMOAD codes [117]. In recent research, mRNA was encapsulated in LNPs featuring aggrecan-targeting peptides on their surface to achieve prolonged joint space retention and enhanced cartilage penetration [71]. The insulin-like growth factor-1 (IGF-1) encoding mRNA was chemically modified, and when delivered with LNPs, stimulated the proliferation of IL1β-stimulated chondrocytes. LNPs were prepared using microfluidic mixing of an acidic aqueous phase with mRNA and an organic phase containing lipids—such as ionizable DLin-MC3-DMA, cholesterol zwitterionic DSPC, and DSPE-PEG2000 with or without the targeting peptide—dissolved in ethanol. Two weeks after IA injection, particles were still present in the mice's joint space, with luciferase-encoding mRNA expression observed up to four days after injection. Both outcomes were at least four times

higher than those without the targeting moiety, highlighting the importance of active targeting following IA injection. This was also significantly greater than recombinant IGF-1 retention, which was no longer present in the joint after two days. The targeted LNPs exhibited deeper and more persistent cartilage penetration over two days in a human cartilage explant. *In vivo*, after a single injection, assessments at 4 and 8 weeks revealed that LNPs significantly decreased the number of apoptotic chondrocytes, enhanced interfacial cellularity, and augmented the presence of type II collagen in different groups. Targeted LNP mRNA delivery outperformed both untargeted delivery and recombinant IGF-1 administration [71]. Taken together, the wide range of RNA-based therapeutics examined present promising avenues for OA therapy, with advancements in lipid-based DDSs promoting enhanced stability, targeted delivery, and extended retention. Targeted approaches appear to hold a distinct advantage over their untargeted counterparts. Further research is needed to examine chondrocyte targeting in physiologically relevant settings with immune cells present, as this may significantly restrict uptake, mirroring challenges faced in systemic administration due to the reticuloendothelial system [118].

1.3 General remarks

In this chapter, we have explored lipid-based DDSs for four major drug classes: NSAIDs, corticosteroids, small molecule DMAODs, and RNA therapeutics. Recent research efforts have demonstrated the multifunctionality of lipid-based DDSs to improve therapeutic outcomes and minimize side effects associated with these drugs when used for IA administration in the treatment of OA. Throughout our discussion, we have observed that the use of advanced DDSs, such as liposomes, lipid nanoparticles, and composite systems, has contributed to enhanced stability, targeted delivery, and prolonged retention of these therapeutics in the joint space. Active targeting strategies have shown a clear advantage over passive targeting; however, more research is necessary to investigate the efficiency of these strategies in physiologically relevant conditions.

Looking ahead, the development of multifunctional DDSs that can deliver combinations of therapeutics, such as RNA molecules and small molecule DMAODs, may provide synergistic effects and improved OA treatment outcomes. A crucial aspect of advancing OA therapy is the design of long-acting systems that resist rapid clearance from the joint space. Particle size and targeting ability are critical factors in achieving this goal, as

they can enhance the localization of DDSs to synovial tissues and prolong their therapeutic effect. Additionally, combining cartilage lubrication properties that reduce cartilage wear with sustained drug delivery has shown promise in animal models. While it is crucial to advance novel DDSs into human clinical trials for OA treatment, comparative analysis between these innovative systems and current standard treatments, like oral and topical NSAIDs as well as IA corticosteroids, is particularly essential. These head-to-head comparisons are vital for assessing the effectiveness, safety, and cost-efficiency of new DDSs. If these novel systems prove superior in these aspects, they could potentially redefine first and second-line treatment regimens for OA, offering a promising and cost-efficient approach to managing the condition. Such comprehensive data would significantly inform clinical decision-making and shape the future of OA therapy. However, the urgency for such comparisons might be less for DDSs encapsulating drugs with unique mechanisms of action, such as small-molecule DMAODs or RNA therapeutics. These treatments may offer substantial potential for patients unresponsive to or unable to tolerate NSAIDs or corticosteroids. Therefore, although they should eventually be compared with standard therapies, their unique benefits could warrant expedited clinical exploration. By pushing the boundaries of DDS innovation, we can strive towards harnessing the full potential of lipid-based DDSs for IA administration in OA therapy.

1.4 Aim of the thesis

The increasing prevalence of OA and the limitations of current treatment options highlight the need for innovative drug delivery systems that effectively address the complex pathogenesis of the disease. We aimed to develop novel lipid-based drug delivery systems that provide sustained release, improved joint retention, and potential cartilage lubrication properties while targeting multiple aspects of OA pathophysiology.

In **Chapter 2**, we established a zinc-based liposomal drug delivery system for local OA therapy. The strategy involved incorporating zinc into negatively charged liposome aggregates to enhance RAPA release and improve cartilage lubrication. We assessed the aggregation kinetics, morphology, and the system's tribological performance on silicon surfaces and ex vivo porcine cartilage. Furthermore, we investigated the attenuation of the fibrotic response in human OA synovial fibroblasts by RAPA.

In **Chapter 3**, we investigated the potential of anti-inflammatory dendrimer peptides as aggregating agents for anionic liposomes to create dendrimer-aggregated liposomes (DendriXALs), aiming to provide an improved intra-articular drug delivery platform for OA treatment. We characterized the DendriXALs system using cryogenic transmission electron microscopy (cryoTEM) and fluorescence microscopy and evaluated the macro-tribological performance on ex vivo porcine cartilage. Additionally, we assessed DendriXALs' low toxicity in vitro and their effect on modulation of phagocytosis by macrophages, which play a vital role in clearing nanoparticles from the articular joints.

Building upon the previous chapters, in **Chapter 4**, we developed an injectable, lipidic mesophase (LMP)-based drug delivery system for RAPA, focusing on controlling the release of RAPA through responsive phase transitions triggered by external stimuli, such as lipases found in the OA microenvironment. We characterized the system using small- and wide-angle X-ray scattering (SAXS and WAXS) and demonstrated the phase transitions in response to lipases. As a proof-of-concept, we prepared RAPA-LMPs in the form of macrobeads, which could be further developed into micro-sized beads for enhanced joint retention. In addition to these developments, we conducted a preliminary macro-tribological study of LMPs on ex vivo cartilage.

Chapter 2.

Liposomal aggregates sustain the release of rapamycin and protect cartilage from friction

This chapter was submitted for publication and it is currently under review. It has been deposited as preprint on 25.03.2023 in bioRxiv: https://doi.org/10.1101/2023.03.23.533793.

Gregor Bordon[a], Shivaprakash N. Ramakrishna[b], Sam G. Edalat[c], Remo Eugster[a], Andrea Arcifa[d], Simone Aleandri[a], Mojca Frank Bertoncelj[e], Lucio Isa[b], Rowena Crockett[d], Oliver Distler[c], Paola Luciani[a,*]

[a] Department of Chemistry, Biochemistry and Pharmaceutical Sciences, University of Bern, Freiestrasse 3, 3012 Bern, Switzerland

[b] Laboratory for Soft Materials and Interfaces, Department of Materials, ETH Zurich, HCl G 501, Vladimir-Prelog-Weg 1-5/10, 8093 Zurich, Switzerland

[c] Center of Experimental Rheumatology, Department of Rheumatology, University Hospital Zurich, University of Zurich, Wagistrasse 14, 8952 Schlieren, Switzerland

[d] Laboratory for Surface Science and Coating Technologies, EMPA, Uberlandstrasse 129, 8600 Dubendorf, Switzerland

[e] BioMed X Institute, Im Neuenheimer Feld 515, 69120 Heidelberg, Germany

[*] Corresponding author; email: paola.luciani@unibe.ch; office number: +41 (0)31 684 41 60

Author's contribution

GB: Conceptualization; Funding acquisition, Investigation; Validation and Visualization; Formal analysis; Data curation; Writing of the original draft. SNR: Methodology (nanotribology); Investigation. SGE: Methodology (cell culture and gene expression). RE: Investigation; Validation. AA: Methodology (macrotribology). SA: Methodology. MFB: Conceptualization; Supervision. LI: Funding acquisition. RC: Funding acquisition; Supervision. OD: Funding acquisition; Supervision. PL: Conceptualization; Supervision; Project administration; Funding acquisition.

2.1 Introduction

Osteoarthritis (OA) is a debilitating chronic joint disease characterised by the degradation of articular cartilage, synovial fibrosis, and low-grade inflammation. It affects 7% of the global population, where women are disproportionately affected by the condition. The current treatment possibilities are very limited, relying primarily on non-steroidal anti-inflammatory drugs and analgesics, and joint replacement. For patients unresponsive to these medications, hyaluronic acid (HA) and glucocorticoids are prescribed, however, their use remains controversial. Several cellular therapies are becoming increasingly available, but they lack consistency of protocols or/and strong clinical data [15,28,119]. Overall, better treatments for OA remain a strongly unmet clinical need.

Rapamycin (RAPA) is an immunosuppressive drug that was first approved for the prevention of rejection in renal transplant recipients [120] and has been since tested for treatment of cancer [121], inflammatory diseases [122–124], and increasing longevity [125,126]. Recently, RAPA showed promise in OA therapy, as it reduces excessive chondrocyte apoptosis and inflammation, protecting the cartilage from further degradation [31,127]. Several in vivo studies have confirmed these effects, demonstrating that RAPA significantly reduces OA severity and damage to the articular cartilage [33,34,128]. The latest evidence shows that OA also perturbs the function of synovial fibroblasts (SFs) in the joint synovial membrane. SFs significantly contribute to cartilage damage in OA, and synovial fibrosis is associated with chronic joint pain [15,129,130]. While research on RAPA's effects on SF inflammation and senescence is gathering momentum [131–133], little is known about its impact on fibrotic OA SFs (OASFs). Additionally, the systemic use of RAPA is hindered by its adverse effects, but a growing body of literature suggests that local intraarticular injection is a promising avenue for OA treatment [33,34].

Previous research has proposed that a combination of pharmacological intervention and cartilage lubrication would yield a synergistically improved treatment for OA, but there are still no therapies available for patients exerting this dual activity [68,134]. Early investigations demonstrated that phospholipid-based liposomes, namely small unilamellar vesicles (SUVs), can improve boundary lubrication and wear of cartilage through

hydration of the phospholipid headgroups [135–138]. More recently, scientists developed a liposomal system that sustained the drug release of D-glucosamine sulfate for OA treatment and succeeded in improving the lubrication [134]. Although liposomes show great promise for OA treatment from the standpoint of biocompatibility, boundary lubrication, and controlled drug release, typical SUVs suffer from several drawbacks. Small SUVs can penetrate deep into cartilage, and when tested on ex vivo cartilage models, they exhibit worse lubrication properties compared to larger phospholipid-based vesicles that can be retained closer to the tissue's surface [139]. Furthermore, a small particle size of below 300 nm was correlated with rapid clearance from the joint, which calls for frequent administration of the formulation and an increased risk of inducing infection [41,49]. In comparison, particles above 10 μm can avoid phagocytosis by macrophages and can be retained in naïve as well as in the inflamed joints for over 6 weeks [49,50,140]. For these reasons, the utility of small phospholipid-based particles, such as SUVs is in practice limited and the development of new drug delivery systems with larger particle size and ability to sustain the drug release is imperative for better treatment of OA. Our group previously reported the ability of calcium and magnesium cations to aggregate the negatively charged liposomes into larger aggregated liposomes (ALs) forming injectable depots [141] and the resulting slower release of bupivacaine *in vitro* [142]. *In vivo* results suggested that the aggregates also increased the drug's area under the curve in plasma compared to the non-depot system and modulated the particle clearance from the injection site. Here, we tested zinc, a divalent cation known for its anti-inflammatory and antioxidant effects [143–145], as an alternative to the aforementioned aggregating agents. Our results demonstrate that aggregating negatively charged liposomes with 150 mM zinc produces irreversible ALs (ZnALs) with a diameter exceeding 90 μm, which has been shown to significantly increase the retention time in synovial joints, as in **Figure 6** [49,50]. The irreversible nature of the particles is not significant only from a pharmacokinetic perspective, but also technological, because it allows downstream processing, such as purification from excess zinc prior to administration. We further characterised the aggregation properties of the system in depth and showed that ZnALs are able to improve lubrication through testing with lateral force microscopy as well as sustain the release of RAPA with 86 % of the drug released after 7 days. These findings suggest that the system has potential for the dual treatment of OA through maintaining a low level of friction in the joint and sustaining the release of RAPA, which can decrease fibrotic markers in OASFs.

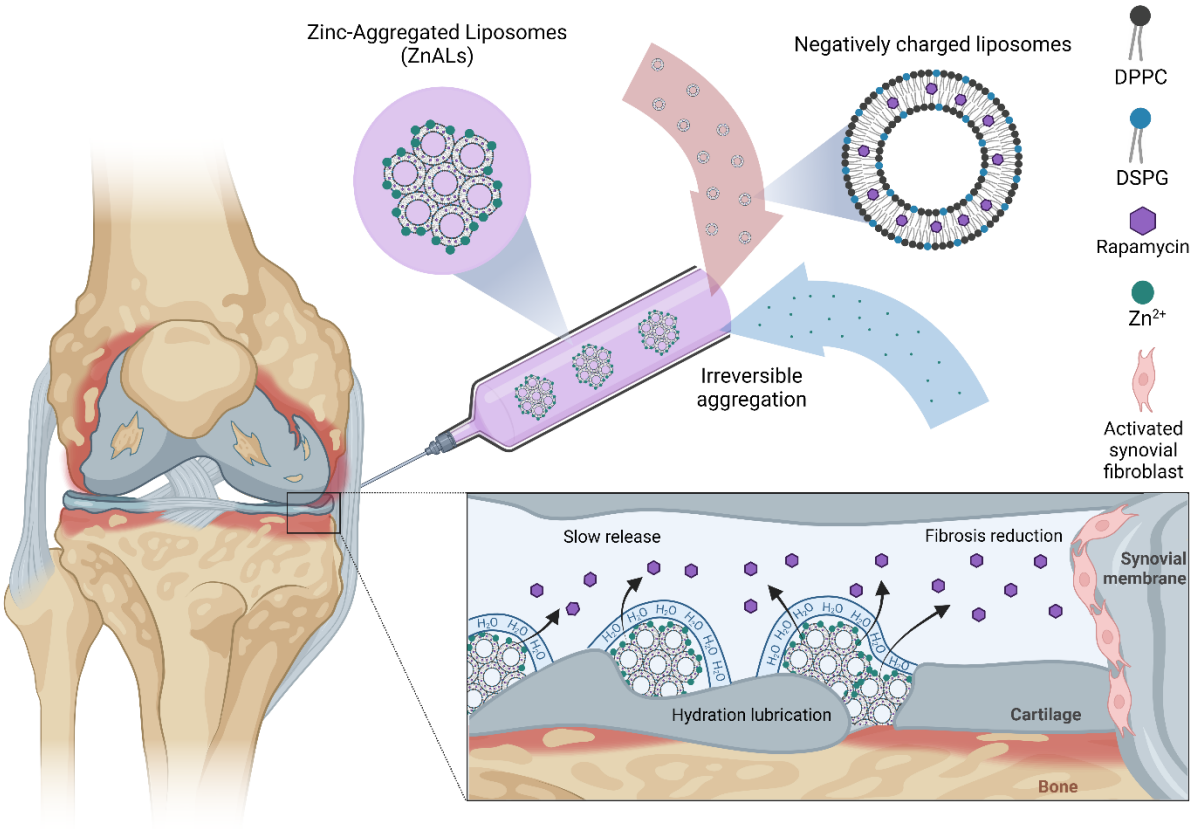

Figure 6: Graphical abstract of the ZnAL technology, depicting its' formation process and its' function for OA treatment. Image was created with BioRender®.

2.2 Materials and methods

2.2.1 Materials

The phospholipids 1,2-dipalmitoyl-*sn*-glycero-3-phosphocholine (DPPC) and 1,2-distearoyl-*sn*-glycero-3-phospho-(10-rac-glycerol) sodium salt (DSPG) were kindly gifted by Lipoid (Ludwigshafen, Germany). Rapamycin (sirolimus) was obtained from R&S Pharmchem (Pudong Districs, Shanghai, China). Zinc chloride (98% purity, reagent grade), ketoconazole (99-101% purity), and cholesterol (≥99% purity) were purchased from Sigma-Aldrich-Merck (St Louis, MO, USA). Trifluoroacetic acid and 1 M HEPES solution were obtained from Carl Roth (Karlsruhe, Germany). 1,1'-dioctadecyl-3,3,3',3'-tetramethylindodicarbocyanine, 4-

chlorobenzenesulfonate salt (DiD, catalog number: D7757) was purchased from Thermo Fisher Scientific (Waltham, MA, USA). Chloroform and methanol were obtained from Fisher Scientific (Schwerte, Germany). All chemicals were used as received. Ultrapure water of resistivity 18.2 MΩ.cm was produced by a Barnstead Smart2 pure device from Thermo Scientific (Pittsburgh, USA). Porcine knee cartilage was obtained from a local slaughterhouse in Münchenbuchsee, Switzerland.

2.2.2 Preparation and characterisation of liposomes

Liposomes with 25 mol% DSPG and varying DPPC/cholesterol content were prepared with thin-film hydration method. Lipid stock solutions in a chloroform/MeOH mixture (75/25 v/v) were dried under nitrogen flow and kept under vacuum overnight to remove residual solvents. Vesicles of 20 mM final lipid concentration were formed by hydration with 20 mM HEPES buffer at pH 7.4, heating to 70 °C, and mixing. The formed vesicles were freeze-thawed 6 times and subsequently extruded 10 times through a 200 nm polycarbonate membrane (Sterlitech Corporation, USA) with a LIPEX extruder at 70 °C (Evonik, Canada). The mean hydrodynamic diameter and polydispersity index (PDI) were measured with dynamic light scattering (DLS) analyser Litesizer 500 (Anton Paar, Austria) at 25 °C with a backscatter angle of 175° and a 658 nm laser. The zeta potential was assessed with laser Doppler microelectrophoresis using the same instrument and Omega cuvette (Anton Paar, Austria). Liposome stability was evaluated for 16 weeks at 4 °C. Formulations were used within 24 h from extrusion for all testing.

2.2.3 Encapsulation efficiency of RAPA

RAPA was dissolved in MeOH and added to the lipid film in varying molar lipid: drug ratios, by keeping the lipid content constant. Encapsulation efficiency was calculated according to the formula below:

$$EE\ \% = \frac{amount\ of\ drug\ encapsulated}{total\ amount\ of\ drug} \times 100\ \%$$

The encapsulated RAPA was quantified after removal of unencapsulated RAPA with preparative size exclusion chromatography (SEC) column (PD MidiTrap, G-25, Cytiva, USA) according to the manufacturer's protocol. The drug concentration in samples was measured with high-performance liquid chromatography (HPLC) using

a reverse phase C_{18} Nucleosil 100-5 (4.0 x 250 mm; 5.0 μm particle size, Macherey-Nagel, Germany) column and mobile phase consisting of MeOH/water (90/10 v/v) + 0.1% trifluoroacetic acid at a flow rate of 1 mL/min, temperature 50° C and UV detection at λ = 278 nm. Ketoconazole was added to all samples as an internal standard at concentration of 0.2 mg/mL.

2.2.4 *In vitro* drug release

Release of RAPA from liposomes and ZnALs was tested in vitro using a custom-made dialysis device (**Figure S1**), with dimensions similar to a 2 mL Slide-A-Lyzer MINI (Thermo Scientific, USA) and a disposable polycarbonate membrane with 100 nm pore size (**Figure S1**). This design allowed us to accommodate a up to 50 mL of release medium and provided the flexibility to select the desired disposable polycarbonate membranes with 100 nm pore size (**Figure S1**), catering specifically to the requirements of our study. The release medium was composed of 10% EtOH in ultrapure water to maintain RAPA stability and achieve sink conditions, as rapamycin is sensitive to chemical degradation, particularly in the presence of higher salt concentrations, and requires an organic solvent to enhance its solubility [146,147]. To confirm the stability of liposomes during the release study, we monitored their size with dynamic light scattering (DLS) throughout the duration of the experiment, as shown in **Figure S2**. A volume of 1 mL of each sample was added into the dialysis device and 48 mL of the release medium were added to the acceptor chamber. The loaded dialysis devices were placed in the incubator at 37 °C while shaking at 10 rpm. Throughout the 7 days of the study's duration, the release medium from the acceptor chamber was aliquoted and fully replaced with a fresh one at each time point. The aliquots were frozen in liquid nitrogen and lyophilised. Each sample was resuspended with the internal standard solution and RAPA content was determined with HPLC.

2.2.5 Preparation and characterisation of ZnALs

Aggregated liposomes (ALs) were prepared through a four-time dilution of 20 mM liposomes with aqueous solutions containing different concentrations of $ZnCl_2$ (Zn^{2+}) and gentle stirring for 5 min. Keeping the volume ratios constant allowed for constant liposome and drug concentration in ZnALs at varying Zn^{2+} concentrations. ALs were characterised via turbidimetric scattering measurements using a microplate reader, as previously

reported [141]. Briefly, 50 µL of liposomes with an initial lipid concentration of 20 mM were mixed with 150 µL Zn^{2+} solution in a quartz 96-well microtiter plate with a clear and flat bottom (Hellma GmbH & Co. KG, Germany). The mixture was gently mixed for 30 min, and the optical density was measured with an Infinite M Pro 200F-PlexNano microplate reader (Tecan, Switzerland) at 450 nm. The zeta potential of ZnALs was measured with the Litesizer 500 in the same manner as for the liposomes. Stability upon dilution was tested by diluting ALs 400 times with ultrapure water and subsequently performing a size measurement with the DLS at different time points. The presence and size of aggregates were determined with laser diffraction measurements, which were performed with PSA 1190 LD (Anton Paar GmbH, Austria) after 400x dilution in water as a dispersion medium where the obscuration parameter was set to 1-7 %. The optimization of input parameters such as stirring and pump speed was defined in order to obtain repeatable measurements. Stirring was set to slow (150 rpm) and the pump speed was put to medium setting (120 rpm). To further confirm the presence of aggregates upon 400x dilution, a nanoparticle tracking analysis (NTA) was performed using Zetaview (Particle Metrix, Germany) with a 488 nm laser, camera sensitivity of 58 and a 100 m/s shutter value. Aggregation kinetic experiments were performed with PSA using a series of 180 measurements with a measurement time of 10 s between each point. D50 was recorded and plotted over time, where 3 time points were averaged together as technical repeats to account for the measurement fluctuations. Prior to testing, the ZnALs underwent a purification process to eliminate excess Zn^{2+}. This was achieved through a 4 h dialysis in 0.5 L of ultrapure water, utilizing Float-A-Lyzers G2, 8-10 kDa MWCO (LubioScience GmbH, Switzerland), and hourly complete replacement of medium. Zn^{2+} concentration was measured using inductively coupled plasma mass spectrometry (ICP-MS, NexION 2000, PerkinElmer, USA). Calibration standards, internal standards, and samples were prepared using a 2% (w/w) HNO_3 solution (BASF SE, Germany) as the matrix. During measurements, a 10 µg/L yttrium solution was utilized as the internal standard during measurements. The ICP-MS system was calibrated with standards (TraceCERT Merck, Germany) ranging from 1 to 500 µg/L Zn^{2+}.

2.2.6 Differential scanning calorimetry (DSC)

Interactions between the phospholipid bilayer and RAPA were examined with a DSC 250 (TA Instruments, USA). Multilamellar liposomes and ZnALs (150 mM Zn^{2+}) with or without RAPA were prepared in a final concentration of 20 mM and 12 µL were transferred in a Tzero® aluminum pan and hermetically sealed. A

volume of 12 µL of 20 mM HEPES was used as a reference. Samples were pre-heated to 60 °C, kept at that temperature for 5 min, and then cooled down to 10 °C. Next, two heating and cooling cycles were performed between 10 °C and 70 °C at the rate of 2 °C/min. The last cycle was used for the evaluation of the thermal profile and the calculation of hysteresis. The enthalpy values were normalized to the phospholipid amounts in the samples.

2.2.7 Microscopic imaging of liposomes and ZnALs

Liposomes and ZnALs were imaged with fluorescence and cryogenic transmission electron microscopy (cryo-TEM) to assess the morphology. For fluorescence microscopy, lipid films for liposome preparation were stained with 0.05 mol% of the non-exchangeable lipophilic dye DiD. Liposomes and ZnALs were prepared as described above, while being protected from light. A volume of 20 µL of formulations was added on a slide and covered with a glass coverslip to be imaged with an inverted fluorescence microscope (Nikon Eclipse-Ti, Canada) through Tx red filter. For cryo-TEM, a volume of 6-8 µL of each sample was applied onto a gold grid covered by a holey gold film (UltrAuFoil 2/1, Quantifoil Micro Tools GmbH, Jena, Germany). Excess of liquid was blotted automatically between two strips of filter paper or only from the backside of the Grid. Subsequently, the samples were rapidly plunge-frozen in liquid ethane (cooled to 180 °C) in a Cryobox (Carl Zeiss NTS GmbH, Oberkochen, Germany). Excess ethane was removed with a piece of filter paper. The samples were transferred immediately with a Gatan 626 cryo-transfer holder (Gatan, Pleasanton, USA) into the pre-cooled Cryo-electron microscope (Philips CM 120, Eindhoven, Netherlands) operated at 120 kV and viewed under low dose conditions. The images were recorded with a 2k CMOS Camera (F216, TVIPS, Gauting, Germany). In order to minimize the noise, four images were recorded and averaged to one image.

2.2.8 Cell culture

SFs were obtained from four consenting OA patients (according to ethics approvals BASEC-Nr. 2019-00674 and BASEC Nr. 2019-00115) and plated onto 25 cm^2 flasks and 6-well (clear, Corning, USA) or 96-well (black with clear bottom, Thermo Fisher Scientific, USA) plates following standard protocols [148]. Cells were cultured at 37 °C in a humidified atmosphere at 5% CO_2 with Dulbecco's modified Eagle's medium (DMEM; Life Technologies) supplemented with 10% fetal calf serum (FCS), 50 U mL^{-1} penicillin/streptomycin, 2 mM L-glutamine, 10 mM HEPES, and 0.2% amphotericin B (all from Life Technologies). OASFs were used for experiments between passages 4 and 6 when they reached confluency.

2.2.9 Toxicity of RAPA and ZnALs

OASFs were counted with Countess 3 FL (Thermo Fisher Scientific, USA) using trypan blue and seeded onto a 96-well plate at a density of 5'000 cells per well. After overnight incubation, the cells were treated with 200 µL of different conditions and incubated for 48 h. Upon incubation, the cells were stained with the LIVE/DEAD™ Viability/Cytotoxicity Assay Kit (Thermo Fisher Scientific, USA) according to the manufacturer's protocol. Briefly, the medium was aspirated, and the cells were washed with DPBS (Thermo Fisher Scientific, USA) before being stained with calcein and Sytox Deep Red dyes. Cells were incubated for 30min at RT and washed with DPBS. The dead control was prepared by fixing the cells in ice-cold ethanol as per manufacturer's recommendations. Fluorescence was measured with a plate reader (BioTek Instruments, USA) in a bottom area scan mode with a 35 gain. Fluorescence intensity of alive cells was measured with a 528/20 nm filter after the excitation at 485 nm wavelength. Dead cells' fluorescence was excited at 530 nm and the emission was detected with 590/35 nm filter. Viability percentage was normalised to the fluorescence intensity of the untreated condition, which was treated with normal medium. Images were taken with a widefield fluorescence microscope (Zeiss AxioObserver Z1, Germany) using GFP (cyan) and DsRed (green) fluorescence filters.

2.2.10 Gene expression

For gene expression experiments, cells were seeded in the same way as described for the toxicity experiments above. The fibrotic response was stimulated by adding 10 ng/mL of TGFβ to the medium together with the tested conditions. After 48 h incubation, cells were lysed, and RNA was extracted with a Quick-RNA Microprep Kit (Zymo Research, USA) as well as on-column DNase I digested according to the manufacturer's protocol. The purity and amount of RNA were determined by measuring the OD at a ratio of 260 to 280 nm with Nanodrop (Thermo Fisher Scientific). RNA was reverse transcribed and SYBRgreen real-time PCR was performed. Data were analysed with the comparative CT methods and presented as $2^{-\Delta\Delta CT}$ (i.e., x-fold) as described elsewhere [149] using RPLP0 as a housekeeping gene for sample normalization. Primer sequences are available in Supplementary Information.

2.2.11 Nanotribology

Nanotribology measurements were performed on silica sliding against silicon with colloidal probe lateral force microscopy (CP-LFM) using a Bruker Dimension Icon AFM with tipless Au-coated cantilevers (CSC-38, Mikromash, Bulgaria). Cantilever spring constants were determined using the thermal-noise method [150] for normal spring constants and Sader's method [151] for torsional spring constants. Approximately 8 μm diameter silica particles (EKA Chemicals AB, Kromasil R) were attached to the end of the cantilever using two-component epoxy glue via a home-built micromanipulator. Four different colloidal probes were prepared and treated with UV/ozone for 30 min before the measurement. Four silicon wafers (~1x1 cm) were treated with UV/ozone and used as substrates. Prior to each measurement, the silicon substrates, but not the silica colloid probe, were immersed in either PBS, Zn^{2+} solution, ZnAL, or liposome solutions (5 mM) for 30 min and rinsed with ultrapure water [134]. CP-LFM measurements were conducted in buffer solution, and friction loops were recorded by scanning the cantilever laterally over the surface. For each applied load, at least five friction loops were acquired, and the average friction values were obtained from trace and retrace curves. Coefficient of friction (COF) values were determined from the slope of the friction force vs normal force graphs. Lateral-force calibration was conducted using the "test-probe method" described by Cannara et al [152] by moving a test probe

(a reference cantilever glued with a silica particle of diameter ~40 μm) laterally into contact with a silicon wafer (1x1 cm) used as a "hard wall" to obtain lateral sensitivity values.

2.2.12 Macrotribology

The macroscopic friction behaviour of cartilage sliding against cartilage in the presence of PBS, Zn^{2+} solution, ZnALs, or liposome solutions was investigated with a UMT-2 tribometer (Bruker, USA) operating in linear reciprocating mode. The counterparts consisted of two portions of cartilage that were cut from porcine knee and stored at -20 °C until use. Cartilage was glued to the upper and lower surfaces of the tribometer shortly before testing. During each experiment, a load of 1 N was applied to the upper specimen (5x5 mm) and sliding took place over a 2 mm stroke length at a frequency of 1 Hz for 10min. The specimens were completely immersed in the lubricant for the entire duration of the test. All tests were conducted at a constant temperature of 20°C and a data acquisition frequency of 500 Hz. The representative coefficient of friction (COF) of each test was computed from the raw data of lateral and normal force as the average of each friction loop, taking only the central 90% portion of each friction loop to avoid transients associated with the two ends of the stroke length. In addition, the first 20% of the loops were excluded so that only the steady-state friction was processed, and the running-in phase was excluded.

2.2.13 Statistical analysis

All experiments were carried out in at least three replicates unless otherwise stated. The reported values are means with ± standard deviation. Microsoft Excel was used for general calculations, while GraphPad Prism 9.5 was used for plotting, performing the one-way ANOVA and Tukey's test.

2.3 Results & Discussion

2.3.1 Preparation of liposomes and drug encapsulation

Drugs with low water solubility, such as RAPA, must be formulated to increase their bioavailability. Encapsulating them in liposomes is an effective way to solubilize the molecules, enhance their therapeutic index,

and enable controlled release [68,153]. A key factor in liposome production is the encapsulation efficiency (EE%), with a low EE% requiring further purification to remove the unencapsulated drug, leading to increased production cost and complexity. The EE% is highly dependent on the drug's chemical properties, the composition of the liposomes, and the lipid-to-drug ratio (L/D) [154]. The impact of both was investigated in **Figure 7a)**, where the higher L/D yielded higher EE%.

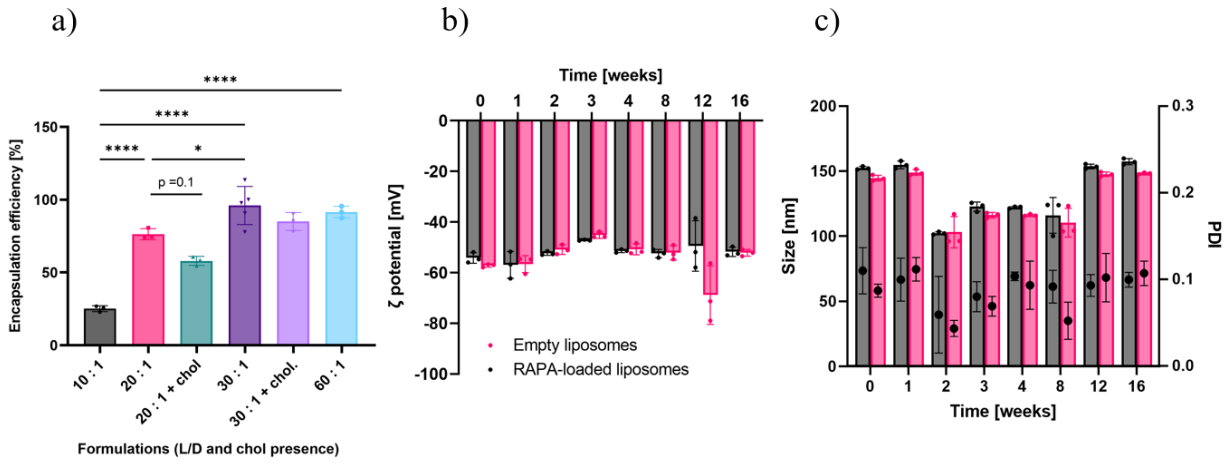

*Figure 7: a) EE% of RAPA in liposomes at different L/D. The formulations without chol had the composition DPPC:DSPG = 75:25 and the formulations with chol DPPC:DSPG:chol = 45:25:30. b) Stability of zeta potential of the formulation with 30 : 1 L/D without chol over 16 weeks. c) Stability of liposomes with 30 : 1 L/D without chol over 16 weeks with size on the left y-axis represented in bars and PDI on the right y-axis represented with the scatter plot. One-way ANOVA with Tukey's multiple comparisons test was run. Statistical significance is designated as: *P < 0.05 **P < 0.01, ***P < 0.001, ****P < 0.0001.*

This is to be expected, as RAPA is highly hydrophobic and a greater amount of phospholipid gives more space for the drug to be encapsulated within the bilayer [155]. Chol is oftentimes added to the formulations to modulate the membrane properties such as thickness, packaging, and fluidity, which in turn can lead to decreased leakage of the drug from the liposomes [154]. On the other hand, the results illustrated in **Figure 7a)** show that the presence of 30 mol% chol decreased the EE%. The highest EE% above 91% was obtained with the L/D of 30:1 and 60:1 without chol and in order to keep a relevant therapeutic dose, the 30:1 formulation was used for all further experiments. These results are congruent with other studies, where RAPA [156] and other hydrophobic drugs were encapsulated in chol-containing liposomes [157]. The accepted explanation for this is that the

addition of chol in the phospholipid bilayer reduces the size of hydrophobic cavities, which leaves less space for the encapsulation of lipophilic drugs, decreasing the drug-lipid interactions and hence, the EE% [155–158]. **Table 2** demonstrates the difference in size between empty and RAPA-loaded liposomes, as measured by DLS in ultrapure water. The size of RAPA-loaded liposomes exhibited a slight but statistically significant increase compared to the empty liposomes, with a p-value <0.01. Both systems displayed a low polydispersity index (PDI) of below 0.2, indicating a relatively uniform size distribution within the liposomal samples. **Figure 7b)** and **c)** show that the liposomes were stable for a period of at least 16 weeks, with a slight decrease in size at week 2, which was already reported for DSPG/PC liposomes previously [141] and subsequent return to normal size at week 12.

Table 2: Liposomes' properties at 30:1 L/D, without chol.

	Size [nm]	PDI	ζ-potential [mV]
Empty	145 ± 2	0.11 ± 0.03	-57.2 ± 0.6
Loaded	152 ± 1	0.087 ± 0.008	-54.0 ± 2.0

2.3.2 Fabrication and characterisation of zinc aggregated liposomes (ZnALs)

Small particles like liposomes are rapidly cleared from synovium and therefore the administration of larger particles is preferable [49]. Cationic vehicles have been recently used to enhance interaction with negatively charged cartilage surface [159,160], but liposomes containing high amounts of positively charged phospholipids can elicit toxicity and inflammation [161,162]. To address this issue, we specifically selected zinc as the aggregating agent for our liposomal formulation, considering its reported anti-inflammatory properties and potential benefits in the context of osteoarthritis treatment. We developed a liposomal formulation with anionic phospholipids that aggregate upon the addition of Zn2+, resulting in slightly positively charged ZnALs in the μm-range (**Figure 8b), c)**).

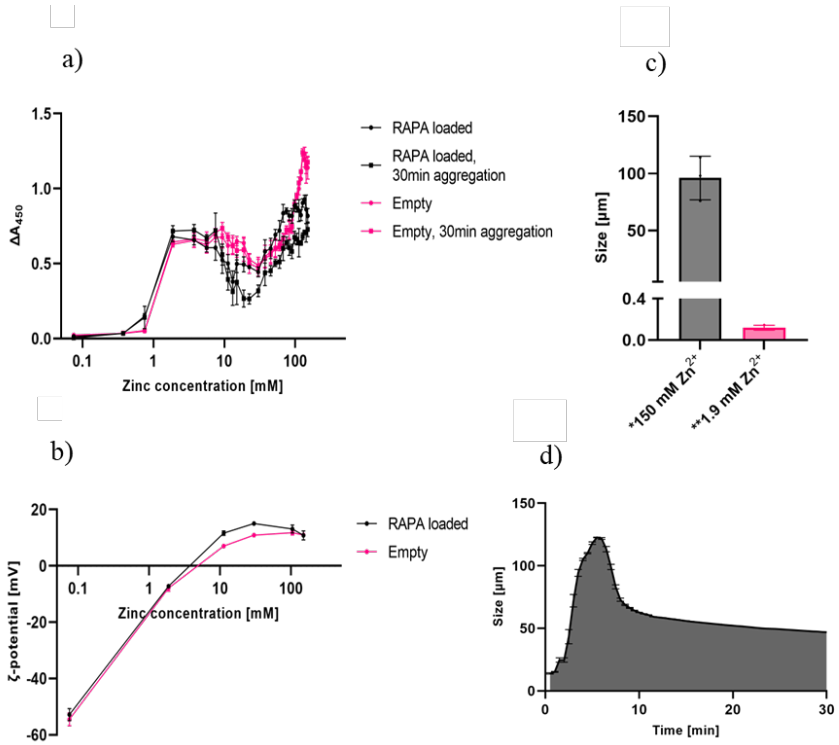

*Figure 8: a) ZnALs' aggregation profile measured at different Zn^{2+} concentrations via a plate reader at 450 nm, immediately after mixing or after 30 min of gentle mixing. Final lipid concentration was 5 mM b) ζ.-potential of ZnALs at different Zn^{2+} concentrations. c) Size after dilution with ultrapure water to a final Zn^{2+} concentration below 0.5 mM. *Measured with PSA. **Measured with DLS. d) Aggregation kinetics of liposomes in 150 mM Zn^{2+} measured with PSA – measurements were performed in 3 technical replicates at 30 s timepoints.*

The aggregation is propagated by the neutralization of negatively charged liposomes with Zn^{2+}, where the attractive van der Waals forces gain the upper hand. This is reflected in the secondary maximum on the aggregation profile on **Figure 8a)**. After further addition of the cation, more Zn^{2+} is bound on the surface of liposomes, which reverses the charge to +15 mV at 20 mM Zn^{2+} content and stabilises smaller particles. This phenomenon is seen as the secondary minimum in **Figure 8a)** and was previously observed in reports that focused on the coating of the anionic liposomes with polycations e.g., polylysine [163,164]. The continued introduction of Zn^{2+} to the final concentration of 150 mM induces a global maximum in the profile, where a dip in the ζ-potential to 11 mV can be observed for both empty and RAPA-loaded systems. The two systems exhibit distinct differences, with the former showing a less pronounced minimum at 20 mM Zn^{2+}. This is likely due to

a lower increase of ζ-potential at 20 mM Zn2+ for the empty system, reaching only +11 mV compared to +15 mV for loaded ZnALs. The lower ζ-potential results in weaker electrostatic repulsion, promoting the formation of larger particles due to enhanced aggregation. These shifts are presumably a consequence of RAPA's perturbation of the phospholipid bilayer. The RAPA's impact on the surface of DPPC-based anionic liposomes has been only recently elucidated [165], while the effect on the lipophilic moiety was studied earlier [166]. **Table 3** shows the results of the differential scanning calorimetry (DSC) analysis, where the impact of RAPA on DPPC/DSPG liposomal bilayer was evaluated on unextruded liposomes (MLVs) and aggregated vesicles (ZnALs). High rigidity of the used unsaturated phospholipids limited the impact of the encapsulated drug on the bilayer's packing, as only a slight decrease in T_m can be observed. A more significant effect is the widening of the transition peak, suggesting that the homogeneity of the bilayers is affected by RAPA. Expectedly, the pretransition peak at 36 °C disappeared in the drug-loaded sample (**Table 3**), which indicates an interaction of the drug with the polar headgroups or acyl chains of the phospholipids. A greater effect of RAPA is observed in ZnALs, where both the transition and the pretransition peaks disappeared in the RAPA-loaded system, suggesting an altered packing of phospholipids. In summary, these DSC results show that RAPA affects the liposomal membrane, which could explain the differences in the aggregation behaviour in **Figure 8a)** and **b)**.

*Table 3: DSC results of empty and RAPA-loaded MLVs and ZnALs (150 mM Zn^{2+}). The change in enthalpy was normalized to the mass of phospholipids in the samples, while the reported results represent the calculated mean values ± standard deviation of at least 3 replicates. Thermograms are available in **Figure S3** in Appendix.*

	T_m [°C]	ΔH [J/g]	Peak width [°C]	T(pretr.) [°C]	ΔH(pretr.) [J/g]
Empty MLVs	43.66±0.03	35±3	3.27±0.03	36.0±0.2	2.0±0.4
Loaded MLVs	43.11±0.02	33±5	4.6±0.2	n.a.	n.a.
Empty ZnAL	43.9±0.1	1.0 ±0.6	2.3±0.2	n.a.	n.a.
Loaded ZnAL	n.a.	n.a.	n.a.	n.a.	n.a.

Subsequently, the size and reversibility of ZnALs were determined by dilution with ultrapure water to below the minimal concentration of Zn^{2+} that is needed for the aggregation (<0.5 mM). The 1.9 mM and 150 mM Zn2+ concentrations were chosen for these measurements as they correspond to the first and second aggregation peaks

respectively, which can be observed in Figure 8a) and 2b). The measurements were performed with dynamic light scattering (DLS) and particle size analyser (PSA) that is based on laser diffraction technology, which is used to analyse particles in µm-range. The PSA measurements showed that the size distribution after 30 min of aggregation in 150 mM Zn^{2+} and subsequent dilution was unimodal with the mean size of 96 µm ± 19 µm (**Table 4** and **Figure 8c**)), indicating that the aggregates are irreversible. Upon performing the same procedure with the ZnALs at 1.9 mM Zn^{2+}, the detector obscuration was found below 0.5%, which points to de-aggregation of ZnALs. Subsequent DLS measurement of the diluted samples revealed the reversion of ZnALs to the single-liposome size of 119 nm, which is the consequence of disaggregation. However, for ZnALs at 150 mM Zn^{2+}, the correlation function was irregular, and the size of aggregates could not be measured.

Table 4:Results of size measurements of ZnALs at different Zn^{2+} concentrations with DLS and PSA reported as mean ± standard deviation of at least 3 replicates.

[Zn^{2+}] in ZnALs	Size after dilution – DLS	Size after dilution – PSA
1.9 mM	119 nm ± 20 nm	Not measurable
150 mM	Not measurable	96 µm ± 19 µm

To confirm the presence of irreversible aggregates at 150 mM Zn^{2+}, a nanoparticle tracking analysis (NTA) was used to capture the ZnALs on video after they were diluted 400x in ultrapure water and can be seen in **Supplementary Video 1** (in Appendix). In contrast, no aggregates can be observed in **Supplementary Video 2** (in Appendix), where ZnALs with 1.9 mM Zn^{2+} were diluted by the same dilution factor. The formation of irreversible aggregates was further studied by the addition of liposomes in excess volume of 150 mM Zn^{2+} solution, while the liquid was continuously flowing through a flow cell that was in a closed loop of PSA instrument. **Figure 8d)** shows the kinetic profile of size change for the period of 30 min. The aggregation reached its peak at 6 min of flowing through the flow cell at 122 µm and was followed by a decrease in size, which stabilised at 10 min. The gradual decrease in size over the following 20 min is likely due to shear stress, caused by the flow through the flow-cell. Taken together, these results demonstrate that ZnALs formed at 150 mM Zn2+ concentration are irreversible, which distinguishes this system from previously reported aggregates [141,142].

Previous studies did not achieve or test the global maximum in the aggregation profile within the explored cation concentrations. The irreversibility of our system enables the removal of excess Zn2+ through dialysis or tangential flow filtration, which was not possible in reversible systems. Our findings also show that the mean size of these aggregates is 96 μm, which exceeds the 10 μm threshold necessary for increased joint retention, as suggested by previous research [49,50]. The formation of irreversible aggregates not only adds value to our liposomal drug delivery system but also demonstrates the potential for enhanced joint retention in osteoarthritis treatment.

The morphology of liposomes and ZnALs were assessed with Cryo-TEM and the representative images are shown in **Figure 9**. The liposomes were mainly unilamellar and nanosized, consistent with the DLS data. The empty liposomes occasionally flattened, wheras the addition of 1.9 mM Zn^{2+}, surprisingly, formed polyhedral structures with a negative curvature of the bilayer. Loaded liposomes only showed slight flattening at 1.9 mM and clear curvature at 150 mM Zn^{2+} (**Figure 9** and **Supplementary Video 3** from the Appendix).

This was not seen in our previous study with DPPC/DSPG/chol liposomes exposed to 10 mM divalent cation, where only aggregation was observed [142]. The obvious explanation for this is that the particles in the present study have an enhanced fluid character due to the lack of chol in the bilayer and the formation of polyhedral structures is energetically favourable under the osmotic pressure imposed by external Zn^{2+}. It has been previously reported that nanosized rigid liposomes can exist in a facetted configuration below their T_m [167]. The fact that RAPA-loaded liposomes exhibit a reduced angularity in up to 20 mM Zn^{2+} concentration suggests that the encapsulation of the drug in the bilayer has a chol-like effect on the membrane. This increased fluidity of the membrane is also supported by the DSC results in **Table 3**. The stabilization of liposomes' spherical morphology by hydrophobic molecules is further supported by earlier investigation of the temoporfin encapsulation, which has comparable solubility in water to RAPA and has similarly reduced the angularity of the particles [168]. These results not only have importance for the design of liposomal drug delivery systems, but have further implications for better understanding of the cell membrane dynamics in different tonicities, as living cells also contain hydrophobic solutes. Furthermore, cryoTEM (**Figure 9**) confirmed the presence of aggregates at 1.9 mM and 150 mM Zn^{2+}, which corroborated the PSA results.

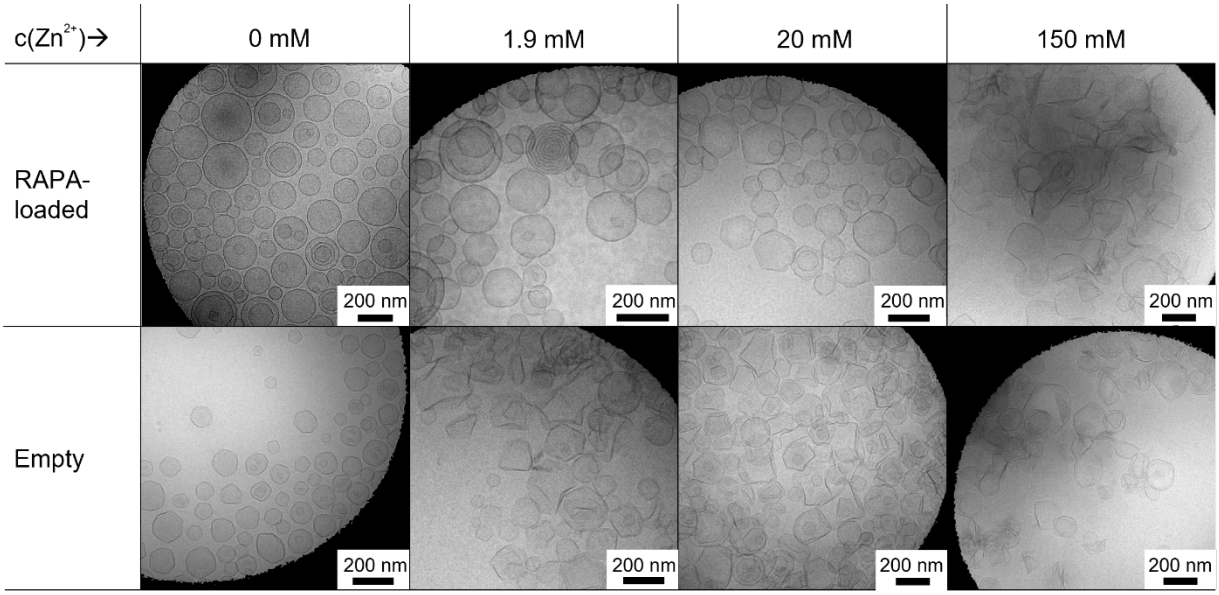

Figure 9: Cryo-TEM images of empty and RAPA-loaded formulations with different Zn^{2+} concentrations.

Empty liposomes had clear aggregation at 20 mM Zn^{2+}, while RAPA-loaded samples showed less pronounced aggregation as seen in **Figure 8a)**. Large aggregates were also scanned three-dimensionally using cryo-TEM tomography and are presented in **Supplementary Video 3** (in Appendix). To observe the system at a larger scale, liposomes were fluorescently labelled with DiD and aggregated as before (*vide supra*). **Figure S4** shows complex morphology of large ZnALs at 150 mM Zn^{2+}.

2.3.3 RAPA release from ZnALs and effect on human OASFs

RAPA release from liposomes and ZnALs was tested in 10% EtOH in water to ensure sink conditions and stability of the drug throughout the experiment. **Figure 10a)** shows that ZnALs could retain the drug for longer than free liposomes with 86% released after 7 days, while 90% of the cargo was released from free liposomes already after 3 days. This difference in release rate can be attributed to the distinct diffusion pathways in aggregated and non-aggregated liposomes. In aggregated liposomes, the drug must navigate through multiple barriers consisting of interconnected phospholipid bilayers, thereby leading to a more prolonged release process. Conversely, non-aggregated liposomes offer a simpler release mechanism, wherein the drug traverses a single membrane of the small unilamellar vesicle, resulting in an accelerated release rate. The use of aggregated liposomes for sustained drug delivery was recently proposed by our group in a study, where bupivacaine's release

was retained *in vitro* by calcium aggregated liposomes and the bioavailability of the drug was increased *in vivo* [142].

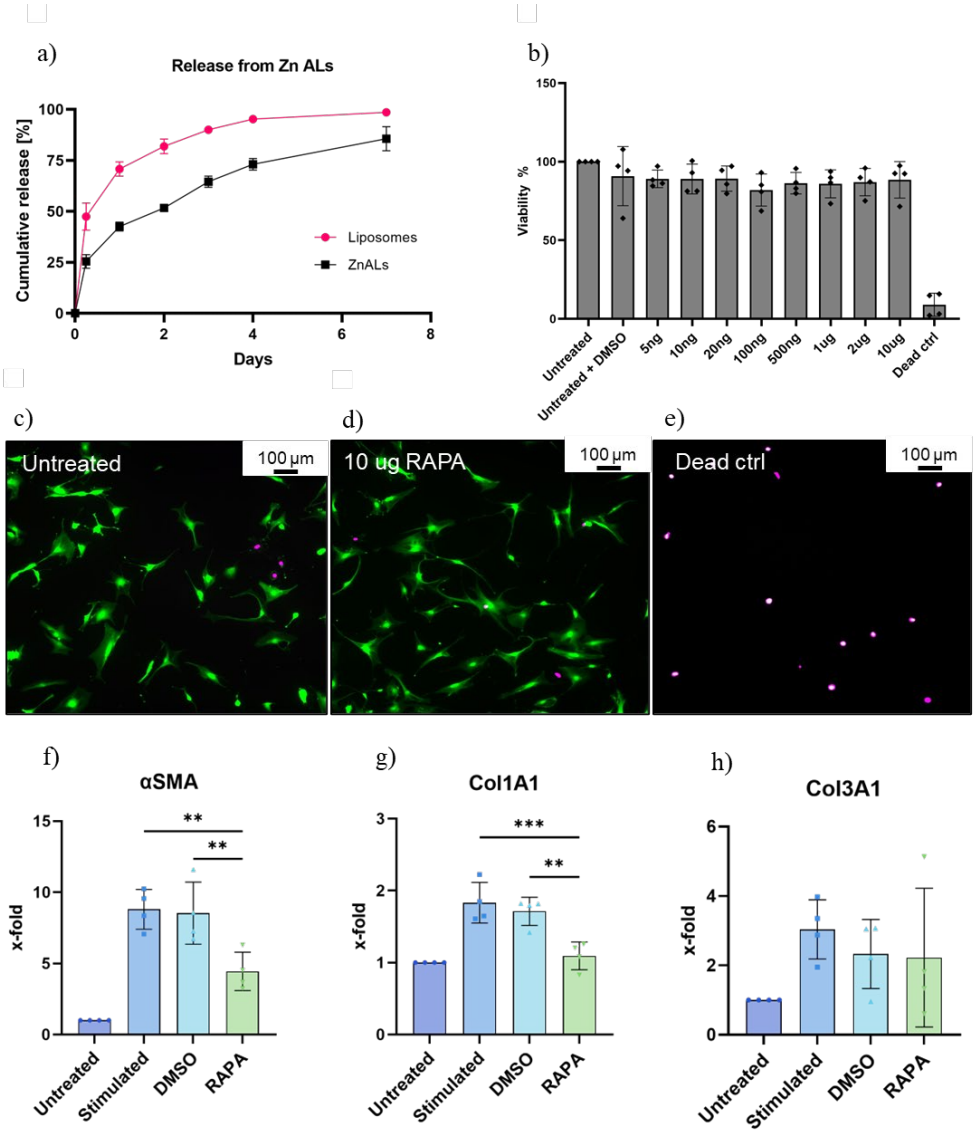

Figure 10: a) Release of RAPA from liposomes and ZnALs at 150 mM Zn^{2+} in 10% EtOH. b) Toxicity of RAPA on human OASFs stained with calcein; fluorescence was measured with a plate reader. c) Fluorescence microscopy image of untreated OASFs after 48 h incubation and subsequent staining with calcein and SYTOX Deep Red. Live cells are coloured in green and dead in magenta. d) Cells at 10 µg/mL RAPA. e) Dead cells treated with 70% EtOH. f) Gene expression of αSMA, g) Col1A1, h) and Col3A1 in OASFs that were stimulated

*with TGFβ (10 ng/mL) and treated with RAPA (1 μg/mL) for 48 h. One-way ANOVA and Tukey's multiple comparisons test were run. Statistical significance is designated as: *P < 0.05 **P < 0.01, ***P < 0.001.*

However, the previously reported aggregates needed an outside source of cations to retain the aggregated state and control the drug release. In our study, however, ZnALs were shown to be irreversible and exhibited a prolonged release even without the addition of Zn^{2+} in the release medium. These results suggest that ZnALs could potentially decrease the need for frequent intraarticular administration, which was previously connected with an increased risk of infections [41]. RAPA did not induce any toxicity in human OASFs after 48 h incubation with the drug in the range of 5 ng/mL up to 10 μg/mL, as reported in **Figure 10b-e)**. Next, the cells were stimulated with transforming growth factor-beta (TGFβ), a key mediator of synovial fibrosis in OA, to induce disease-like fibrotic response [15,129,130]. **Figure 10f)** and **g)** show that 1 μg/mL RAPA was able to decrease the gene expression of key profibrotic markers, in the OASFs, namely αSMA and Col1A1. Previous studies reported that RAPA can decrease inflammation and chondrocyte senescence in the synovial joints [32,34,169]. Our results add to this by showing that RAPA dampens fibrotic signaling in human OASFs *in vitro*. Furthermore, the toxicity of Zn^{2+} and RAPA in ZnALs was tested to find the dose for gene expression experiments. ZnALs were purified with dialysis prior to testing and the final Zn^{2+} concentration was measured with ICP-MS. RAPA content in purified ZnALs with 0.5 mM Zn^{2+} was 100 ng/mL and the ratio between the two was kept constant for higher doses (**Table S1**). No significant toxicity was observed at 0.5 mM of Zn^{2+}, while 5 mM induced cell death (**Figure 11**).

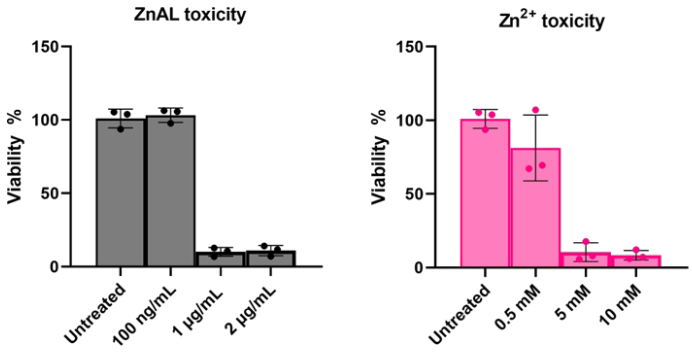

*Figure 11: a) Toxicity of purified ZnALs with RAPA doses 100 ng/mL, 1 µg/mL, and 2 µg/mL. b) Toxicity of free zinc in concentrations that are present in purified ZnALs at above RAPA doses (**Table S1**).*

The same zinc concentration is present in purified ZnALs with 1 µg/mL RAPA content (**Table S1**), where a similar toxic effect was observed. For these reasons, purified ZnALs with 100 ng/mL dose of RAPA were used for further cell experiments. The gene expression data in **Figure 12a)-c)** show that 100 ng/mL RAPA did not decrease fibrotic markers as effectively as 1 µg/mL. This calls for further research to find a more potent drug or a less toxic aggregating agent.

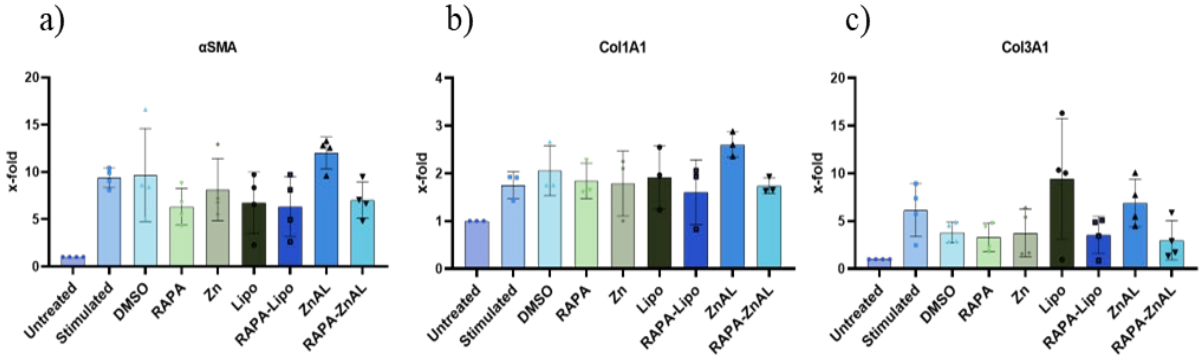

Figure 12: Gene expression of a) αSMA, b) Col1A1, n) and Col3A1 in OASFs that were stimulated with TGFβ (10 ng/mL) and treated with specified conditions for 48 h.

2.3.4 Lubrication of cartilage

Lubrication properties of the system were analysed with colloidal probe lateral force microscopy (CP-LFM) on silicon surface and a UMT-2 macro-tribometer with self-mated *ex vivo* porcine cartilage. The silicon used as a substrate for CP-LFM measurement was thoroughly cleaned to ensure a negative surface charge, in order to mimic the chemistry of the cartilage surface. **Figure 13a)** shows the change in friction force as the applied normal force is increased for the silicon surfaces treated with different conditions, as previously described [134]. The measured friction coefficient (COF) values obtained from the slope of the curve, drastically decreased when the surface was treated with liposomes and purified ZnALs (0.017) in comparison to PBS (0.279). It is generally accepted that the superior lubrication of liposomes stems from the formation of a hydration shell around the dipole of phospholipids, which can support high compressive loads and is very fluid [136,170]. A similar mechanism is expected here after the treatment with ZnALs, whose mean COF is lower compared to the liposomes', which is 0.028. While hydration is also anticipated in the case of Zn^{2+} treatment, the results demonstrate a significant increase in friction (0.421). The plot of normal force versus friction force ***Figure 13*****a)** for silica sliding against silicon submerged in a Zn^{2+} solution does not pass through zero, indicating a substantial adhesive component. This can be attributed to the positively charged Zn^{2+} surface interacting with the negatively charged silica countersurface. This observation suggests that the hydration shell formed around the zinc ions is not sufficient to counterbalance the adhesive forces between the probe and the Zn^{2+}-coated silica surface, increasing the COF.

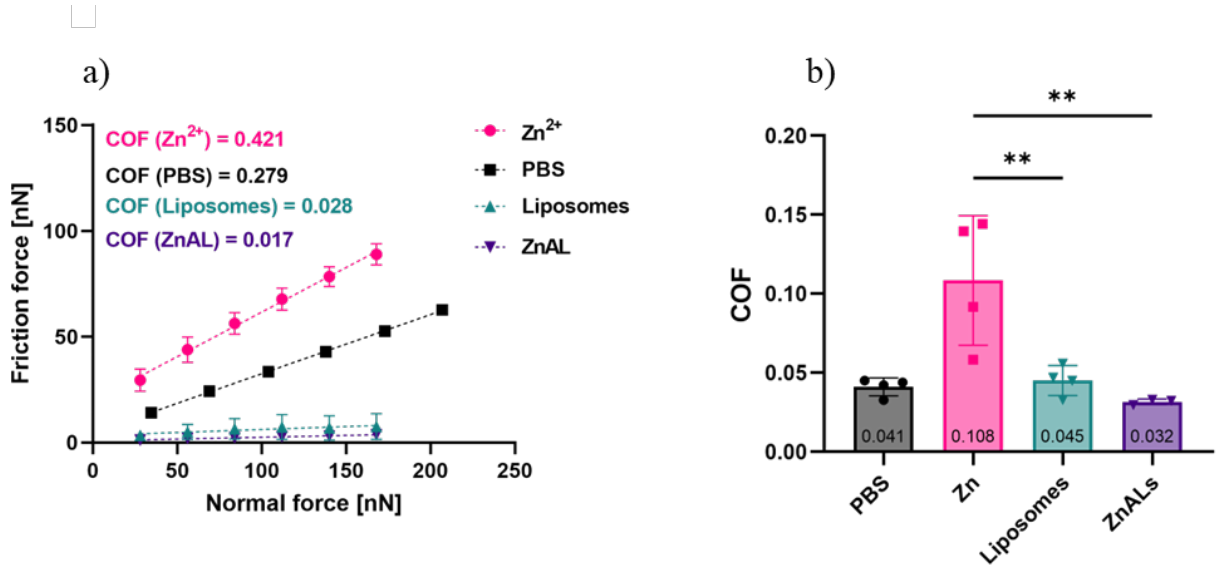

*Figure 13: a) Friction as measured with CP-LFM on silica surface. b) Friction as measured with UMT on ex vivo porcine cartilage. ZnALs were purified before testing as described above. One-way ANOVA with Tukey's multiple comparisons test was run. Statistical significance is designated as: *P < 0.05 **P < 0.01, ***P < 0.001, ****P < 0.0001. In all tests, liposomes and ZnAL had a total lipid concentration of 5 mM, while 23 mM was the final Zn^{2+} concentration in ZnALs after dialysis and in Zn^{2+} condition.*

A similar trend can be observed **Figure 13b)**, where the COF was measured on *ex vivo* cartilage with a macro-tribometer. The presence of zinc drastically increased the friction on the cartilage to a COF of 0.108 compared to the PBS of 0.041. Zn^{2+} is classed as strongly kosmotropic and may be influencing the aggregation of proteins and their hydration within the cartilage. As the mechanical and tribological behaviour of cartilage is strongly dependant on hydration, a change is expected to have an influence on the friction properties. Ionic kosmotropes tend to reduce the diffusion of water and separate into more dense water. This increase by the metal cations was negated by the electrostatic adsorption on the negatively charged liposomes and the formation of ZnALs, which significantly decreased the COF to 0.032. It is proposed that the liposomes hold the Zn^{2+} at the surface, thus reducing its influence on the bulk cartilage and forming a protective coating on the surface. The mean COF of the free liposomes was measured at 0.045. To our knowledge, this is the first tribological study of liposomal aggregates. Taken together, the formation of aggregates improved the friction on nano-tribological scale and protected cartilage on macro-tribological scale, which indicates the potential of

the formulation for the treatment of damaged cartilage in OA. More research is needed to confirm the observed responses under physiological conditions and determine the influence of liposomes and ZnALs on wear.

2.4 Conclusion

In the present report, we show that the aggregation of negatively charged liposomes with 150 mM Zn^{2+} yields irreversible aggregates (ZnALs) with a diameter above 90 µm, which was reported to drastically increase retention in synovial joints. We characterised the aggregation properties in depth and showed that ZnALs can sustain the release of RAPA, which decreases fibrotic markers in human OASFs. While necessary for the aggregation and the controlled release, Zn^{2+}'s toxicity limits the therapeutic window of ZnALs. Aggregate formation prevents the increase of friction due to the presence of Zn^{2+} *ex vivo*, significantly decreasing the friction coefficient (COF) to 0.032, below the PBS control. The same effect was observed in a nanotribological setting, where ZnALs lowered the COF compared with free zinc and outperformed PBS. In summary, ZnALs are a drug delivery system that can sustain the release of RAPA longer than free liposomes, with 86 % of the drug released at 7-day mark. Future research should focus on improvements in the toxicity profile of the aggregated liposomes by finding new aggregating agents and thus improving the therapeutic effect of the formulation.

2.5 Acknowledgments

This work was supported by The Open Round grant by the Faculty of Science of the University of Bern. The authors thank the Center for Microscopy and Image Analysis at the University of Zurich for maintaining the imaging equipment and Dr. Elena Pachera for her support in acquiring images, as well as Peter Künzler and Benvinda Henriques Campos for their valuable support in the cell culture laboratories. Aggregation kinetics and aggregates' size were measured and analysed with the support of Anton Paar TriTec SA in Neuchâtel. Fresh preparation of liposomes for cell experiments was possible thanks to the hospitality of Prof. Jean-Christoph Leroux and his team at ETH Zürich. The authors are grateful to Nicola Lüdi at Department of Chemistry, Biochemistry and Pharmaceutical Sciences of University of Bern for his support with ICP-MS

measurements. The authors would also like to thank the workshop of Department of Chemistry, Biochemistry and Pharmaceutical Sciences of the University of Bern for making the dialysis devices for *in vitro* drug release experiments. Frank Steiniger of the University of Jena, Germany, is warmly acknowledged for his support with the cryo-TEM image acquisition and analysis of RAPA-loaded liposomes.

Chapter 3.

Anti-fibrotic peptide dendrimers aggregate liposomes enhancing cartilage lubrication and retention

This chapter is to be submitted for publication.

Gregor Bordon[a], Kapila Gunaskera[a], Hyppolite Personne[a], Adrian Madarasz[b], Andrea Arcifa[c], Oliver Distler[d], Steven T. Proulx[b], Rowena Crockett[c], Jean-Louis Reymond[a], Paola Luciani[a,*]

[a] Department of Chemistry, Biochemistry and Pharmaceutical Sciences, University of Bern, Freiestrasse 3, 3012 Bern, Switzerland

[b] Theodor Kocher Institute, University of Bern, Freiestrasse 1, 3012 Bern, Switzerland

[c] Laboratory for Surface Science and Coating Technologies, EMPA, Uberlandstrasse 129, 8600 Dubendorf, Switzerland

[d] Center of Experimental Rheumatology, Department of Rheumatology, University Hospital Zurich, University of Zurich, Wagistrasse 14, 8952 Schlieren, Switzerland

* Corresponding author; email: paola.luciani@unibe.ch; office number: +41 (0)31 684 41 60

Author's contribution

GB: Conceptualization; Funding acquisition, Investigation; Validation and Visualization; Formal analysis; Data curation; Writing of the original draft. KG: Methodology; Investigation. HP: Methodology; Investigation; AM: Methodology; AA: Methodology. OD: Funding acquisition; Supervision. STP: Supervision; Methodology. RC: Funding acquisition; Supervision. JLR: Funding acquisition; Supervision. PL: Conceptualization; Supervision; Project administration; Funding acquisition.

3.1 Introduction

Osteoarthritis (OA) is a persistent joint condition affecting over 500 million people worldwide, which in 2019 cost the healthcare systems $460 billion globally [1,6]. The pathogenesis of OA involves mechanical, inflammatory, fibrotic, and metabolic factors that ultimately culminate in joint failure [14,15]. As the disease progresses, alterations in cartilage composition can cause erosion, leading to heightened susceptibility to mechanical disruption and the formation of cartilage wear particles [11,14]. These particles contribute to the activation of synovial macrophages and synovial fibroblasts, which drive synovial fibrosis, joint stiffness, and chronic pain in OA patients [15–17]. The presence of wear particles is also closely linked to increased roughness of the cartilage surface, resulting in elevated friction and further cartilage degradation [18]. Current management strategies for OA include lifestyle changes, small-molecule pain medication, large-molecule viscosupplementation, cell therapy, and surgical procedures [24]. However, these treatments are insufficient in reversing the disease progression, and the development of disease-modifying OA drugs (DMOADs) has emerged as a promising strategy. The potential side effects associated with long-term systemic administration of DMOADs may undermine their therapeutic benefits, leading to an increased interest in intra-articular (IA) administration of lipid-based drug delivery systems (DDSs) [39,40]. This approach reduces systemic exposure, minimizes side effects, and increases local bioavailability. Combining cartilage lubrication with drug delivery has shown promise in treating OA, as DDSs can improve drug retention, provide on-demand drug release, and reduce cartilage wear and tear [21].

Liposomes have shown promise in clinical settings for improving corticosteroid therapy in OA treatment [58]. However, they possess some limitations that need to be addressed. One of the main concerns is their small size, which may lead to their rapid removal from the joint space, thereby reducing their therapeutic efficacy [43,49,50]. The small particle size of below 300 nm has been associated with rapid clearance from the joint, necessitating frequent administration of the formulation and increasing the risk of inducing infection. This rapid clearance is partly due to phagocytosis by macrophages, which engulf and eliminate smaller particles more efficiently. In contrast, particles above 10 μm can avoid phagocytosis and be retained in both naïve and inflamed joints for over six weeks [49,50]. Moreover, although small unilamellar liposomes exhibit excellent lubricating

properties *in vitro* [134,137], *ex vivo* studies on cartilage have revealed a lack of lubricating effect [69,139]. The superior lubrication by liposomes *in vitro* is linked to the hydration property of phospholipids that form a hydration shell, which is resistant to pressure and effectively reduces friction [137]. However, this discrepancy in *ex vivo* studies could be attributed to the penetration of liposomes into the porous cartilage structure, which results in poor retention on the surface necessary for providing an efficient lubrication [139].

Our group previously reported the development of calcium aggregated liposomes (ALs) that have the ability to sustain drug release by increasing the barrier for drug diffusion through layering multiple phospholipid membranes aggregated together [141,142]. Building on this system, we formed irreversible aggregates of nearly 100 μm in diameter by using zinc as the aggregating agent [69], which has been reported to possess anti-inflammatory activity [143–145]. The data showed a prolonged release of a potential DMAOD, rapamycin, beyond that of plain liposomes. These ALs were efficient in significantly reducing friction *in vitro*, and *ex vivo* they protected cartilage from increased friction caused by the aggregating agent. However, the study on human OA synovial fibroblasts (OASFs) demonstrated significant toxicity of the aggregating agent, limiting the system's ability to deliver the drug in a therapeutic dose [69]. To enable the use of this system for OA management, finding an alternative aggregating agent that is charged, enabling aggregation, non-toxic to human synovial cells, and potentially possessing added anti-inflammatory and/or anti-fibrotic activity is crucial for further development and optimization.

Dendrimers are branched core-shell structures with a precisely defined number of focal points between the core and the shell, determining their generation (G1, G2, G3, etc.). By displaying cationic lysine amino acids as terminal groups of the branches, dendrimers are positively charged. This characteristic, along with the known biocompatibility of peptide dendrimers, makes them ideal candidates for the preparation of ALs [171,172]. Our recent study reported the development of anti-inflammatory peptides with G3 dendrimer architecture through solid-phase peptide synthesis. The dendrimers displayed no toxicity *in vitro* and exerted an anti-inflammatory effect on monocytes [173]. In the present report, we evaluated the ability of two best performing dendrimers (DendriXs) to aggregate anionic liposomes and their potential to repress fibrotic markers in OASFs. Subsequently, we tested the toxicity of the DendriXs and dendrimer-aggregated liposomes (DendriXALs) *in*

vitro and characterized the system using cryogenic transmission electron microscopy (cryoTEM) and fluorescence microscopy. Our findings demonstrate for the first time that the dendrimer-liposome complexes are capable of significantly suppressing friction on a macro-tribological scale in *ex vivo* porcine cartilage and improving particle retention on the cartilage surface. These results indicate that DendriXALs have the potential to be a platform for the intra-articular delivery of drugs for OA treatment. Further studies are needed to evaluate their therapeutic efficacy in preclinical models of OA. With a synergistic combination of anti-inflammatory and anti-fibrotic properties, as well as enhanced cartilage retention, we envision that DendriXALs can significantly improve the management of OA and reduce the burden of this debilitating disease.

3.2 Materials and methods

3.2.1 Materials

The phospholipids 1,2-dipalmitoyl-*sn*-glycero-3-phosphocholine (DPPC) and 1,2-distearoyl-sn-glycero-3-phospho-(10-rac-glycerol) sodium salt (DSPG) were kindly given by Lipoid (Ludwigshafen, Germany). A HEPES solution (1 M) was obtained from Carl Roth® (Karlsruhe, Germany). 1,1'-Dioctadecyl-3,3,3',3'-tetramethylindodicarbocyanine, 4-chlorobenzenesulfonate salt (DiD, catalog number: D7757) was obtained from Thermo Fisher Scientific™ (Waltham, MA, USA). DMF (N,N-dimethylformamide) was purchased from Thommen-Furler AG (Switzerland), Oxyma Pure (hydroxyiminocyanoacetic acid ethyl ester) from SENN AG (Switzerland), DIC (N,N'-diisopropyl carbodiimide) from Iris BIOTECH GMBH (Germany) and piperidine from Acros Organics (Thermo Fisher Scientific™, USA). DODT (2,2'-(Ethylenedioxy)diethanethiol) was obtained from Merck® (Germany), while triisopropylsilane and trifluoroacetic acid were purchased from Fluorochem Ltd (United Kingdom). All amino acids were supplied by Shanghai Space Peptides Pharmaceuticals Co., Ltd. Chemicals were used as supplied and solvents were of technical grade. Amino acids were used as the following derivatives: Fmoc-Lys(Boc)-OH, Fmoc-Lys(Fmoc)-OH, Fmoc-Glu(tBu)-OH, Fmoc-Gly-OH, Fmoc-Tyr(tBu)-OH, Fmoc-Cys(Trt)-OH. Rink Amide AM LL resin was purchased from Novabiochem® (Merck®, Germany). Ala-Wang resin was purchased from Iris BIOTECH GMBH. Porcine knee cartilage was procured from a regional abattoir located in Münchenbuchsee, Switzerland. Chloroform and methanol were purchased

from Fisher Scientific (Schwerte, Germany). Water with a resistivity of 18.2 MΩ.cm was generated using a Barnstead Smart2 pure system from Thermo Scientific™ (Pittsburgh, USA).

3.2.2 Dendrimer preparation

Dendri1 and Dendri4 (DendriXs) dendrimers were synthesized using standard 9-fluorenylmethoxycarbonyl (Fmoc) Solid Phase Peptide Synthesis at 60 °C under nitrogen bubbling as previously reported [173]. Branching points consisted of Fmoc-Lys(Fmoc)-OH to obtained two free amines after Fmoc deprotection (mainchain and sidechain).

Synthesis: 400 mg of resin (Rink amide, 0.29 mmol/g for Dendri1, and Ala-Wang, 0.32 mmol/g for Dendri4) was first swollen 10 min in DMF. Double deprotections of Fmoc groups were performed using a solution of 20% v/v piperidine in DMF. during one and four minutes. Resin was washed five times (5 x 8 mL of DMF) after deprotection. Double coupling (2 x 8min) for the two first generations G0 and G1, quadruple coupling (4 x 8 min) for second generation G2 and septuple coupling (7 x 8 min) for third generation G3 were performed using 3 mL amino acid (0.2 M), 2 mL of DIC (0.8 M) and 1.5 mL Oxyma (0.8 M) in DMF for each coupling. Resin was washed twice with 8 mL of DMF between couplings and three times after the last one. All Fmoc deprotections were performed as described above. After last Fmoc deprotection, resin was washed three times with DMF and three times with MeOH at room temperature.

Cleavage: Peptide was then cleaved from the resin using a 7 mL mixture of TFA/TIS/DODT/H2O (94/2.5/2.5/1, v/v/v/v) for Dendri1 and TFA/TIS/H2O (94/5/1, v/v/v) for Dendri4. Peptide solutions were then precipitated with 25 mL cold terbutylmethyl ether, centrifuged for 10 minutes at 3500 rpm, evaporated and dried with argon before purification.

Purification: The dried crudes were dissolved in a water/MeCN mixture, filtered (pore size 0.22 µm) and purified by preparative RP-HPLC with gradient of 60 min from 100% solvent A to 100% solvent D described above. Collected fractions were analysed by analytical LC-MS. Peptides were obtained as foamy white solids after lyophilization. Yields were calculated for the TFA salts

Quantification of dendrimers: Analytical RP-HPLC was performed with an Ultimate 3000 Rapid Separation LC-MS System (DAD-3000RS diode array detector) using an Acclaim® RSLC 120 C18 column (2.2 µm, 120 Å, 3×50 mm, flow 1.2 mL/min) from Dionex. Data recording and processing was done with Dionex™ Chromeleon™ Management System Version 6.80 (analytical RP-HPLC). All RP-HPLC were using HPLC-grade acetonitrile and Milli-Q deionized water. The elution solutions were: A: MilliQ deionized water containing 0.05% TFA; D: MilliQ deionized water/acetonitrile (10:90, v/v) containing 0.05% TFA. Preparative RP-HPLC was performed with a Waters® automatic Prep LC Controller System containing the four following modules: Waters2489 UV/Vis detector, Waters2545 pump, Waters® Fraction Collector III and Waters® 2707 Autosampler. A Dr. Maisch® GmbH Reprospher® column (C18-DE, 100×30 mm, particle size 5 µm, pore size 100 Å, flow rate 40 mL/min) was used. Compounds were detected by UV absorption at 214 nm using a Waters® 248 Tunable Absorbance Detector. Data recording and processing was performed with Waters® ChromScope™ version 1.40 from Waters Corporation®. The elution solutions were: A MilliQ deionized water containing 0.1% TFA; D MilliQ deionized water/acetonitrile (10:90, v/v) containing 0.1% TFA. MS spectra, recorded on a Thermo Scientific™ LTQ OrbitrapXL™, were provided by the MS analytical service of the Department of Chemistry, Biochemistry and Pharmaceutical Sciences at the University of Bern (group PD Dr. Stefan Schürch).

3.2.3 Cell culture

Synovial fibroblasts (SFs) were obtained from four OA patients and plated onto 25 cm² flasks and 6-well clear Corning® plates (USA) or 96-well black plates with clear bottoms from Thermo Fisher Scientific™ (USA). The cells were maintained at 37 °C in a 5% CO2-enriched humid atmosphere using Dulbecco's modified Eagle's medium (DMEM) supplemented with 10% fetal calf serum (FCS), 50 U/mL penicillin/streptomycin, 2 mM L-glutamine, 10 mM HEPES, and 0.2% amphotericin B (all from Thermo Fisher Scientific™, USA) as per standard protocols [148]. Once confluent, the OASFs were utilized for experiments between passages 4 and 6. Meanwhile, mouse monocyte macrophages (RAW264.7), which are semiadherent, were grown in the incubator under the same conditions as OASFs. DMEM (4.5 g L^{-1} glucose and phenol red) was added with 1% v/v penicillin/streptomycin mixture, 1% v/v L-glutamine (200 nM), and added 10% v/v FCS, as previously reported

[174]. Once 70-80% confluence was achieved, the cells were harvested using a cell scraper and employed for additional subcultivation.

3.2.4 Toxicity of dendrimers

The OASFs were quantified using Countess™ 3 FL (Thermo Fisher Scientific™, USA) and trypan blue, and then seeded at a density of 5'000 cells per well onto a 96-well plate. After overnight incubation, the cells were subjected to 200 µL of various conditions and incubated for 48 h. Following the incubation, cell viability was determined using the Cell Counting Kit-8 (CCK-8) according to the manufacturer's (Merck®, Germany) instructions. Briefly, medium was aspirated, and the cells were washed with DPBS (Thermo Fisher Scientific™, USA) before being stained with 100 µL of 10x diluted CCK-8 in medium. Cells were incubated for 2 h at 37 °C and subsequently, the absorbance was measured at 450 nm using a plate reader (BioTek Instruments®, USA).

3.2.5 Gene expression

For gene expression studies, the cells were seeded as previously described for the toxicity experiments. To stimulate a fibrotic response, 10 ng/mL of TGFβ was added to the medium along with the test conditions. After 48 h incubation, the cells were lysed and RNA was extracted using the Quick-RNA™ Microprep Kit (Zymo Research®, USA) and on-column DNase I digestion according to the manufacturer's instructions. The purity and quantity of RNA were evaluated by measuring the OD ratio at 260 and 280 nm using Nanodrop (Thermo Fisher Scientific™). Subsequently, the RNA was reverse-transcribed, and SYBR®green real-time PCR was conducted (primers: αSMA Fwd: 5' GAC AAT GGC TCT GGG CTC TGT AA 3', Rev: 5'ATG CCA TGT TCT ATC GGG TAC TT 3'; Col1A1 Fwd: 5' CAG CCG CTT CAC CTA CAG C 3', Rev: 5' TTT TGT ATT CAA TCA CTG TCT TGC C 3'; Col3A1 Fwd: 5' GGA CCT CCT GGT GCT ATA GGT 3', Rev: 5' CGG GTC TAC CTG ATT CTC CAT 3'). Data were analyzed with the comparative CT methods and presented as $2^{-\Delta\Delta CT}$ (i.e., x-fold) as described previously [149] using RPLP0 as a housekeeping gene for sample normalization (Fwd: 5'-GCG TCC TCG TGG AAGTGA CAT CG 3', Rev: 5'-TCA GGG ATT GCC ACG CAG GG 3').

3.2.6 Liposome preparation and characterization

Liposomes containing 25 mol% DSPG and varying amounts of DPPC/cholesterol were produced using the thin-film hydration technique. The lipid stock solutions in a chloroform/MeOH mixture (75/25 v/v) were appropriately measured and dried under a mild nitrogen flow in a glass vial, followed by the removal of residual solvents through overnight incubation under vacuum in a desiccator. The lipids were hydrated with 20 mM HEPES buffer at pH 7.4, heated to 70 °C, and mixed to produce vesicles of 20 mM final lipid concentration. These vesicles were then subjected to six freeze-thaw cycles and extruded ten times via a 200 nm polycarbonate membrane (Sterlitech® Corporation, USA) using a LIPEX® extruder at 70 °C (Evonik®, Canada). The mean hydrodynamic diameter and polydispersity inDendriX (PDI) of the formed vesicles were determined via dynamic light scattering (DLS) analysis using a Litesizer 500 instrument (Anton Paar®, Austria) with a backscatter angle of 175° and a 658 nm laser at 25 °C. Furthermore, the zeta potential was measured using the same device and Omega cuvette (Anton Paar®, Austria) with laser Doppler microelectrophoresis.

3.2.7 Dendrimer-Aggregated Liposomes (DendriXAL) preparation and characterization

Aggregated liposomes (ALs) were generated by four-fold dilution of 0.4 mM liposomes with dendrimer solutions (DendriXs - Dendri1 and Dendri4) of varying concentrations in 20 mM HEPES followed by gentle stirring for 5 min. The resultant DendriXALs were evaluated using a plate reader, as per previous reports [141]. Briefly, 50 µL of liposomes, with an initial lipid concentration of 0.4 mM, were combined with 150 µL of differing concentrations of DendriXs in a 96-well microtiter plate with a clear and flat quartz bottom (Hellma® GmbH & Co. KG, Germany). The mixture was gently stirred for 5 min, and the optical density was assessed at 450 nm using an Infinite M Pro 200F-PlexNano microplate reader (Tecan®, Switzerland). Zeta potential of DendriXALs was measured in the same manner as for liposomes using the Litesizer® 500. For the aggregation process involving salts, DendriXs were combined with varying concentrations of NaCl, following which DendriXALs were prepared using the same method as previously mentioned, and subsequently, the optical density was measured as described earlier.

To investigate if the aggregation process induces a burst release of the encapsulated model drug, rapamycin was incorporated into the liposomes at a lipid-to-drug ratio of 30:1, following the previously described method [69]. The *in vitro* release profile was assessed over a seven-day period using a custom dialysis device and a solution of 10% ethanol in ultrapure water. This method, reported earlier [69], ensured the drug's stability and maintained sink conditions without affecting the liposome composition.

3.2.8 Microscopic imaging of liposomes and DendriXALs

To evaluate the morphology, liposomes and DendriXALs were imaged using fluorescence and cryogenic transmission electron microscopy (cryo-TEM). To prepare for fluorescence microscopy, lipid films were stained with 0.05 mol% of the non-exchangeable lipophilic dye DiD, and liposomes and DendriXALs were prepared following the same method described previously, while being shielded from light. Then, 20 µL of the formulations were placed on a slide and covered with a glass coverslip, and an inverted fluorescence microscope (Nikon Eclipse-Ti, Canada) was used to capture images through a Tx red filter. For cryo-TEM imaging, 6-8 µL of each sample was added onto a gold grid covered by a holey gold film (UltrAuFoil® 2/1, Quantifoil® Micro Tools GmbH, Jena, Germany). The excess liquid was blotted automatically between two strips of filter paper or only from the backside of the grid. Subsequently, the samples were rapidly plunge-frozen in liquid ethane (cooled to 180 °C) in a Cryobox™ (Carl Zeiss NTS® GmbH, Oberkochen, Germany). Excess ethane was removed with a piece of filter paper, and the samples were immediately transferred with a Gatan™ 626 cryo-transfer holder (Gatan®, Pleasanton, USA) into the pre-cooled Cryo-electron microscope (Philips CM 120, Eindhoven, Netherlands) operating at 120 kV under low-dose conditions. The images were recorded with a 2k CMOS Camera (F216, TVIPS, Gauting, Germany), with four images being recorded and averaged into one image to minimize noise.

3.2.9 Uptake of Dendri4ALs and liposomes

RAW264.7 cells (2.4 million) were initially cultured in T25 flasks and left to incubate overnight. On the following day, the cell medium was removed, and the cells were washed with PBS. They were then incubated for 3 h with freshly prepared and fluorescently labelled DiD-liposomes, serving as a positive control, and with

DiD-Dendri4ALs. As a negative control, DMEM was used. The samples were prepared in a phenol red-free medium with reduced FCS content (2 v/v%), following a previously reported protocol [29]. After incubation, the cells were washed twice with PBS and collected using a cell scraper. Subsequently, the cells were centrifuged for 3 min at 500 g and resuspended in 150 µL buffer at 4 °C containing 0.02% EDTA, 2% v/vFCS, 1% v/v L-glutamine (200 nM), and 1 mM pyruvate. The resuspended cells were stored on ice until analysis.

An imaging flow cytometer (ImageStream® X Mark II, Cytek Biosciences®, USA) was used for analysis. Initially, the cell suspension was filtered to remove aggregates, followed by the addition of 100 ng/mL propidium iodide (PI, BioLegend®, USA) to label dead cells, and 5 µg/mL Hoechst reagent (Thermofisher Scientific™, USA) to label all cells. This mixture was then incubated for 3 min at 37 °C. Following this, the suspension was analysed using the flow cytometer, with a minimum of 5000 cells being measured for each sample. Subsequent gating was applied to select single, focused, and live cells, with the procedure ensuring that the count of live cells remained above 500 for all samples. The detailed gating strategy is provided in the Appendix (**Figure S5**). Analysis and generation of histograms and statistics of DiD intensity were conducted using IDEAS® 6.3 software (Amnis Corporation®, USA). The fluorescence intensity of cells was normalized to the count. The signal from DMEM-treated cells was subtracted from both the liposome and Dendri4AL samples, and the Dendri4AL sample was further normalized to its respective liposome positive control.

3.2.10 Cartilage retention

Procine cartilage explants were cut in 0.5x0.5 cm pieces, washed with PBS and placed in 12-well microtiter plates. Next, the samples were submerged in 1.5 mL 20 mM HEPES, Dendri1AL (50 µg/mL Dendri1), Dendri4AL (50 µg/mL Dendri4), and liposome solutions containing equivalent concentrations as in DendriXALs. All liposomal preparations were labelled with 0.05 mol% lipophilic DiD dye. Following a 24-h incubation at 37 °C, the samples were washed with 1.5 mL of PBS. Fluorescent stereo microscope imaging (Zeiss AxioZoom® V16, Germany) was performed, and images were captured at 10X and 50X magnification with GFP and Cy5 filters. Fluorescence intensities were analyzed using Zeiss's ZEN 2.5 software, focusing on a consistent area of interest on the cartilage surface.

3.2.11 Tribology

The UMT-2 tribometer (Bruker®, USA) was utilized to investigate the friction behavior of self-mated cartilage in the presence of measured samples, operating in linear reciprocating mode. The counterparts comprised two sections of porcine cartilage that were bonded to the upper and lower parts of the tribometer shortly before testing. During each experiment, the upper specimen (10x10 mm) was subjected to a 1 N load against the lower specimen (30x15 mm) and moved over a 2 mm stroke length at a frequency of 1 Hz for 10 minutes. The pair was fully immersed in the lubricant throughout the duration of the test. All tests were performed at a constant temperature of 20 °C and a data acquisition frequency of 500 Hz. The representative coefficient of friction (COF) of each test was determined from the raw data of lateral and normal force as the average of each friction loop, considering only the central 90% portion of each friction loop to avoid transients associated with the two ends of the stroke length. Additionally, the first 20% of the loops were disregarded to account for the steady-state friction behavior of the self-mated contact, thus eliminating possible running-in transients.

3.2.12 Statistical analysis

All experiments were conducted with a minimum of three replicates, except where noted otherwise. The presented values represent the mean ± standard deviation. General calculations were performed using Microsoft Excel, while GraphPad Prism 9.5 was utilized for generating graphs, executing one-way ANOVA, and conducting Tukey's test for multiple comparisons and unpaired t-test for single comparisons.

3.3 Results & Discussion

Intra-articular (IA) administration of corticosteroids and disease-modifying anti-OA drugs (DMAODs) has recently emerged as a promising avenue for OA treatment, as it delivers therapeutics directly to the affected site while minimizing systemic side effects [39]. Nevertheless, the efficacy of this treatment strategy is strongly influenced by the rapid clearance of drugs from the joint, necessitating frequent IA injections and increasing the risk of opportunistic infections [41]. Liposomes have been extensively investigated for their potential to prolong drug residence time in the joint, and have even been successfully employed in clinical settings for IA delivery

of dexamethasone [58]. Here, we produced anionic liposomes, which have been previously reported and characterized by our group, with an average diameter of 145 nm, a polydispersity index (PDI) below 0.2, and a negative zeta potential of -57 mV [69]. In addition to facilitating sustained drug release, liposomes have been demonstrated to significantly reduce friction *in vitro* by forming a hydration layer around phospholipid molecules, potentially leading to decreased cartilage wear [69,175]. However, research indicates that nanoparticles of this size exhibit insufficient retention on the cartilage surface, resulting in suboptimal performance in more physiologically relevant models, such as *ex vivo* cartilage [139]. Consequently, we previously reported the development of liposomal aggregates using divalent zinc cations, which exhibit some anti-inflammatory activity. Although this system successfully sustained the release of rapamycin beyond that of plain liposomes, zinc induced significant toxicity in human OA synovial fibroblasts (OASFs), severely limiting the applicability of such a system. While the initial results were encouraging, the design of tailored aggregating agents is crucial for liposomal aggregates to possess therapeutic potential [69]. These alternative aggregating agents should exhibit multiple cationic centers at physiological pH, low toxicity, and potentially possess anti-inflammatory as well as anti-fibrotic properties.

3.3.1 Choice of the aggregating agent

We recently reported the development of peptide dendrimers exhibiting potent anti-inflammatory activity on monocytes and demonstrated no observable toxicity *in vitro* [173]. To evaluate whether these dendrimers could be employed in the preparation of dendrimer-aggregated liposomes (DendriXALs), we selected the two best-performing peptides, Dendri1 and Dendri4 (DendriXs), and conducted an aggregation study by measuring changes in optical density and zeta potential at different charge ratios. To calculate these charge ratios, we first determined the liposomal surface area based on the average diameter, and then estimated the number of phospholipid headgroups on the surface by utilizing the average surface area of DPPC molecules and weighing it by the proportion of DSPG molecules in the formulation (i.e. 25 mol%). Although the number of positive charges on Dendri1 and Dendri4 molecules differs, with 12 for the former and 17 for the latter, the aggregation profiles depicted in **Figure 14** are similar. A sharp increase in optical density is observed at a charge ratio of 1, which correlates well with the zeta potential crossing the x-axis. This correlation has also been observed with

divalent cations in previous studies [69,141]. The observed behavior can be readily explained by the diminishing repulsive forces between colloidal particles as the negative charges on anionic liposomes are neutralized by the increasing presence of positively charged dendrimers, until the overall charge reaches zero and the system becomes unstable. The subsequent decline in optical density following the aggregation peak is likely due to the increasing charge leading to the formation of water-soluble "dendriosomes," a phenomenon previously observed in the case of poly(amidoamine) (PAMAM) dendrimers and anionic liposomes [176,177]. Aggregation in the presence of salt is presented in **Figure S6**, where the results indicate that the most pronounced aggregation occurs at physiological concentrations of NaCl. Conversely, elevated salt concentrations beyond 150 mM NaCl resulted in diminished aggregation, which is consistent with previous reports [178].

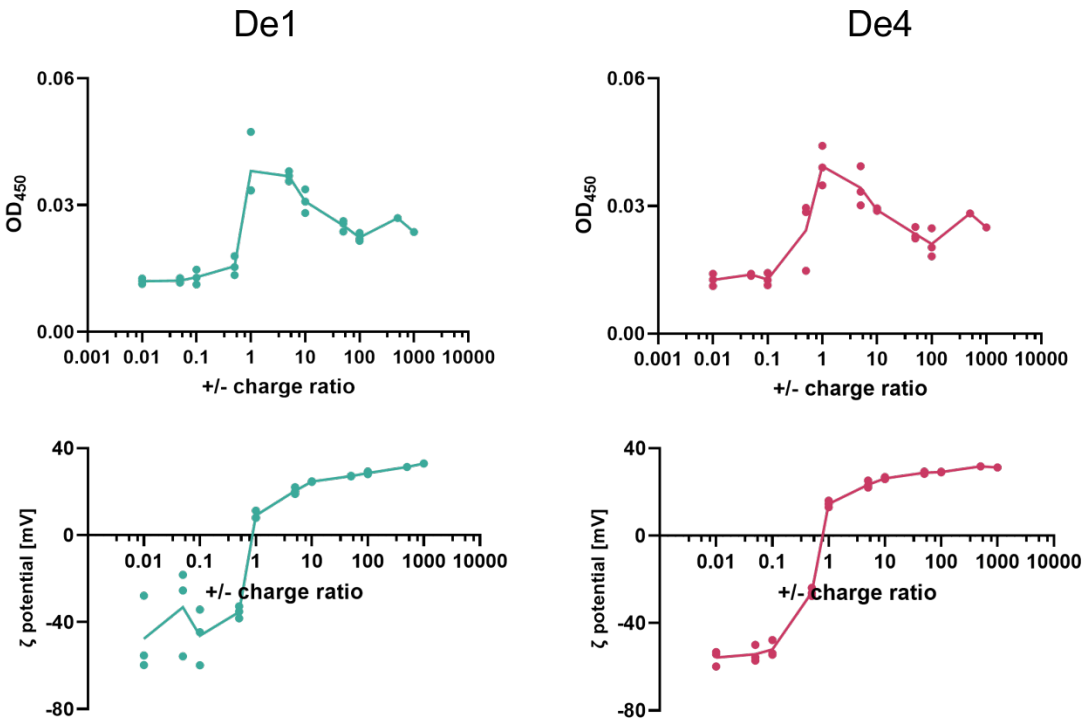

Figure 14: Aggregation profile of DendriXALs with changes of optical density at λ = 450 nm and changes in zeta potential in dependence of the charge ratio (+ from DendriXs and - from DSPG molecules on liposomes). Each data point on the graph represents the measurement of one replicate, while the connecting line represents the mean value of each replicate. Each measurement was performed with 3 replicates, while the charge ratios at 500 and 1000 were performed with 1.

Subsequently, the DendriXs were evaluated in an *in vitro* fibrosis model using human OASFs. The results depicted in **Figure 15** reveal that both DendriXs significantly reduced the expression of the gene for alpha smooth muscle actin (αSMA), while the decrease of collagen type I (Col1A1) expression was significant only for Dendri4. While these findings were encouraging, the past concerns over toxicity from the study with zinc-aggregated liposomes [69] made evaluating this facet of the of DenriXs and DendriXALs crucial. Thus, OASFs were incubated with both DendriXs and DendriXALs, containing 50 µg/mL of DendriXs and corresponding concentrations of liposomes, for 48 h. Subsequently, cell viability was assessed using the CCK8 kit.

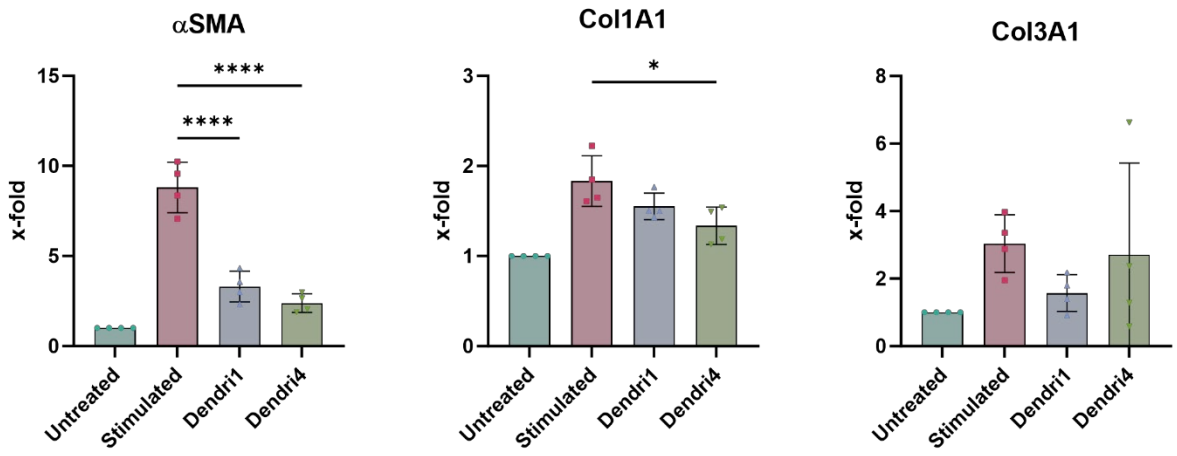

*Figure 15: Expression of pro-fibrotic genes a) αSMA, b) Col1A1, and c) Col3A1 on OASFs that were stimulated with 10 ng/mL TGFβ and treated with DendriXs for 24 h. One-way ANOVA and Tukey's multiple comparisons test were run. Statistical significance is designated as: *p<0.05, **p<0.01, ***p<0.001, ****p<0.0001.*

Results on **Figure 16** show that no significant toxicity was induced in the tested conditions with the lowest viability observed in Dendri4AL containing 50 µg/mL Dendri4. Collectively, these findings highlight that DendriXs are effective aggregating agents capable of attenuating the expression of fibrotic markers in human OASFs, as well as the previously reported inflammatory response in monocytes, both of which are pertinent to the treatment of pathologies such as OA. Furthermore, the low toxicity of this system unlocks the previously constrained potential of aggregated liposomes for osteoarthritis treatment.

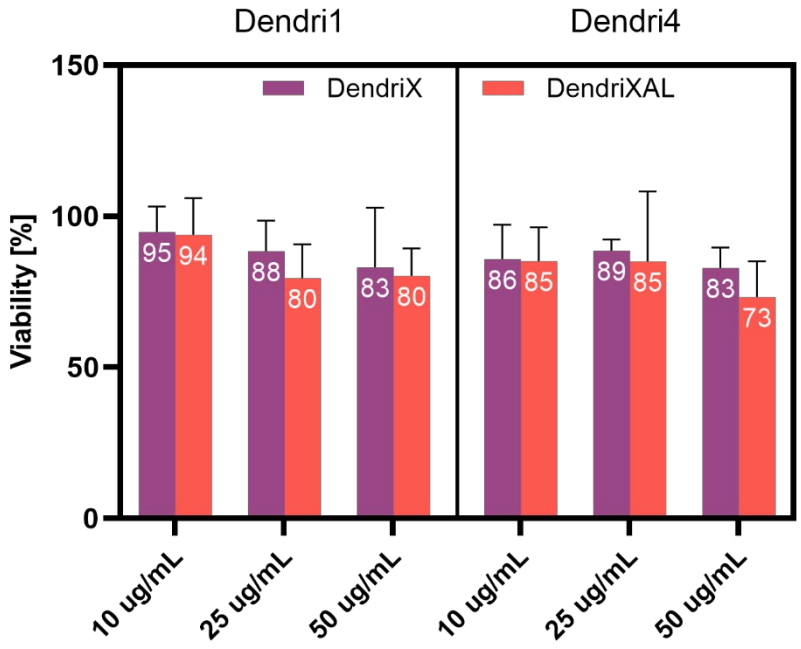

Figure 16: Toxicity of DendriXs and DendriXALs as measured with a CCK8 cell viability assay. The OASFs were in concentration of 5k cells per well in a 96-well plate. They were then treated with conditions of varying dendrimer concentrations for 48 h and the viabilities were normalized to the measured fluorescence signal of the condition treated with DMEM (100%).

3.3.2 Visualization of DendriXALs

Next, the aggregates were imaged with cryoTEM and representative images are displayed in **Figure 17**. The images display liposomes as mainly unilamellar and nanosized, consistent with DLS data. Upon addition of DendriXs into the system, clear aggregation is observed with membranes tightly packed together and bound by DendriXs. This is evident from the minimal distance between the occasionally curved membranes, which corresponds to the size of the DendriX, particularly noticeable in the Dendri1AL images. No discernable penetration of DendriXs into the liposomal core was observed, which might otherwise induce a burst release of the encapsulated cargo. It was indeed confirmed through an *in vitro* release study of rapamycin encapsulated in liposomes at a 30:1 lipid-to-drug molar ratio. **Figure S7** shows that there is no variation in the release between plain liposomes, Dendri1ALs, and Dendri4ALs. Dendrimers' interactions with phospholipid bilayers have been

thoroughly investigated, revealing that dendrimer generation plays a significant role and that higher generation dendrimers tend to perturb the membrane more extensively than their lower generation counterparts. Since both Dendri1 and Dendri4 are G3 dendrimers, their impact on the surface is limited, further corroborating the findings from the cryoTEM images and rapamycin release study.

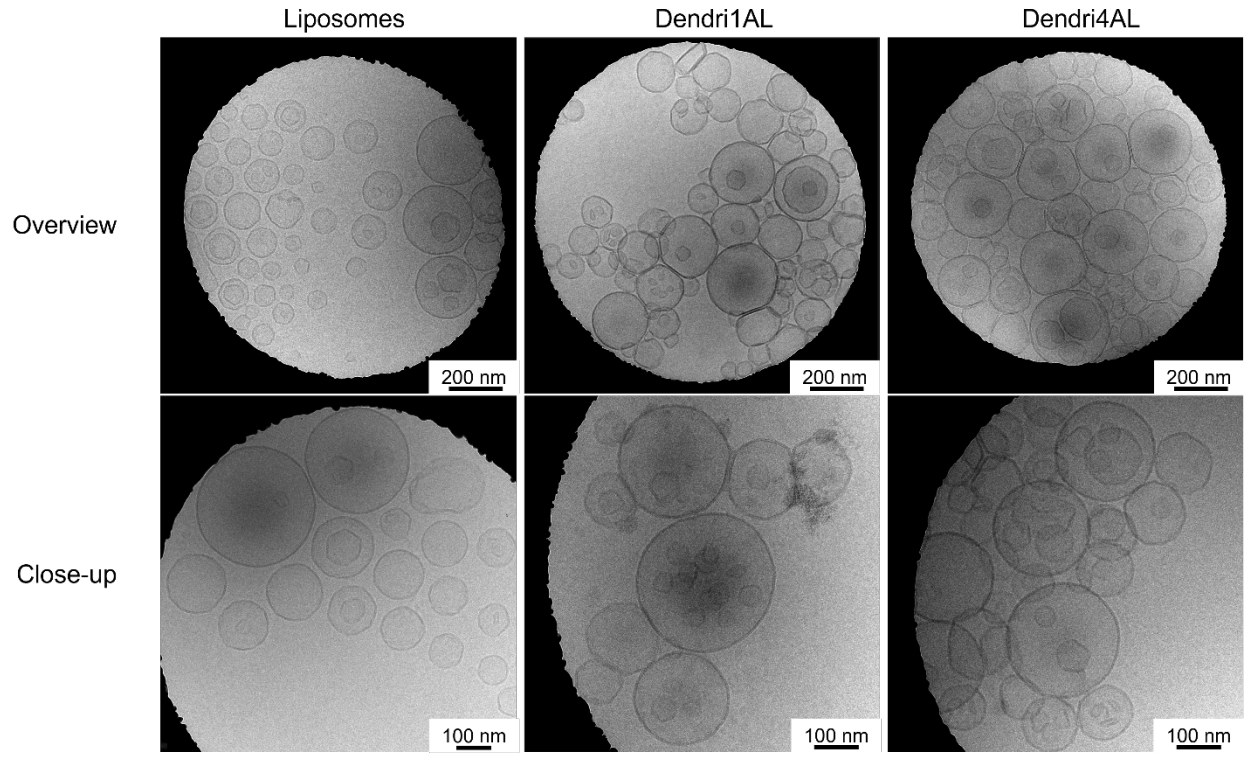

Figure 17: CryoTEM images of liposomes and DendriXALs. The total lipid concentration for all samples is 2 mM with adjusted DendriX concentration (152 µg/mL Dendri1 and 139 µg/mL Dendri4).

To further elucidate the system's morphology on a macroscopic level, DendriXALs were imaged using fluorescence microscopy. The images presented in **Figure 18** depict complex morphological features and micrometer-sized structures, reminiscent of those previously reported for zinc-aggregated liposomes [69]. This evidence suggests that while employing a different aggregating agent reduces toxicity and imparts both anti-fibrotic and anti-inflammatory properties to the drug delivery system, the overall structure of the dosage form remains largely unaltered. The absence of toxicity also eliminates the need for purification after aggregation,

which was necessary for the previous system. This simplification of the preparation process subsequently reduces the associated costs and complexity.

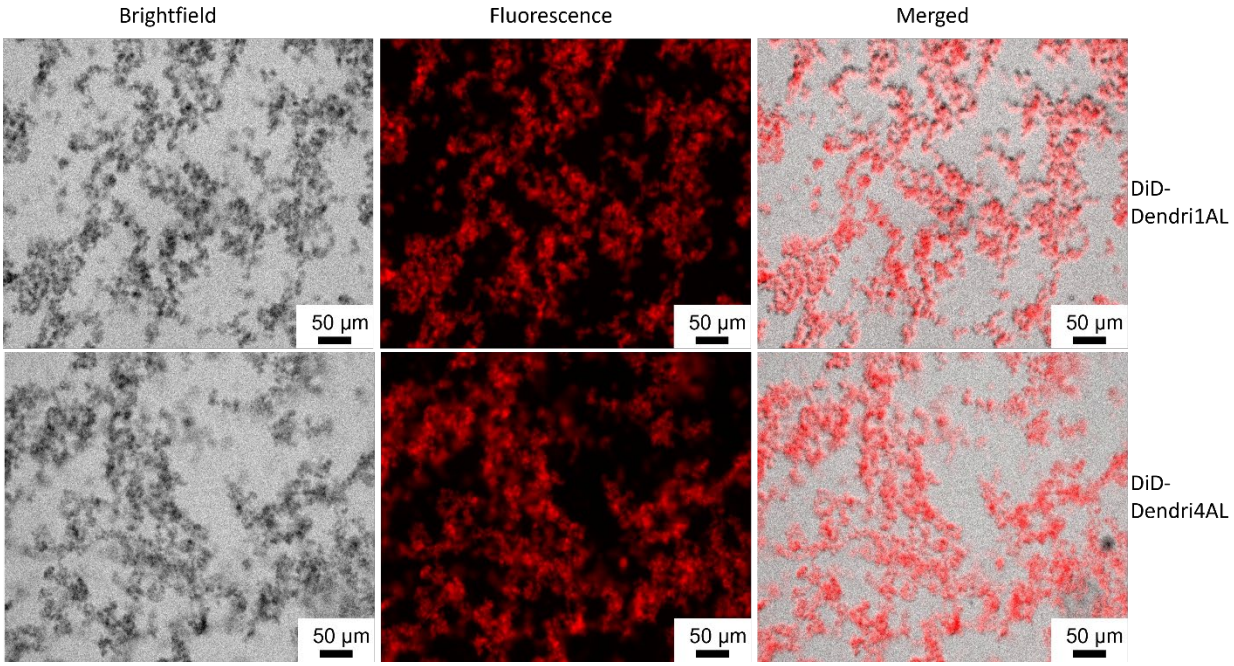

Figure 18: Morphology of DendriXALs on a macro-level. Liposomes were labelled with DiD fluorescent probe, aggregated with DendriXs, and imaged with a fluorescence microscope using Tx red filter and brightfield. The total lipid concentration was 5 mM and DendriX concentration was adjusted (381 µg/mL Dendri1 and 347 µg/mL Dendri4).

3.3.3 Cartilage lubrication

Synovial fibroblast activation, closely associated with pro-inflammatory and pro-fibrotic factors, is strongly correlated with the presence of cartilage wear particles generated during cartilage erosion [18,19]. This process is further exacerbated by the increased roughness of the cartilage surface in OA, resulting in higher friction and mechanical wear. Natural biolubricants, which prevent cartilage wear in healthy joints by providing effective lubrication, are diminished in OA, impairing synovial fluid lubrication and leading to increased friction and cartilage degradation [20–22]. While small liposomes initially demonstrated promise in reducing friction *in vitro*, their small size led to suboptimal performance compared to larger particles in *ex vivo* studies [139]. We reported

recently that liposomal aggregates could protect cartilage from friction induced by the aggregating agent and form a protective layer on *ex vivo* porcine cartilage. However, the coefficient of friction (COF) was not significantly reduced compared to that observed with liposomes. To determine whether DendriXALs are more efficient in reducing COF, we tested their macro-tribological effect on the same *ex vivo* porcine model, with results illustrated in **Figure 19**. The results indicate that Dendri1AL performed better (COF = 0.02) than plain liposomes (COF = 0.08) in reducing COF and successfully protected the cartilage from the negative impact of free Dendri1 (COF = 0.12) on the cartilage surface. Similar observations were made for Dendri4ALs, which reduced friction more effectively than all other controls. The increased friction in DendriXs is likely due to the strong electrostatic interaction between the highly cationic peptides and the negatively charged cartilage surface, which could damage the surface. Liposomes in the DendriXAL system sequester the cations and bind them tightly to the surface, preventing surface deformation. The mechanism of lubrication has been previously discussed by our and other groups, explaining the liposomal lubricating effect through the formation of a hydration shell at the phospholipid headgroup region, which is highly pressure-resistant and capable of reducing friction. In the case of DendriXAL, we hypothesize that the large particles observed in Figure 18 form an extensive protective layer on the cartilage surface, preventing excessive friction or wear on the tissue's surface. However, further research is needed to confirm these effects under more physiological conditions and demonstrate their efficacy in reducing wear in animal models.

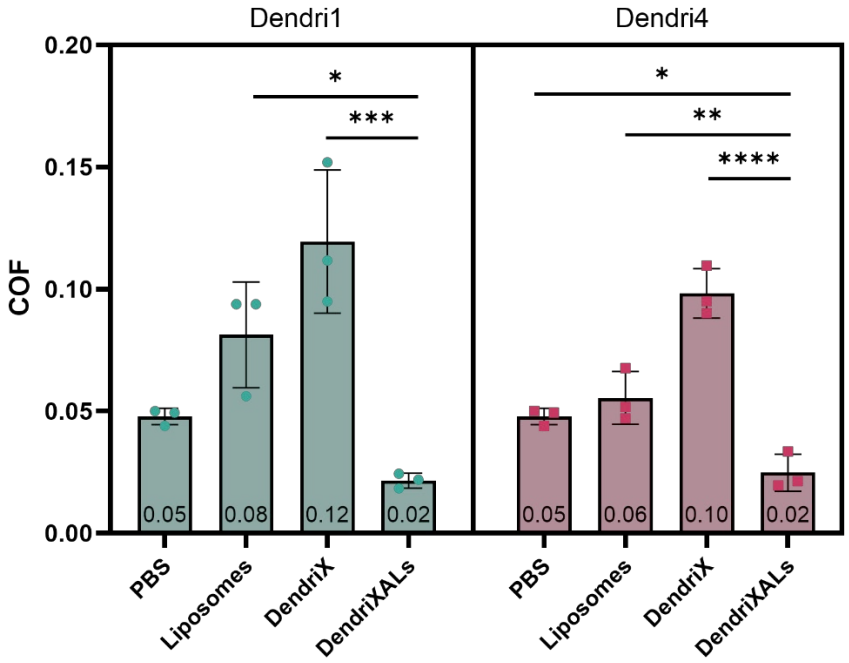

*Figure 19: Lubrication of ex vivo porcine cartilage with liposomes, DendriXs and DendriXALs. For all samples, DendriX content was kept constant at 50 µg/mL while the liposomal concentration was adjusted for Dendri4ALs (0.73 mM) and Dendri1ALs (0.66 mM). A One-way ANOVA with Tukey's multiple comparisons test was run. Statistical significance is designated as: *P < 0.05 **P < 0.01, ***P < 0.001, ****P < 0.0001. The mean COF values are specified within the bars for each condition.*

3.3.4 DendriXAL retention on cartilage

An important aspect of cartilage lubrication and protection from wear is the retention on the cartilage surface, as the material can only lubricate if it is present at the interface. Small nanosized particles are known to undergo quick clearance from the joint through the lymphatic drainage system and phagocytosis [49,50]. To increase the residence time in the joint, researchers developed cartilage targeting systems, which are often designed to penetrate the cartilage pores [39] and don't necessarily offer the lubricating effect, as they are not sufficiently retained at the surface [139]. To test whether the DendriXALs increase the retention on the cartilage surface, we cut porcine cartilage, placed it in 12-well plates, and incubated it for 24 h with buffer, DiD-labelled plain liposomes, and DendriXALs. A fluorescence stereomicroscope was used to image the retained samples and

measure the intensity. **Figure S8** and **Figure** S9 show the samples under 10X magnification, where the area of interest was selected at the center of the cartilage and was kept constant for all samples. **Figure 20a** reports the comparison of intensity measurements for liposomes and DendriXALs, while **Figure 20b** and **c** show the treated cartilage surface with Dendri1Al and Dendri4AL, respectively, under 50X magnification. While there was no difference between the retention of the plain liposomes and Dendri1ALs, significantly higher retention was observed in the case of Dendri4ALs. The observed increase in retention for Dendri4ALs can be attributed to the ~2 kDa greater molecular weight and increased number of positive charges of the Dendri4 dendrimer (9.4 kDa and 17 positive charges) relative to the Dendri1 dendrimer (7.4 kDa and 12 positive charges). This disparity in molecular weight and charge density may foster more robust interactions between the Dendri4ALs and the cartilage surface, ultimately leading to improved retention. This enhanced interaction could be the result of a heightened electrostatic attraction between the Dendri4 dendrimer and the anionic liposomes, as well as the negatively charged cartilage surface. Moreover, the larger size of the Dendri4 dendrimer could also play a role in the increased retention via steric effects, thereby promoting a more stable association with the cartilage surface. These results offer an explanation of the better performance of Dendri4ALs in the lubrication study in Figure 19, where the COF was reduced significantly compared to plain liposomes. However, the lack of increased retention of Dendri1ALs is interesting, as this system also reduced friction beyond free liposomes. The possible explanation for this result is that the increased retention on the surface is not the only mechanism for the lubrication of the system. Indeed, during the macro-tribological measurements, the cartilage was incubated with DendriXALs and was not exposed to any washing step, which kept the aggregates on the surface of the cartilage.

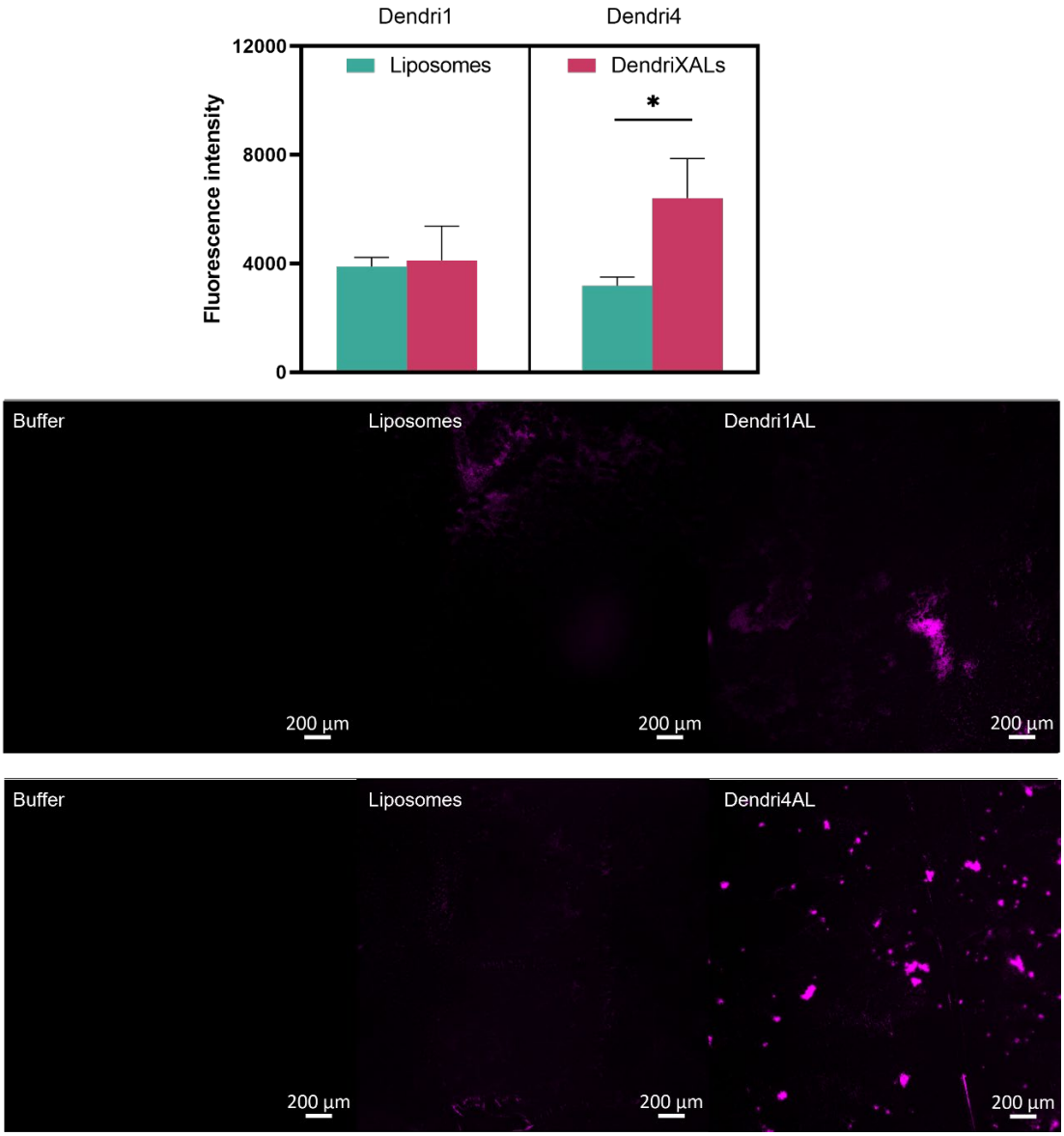

*Figure 20: Retention on cartilage surface. a) comparison of fluorescence intensities from the measured area of interest, which was kept constant among all samples. Each condition was tested in 3 replicates. For statistical analysis the two groups were compared with a t-test and statistical significance is designated as *p < 0.05. b) Representative images of Dendri1ALs, liposomes and buffer samples with 50X magnification. c) Representative images of Dendri4ALs, liposomes and buffer samples with 50X magnification. For all samples, DendriX content was kept constant at 50 µg/mL while the liposomal concentration was adjusted for Dendri4ALs (0.73 mM) and Dendri1ALs (0.66 mM).*

3.3.5 Cellular uptake of Dendri4ALs

Building on the key role of particle size and retention within the joint space, it is essential to address the cellular uptake by immune cells as a pivotal consideration in the formulation of a proficient drug delivery system. The rate of uptake by these immune cells can significantly dictate the therapeutic efficacy of the delivered drugs by impacting their clearance. In the context of liposomes, despite their documented effectiveness in amplifying drug retention within the joint space, their relatively small size often predisposes them to expedited clearance [179]. This rapid removal is mediated primarily by phagocytosis, a biological process which is especially responsive to the size of the vesicles [180,181]. Research suggests that particles larger than 10 µm can substantially evade immune cell uptake, thereby enhancing their retention in the target area [49,50,182]. However, particle size is only one side of the coin; the composition of these vesicles plays an equally significant role. Specifically, liposomes containing cationic lipids, though associated with toxicity challenges, exhibit a propensity to form a protein corona. This results in an increased attraction of surrounding proteins to their surface, enhancing the phagocytosis process and consequently, clearance from the joint space. Contrastingly, neutral nanoparticles are found to have a prolonged presence in plasma due to their reduced ability to adsorb proteins [181]. These aspects – size and composition – are therefore integral to the development of an optimal drug delivery system for OA therapy. Hence, by mindfully tailoring these parameters, we can potentially enhance the therapeutic effect and manage OA more effectively.

In order to evaluate this aspect, we chose Dendri4AL for testing uptake into RAW264.7 macrophages. This decision was based on its compelling performance in joint lubrication and its ability to improve cartilage retention. The DiD-labelled system was incubated with cells and compared with a negative DMEM control and a positive liposome control. After a 3-h treatment, the cells were harvested and analyzed using Image Stream®, a fluorescent imaging flow cytometer. The results depicted in **Figure 21** show a significant reduction in DiD intensity in live cells. These findings are likely associated with the presence of large macroscopic Dendri4AL structures — as shown in **Figure 18** — which may sterically hinder phagocytosis. The representative images in Figure 21c show that the uptaken particles are integrated within the cell cytoplasm and distributed around the nucleus. This subcellular distribution of liposomes aligns with findings reported by other research teams

[183,184]. The fact that Dendri4ALs are still phagocytosed by the macrophages, albeit to a lower extent, can be explained with the softness of the liposomal material, which was correlated with facilitated cellular uptake [185]. Moreover, to confirm these results, the validation should be run under more physiological conditions, as the protein corona formation and composition is dependent on the proteins present in the medium [180,181].

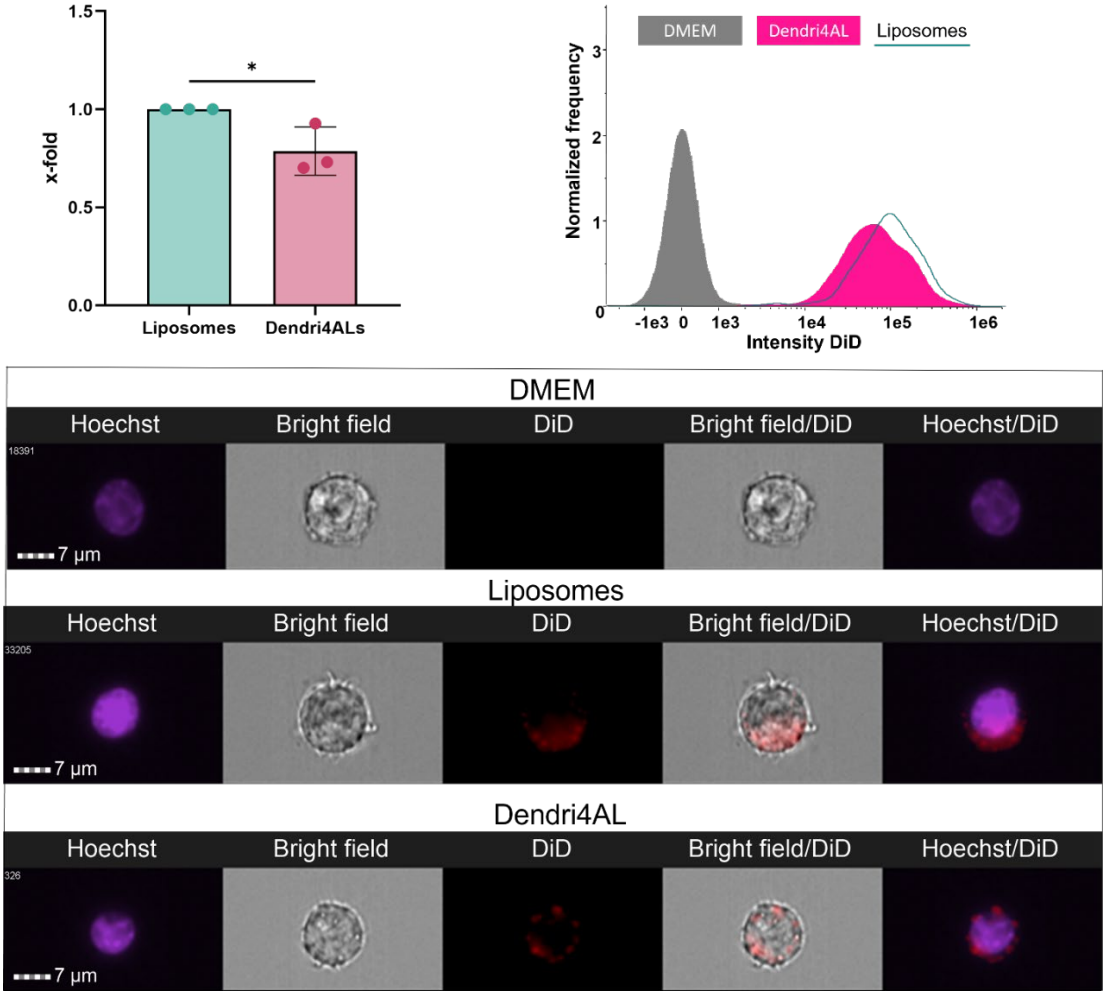

*Figure 21: Uptake of DiD labelled Dendri4ALs by macrophages after 3 h incubation. a) DiD intensity normalized to the cell count and the positive liposome control to account for the variability in the independently prepared DiD labelled liposomes. b) A representative histogram of the DiD intensity within live macrophages for DMEM negative control, liposome positive control and Dendri4AL. c) Images of representative cells, acquired with Image Stream fluorescent imaging flow cytometer. For statistical analysis the two groups were compared with the unpaired t-test and statistical significance is designated as *p < 0.05.*

3.4 Conclusion

Liposomal aggregates have emerged as promising platforms for drug delivery, exhibiting a synergistic ability to facilitate efficient drug transportation while concurrently offering a protective shield against cartilage friction. Yet, the practical *in vivo* application of such systems has been limited by the toxicity associated with the aggregating agents previously employed in these models. Our study introduces a new approach harnessing dendrimer-aggregated liposomes (DendriXALs). Capitalizing on the unique properties of dendrimers—highly branched, multicationic structures with excellent biocompatibility—DendriXALs serve as ideal candidates for the aggregation of anionic liposomes. Crucially, we established that DendriXALs are non-toxic to human synovial fibroblasts and demonstrate efficient biolubrication capabilities. These attributes can be traced to their phospholipid composition and macroscopic size and morphology. Of particular interest is the Dendri4AL variant, which displayed enhanced cartilage retention and a lower uptake rate by macrophages indicating a potential for decreased clearance from the joint space. These findings highlight Dendri4ALs as a candidate for an effective intra-articular drug delivery platform in the treatment of OA. However, in order to validate these findings and enable their practical application in a clinical setting, further *in vivo* studies are required.

3.5 Acknowledgments

This work was supported by The Open Round grant by the Faculty of Science of the University of Bern. The authors thank Peter Künzler and Benvinda Henriques Campos for their valuable support in the cell culture laboratory. Thanks are also due to Dr. Stefan Müller from the Flow Cytometry and Cell Sorting core facility of the Department of BioMedical Research (DBMR) at University of Bern for his assistance with flow cytometry measurement, and we acknowledge this core facility for diligently maintaining the flow cytometry equipment. The authors would also like to thank the workshop of Department of Chemistry, Biochemistry and Pharmaceutical Sciences of the University of Bern for making the dialysis devices for in vitro drug release experiments. Frank Steiniger of the University of Jena, Germany, is warmly acknowledged for his support with the cryo-TEM image acquisition and analysis of loaded liposomes and DendriXALs.

Chapter 4.

Lipidic mesophases for enzyme-triggered localized therapy of osteoarthritis

This chapter is part of a manuscript in preparation for an on-going project.

Gregor Bordon developed the RAPA-LMP formulation and performed release and tribology studies. Elena Allegritti developed and characterised the macrobeads, Shivaprakash N. Ramakrishna assisted with nanotribological measurements, Rowena Crockett co-supervised the macro-tribological experiments, Lucio Isa co-supervised the nano-tribological experiments, Simone Aleandri performed SAXS measurements and analysis and co-supervised the project, Paola Luciani co-supervised and administered the project.

4.1 Introduction

The challenge of extending drug retention time in the joint space is a critical aspect for improving intra-articular (IA) administration in the treatment of osteoarthritis (OA). This issue, thoroughly discussed in Chapter 1, has prompted the development of numerous drug delivery systems. These solutions range from polymer-based approaches, such as hydrogels and microspheres, to lipid-based systems like liposomes [68,134,137,186–188]. However, these systems are not without their limitations. With liposomes, their small size can lead to quicker clearance by immune cells, decreasing the residence time in the joint. In certain cases, particularly with small, hydrophilic drugs, short-term release can also be a concern [49,189]. Lipidic mesophases (LMPs) recently emerged as a promising drug delivery platform that provides extended drug release and hold promise for increased retention in synovial space [190,191]. These self-assembled structures consist of monoacylglycerol lipids (such as monoolein, monolinolein and phytantriol) and water, forming various ordered phases such as lamellar, cubic, (with an Ia3d and Pn3m symmetry) and hexagonal mesophases [110,192]. The lamellar phase comprises a two-dimensional stack of amphiphilic bilayers separated by aqueous layers, where each bilayer consists of two monolayers packed tail-to-tail to minimize contact between the hydrocarbon chains and water [16]. Increasing the water content causes the lamellar phase to transform first to an Ia3d and then to a Pn3m cubic phase, which swells until reaching maximum hydration, beyond which Pn3m and water coexist [16]. In contrast, increasing the system's temperature induces a transition from the cubic phase to an inverse hexagonal phase [110]. The cubic phase resembles an ordered molecular sponge consisting of a lipid bilayer curved in three dimensions, surrounded by two identical, yet nonintersecting aqueous channels [193]. The hexagonal phase is composed of an ensemble of cylindrical micelles packed on a hexagonal lattice, with water-lipid heads forming the cylinders and lipid tails filling the continuous matrix [110]. LMPs exhibit biocompatibility, thermodynamic stability, and predictable phase transitions, making them suitable for drug delivery applications. One of the critical factors in developing drug delivery systems for poorly soluble drugs is solubility enhancement. LMPs can encapsulate these drugs within their hydrophobic domains, providing a means for solubility enhancement and sustained drug release. The internal nanostructure of LMPs influences the diffusional behaviour of incorporated solutes through the aqueous domains, which can be tailored to control the drug release kinetics

[192,194]. The responsive phase transitions can be exploited to trigger on-demand drug release upon exposure to specific stimuli such as temperature, water absorption, pH, or enzymes. For example, in a pH-responsive system, an inverse hexagonal phase could be stabilized at neutral pH, corresponding to plasma conditions and slow drug release. Upon exposure to a lower pH environment – for example in the tumor microenvironment, the system can spontaneously change the phase geometry, leading to increased diffusion coefficients and accelerated drug release [195,196]. Similarly, LMPs can be designed for temperature-triggered release, such as our group's recently reported *in situ* forming system for local treatment of ulcerative colitis, where the LMPs undergo a phase shift in response to the higher temperature of the intestine, resulting in sustained drug release [197]. Enzyme-triggered release is also a promising application of LMPs for OA treatment, as the OA microenvironment is known to have high concentrations of lipases and MMPs that can be exploited to trigger on-demand drug release. In fact, recent investigations have demonstrated the potential of LMPs to provide sustained release of triamcinolone acetonide in response to the addition of MMPs or lipases, suggesting their promise for OA treatment [191]. Furthermore, monoolein (MO)-based LMPs with kartogenin showed encouraging results in protecting and regenerating cartilage, which is key for successful OA therapy [198].

Rapamycin (RAPA), as elaborated in Chapters 1 and 2, is an immunosuppressive drug with potential benefits in treating OA by reducing inflammation and cartilage damage. Its systemic administration, however, can lead to complications such as nephrotoxicity [199]. To avoid these side effects, local administration of RAPA has been proposed, making LMPs a promising drug delivery system due to their ability to provide sustained drug release for a chronic disease like OA. In our study, we used MO, which is relatively inexpensive and generally recognized as safe (GRAS) by the FDA [200]. Our results show that RAPA can be effectively encapsulated in the MO lamellar phase with homogeneous distribution of the drug in the bulk LMP, which is easily injectable through a syringe needle. Characterization of the system with small- and wide-angle x-ray scattering (SAXS and WAXS) confirmed past results [201] that a phase transition from lamellar to inverse cubic Pn3m in the excess medium occurs within 2 h. Additionally, the presence of lipases in the buffer, mimicking the OA microenvironment, shifted the phase towards the inverse hexagonal mesophase, as recently reported [202]. Recent research has shown that small particulate suspensions could be useful for OA treatment due to their increased retention in the joint and potential lubrication of the cartilage [49,68]. In a proof-of-concept study, we

prepared RAPA-LMPs as macrobeads. These beads exhibited a homogeneous size distribution, with only a very slight influence on the average size observed due to the encapsulation of RAPA.. Upon injection, the beads morph into rod-like structures. Finally, our study demonstrated that LMPs can retain drug release for over a month in sink conditions and that lipases triggered the releases. These findings suggest that LMPs have the potential to serve as an on-demand delivery system for RAPA, a promising avenue for treating OA.

4.2 Materials and methods

4.2.1 Materials

Materials used in this study include Dimodan MO 90D (>90% purity), gifted by Danisco (Denmark), and rapamycin (sirolimus), obtained from R&S Pharmchem (Pudong Districs, Shanghai, China). Ketoconazole (99-101% purity) was purchased from Sigma-Aldrich-Merck (St Louis, MO, USA). Trifluoroacetic acid and 1 M HEPES solution were obtained from Carl Roth (Karlsruhe, Germany), while chloroform and methanol were obtained from Fisher Scientific (Schwerte, Germany). All chemicals were used as received. Ultrapure water with a resistivity of 18.2 MΩ.cm was produced using a Barnstead Smart2 pure device from Thermo Scientific (Pittsburgh, USA). Lyophilized lipases from *Candida rugosa* were obtained from Merck (Germany).

4.2.2 Preparation of LMPs and macrobeads

Monoolein (MO) was weighed and melted at 40 °C. Rapamycin (RAPA) powder was then added to the molten MO at different mass concentrations and mixed until homogenous. Ultrapure water, comprising 10% of the total mass, was added to the mixture to obtain a lamellar phase. To equilibrate the lipidic mesophase (LMP), the bulk was mixed with a spatula and centrifuged at 4400 rcf for 3 min. This process was repeated three times. The following day, the LMP was ready for use. To test RAPA distribution within the bulk LMP, samples were taken from the top, middle-top, middle-bottom, and bottom of a 15 mL tube and analyzed using high-performance liquid chromatography (HPLC) with a reverse-phase C18 Nucleosil 100-5 column (4.0 x 250 mm; 5.0 µm particle size, Macherey-Nagel, Germany). The mobile phase consisted of methanol/water (90/10 v/v) + 0.1%

trifluoroacetic acid, with a flow rate of 1 mL/min, temperature of 50 °C, and UV detection at λ = 278 nm. Ketoconazole was added to all samples as an internal standard at a concentration of 0.2 mg/mL.

Due to the viscoelasticity of the system, it was crucial to determine the relationship between the amount of the formulation loaded into a 1 mL syringe with Luer lock (Fisher Scientific, MA, USA) and a 20 G needle. This relationship was evaluated by loading different masses of the formulation into the syringe and injecting the formulation onto a balance after 24 h, where the injected mass was weighed.

Macrobeads were prepared by injecting the molten MO-RAPA mixture with a 1 mL Hamilton glass syringe and 18G needle into cold ultrapure water (4 °C) in a beaker while mixing at 200 rpm. The beads were incubated in the water for a pre-determined period of time and then filtered under vacuum. The diameter of the beads was measured using a Vernier caliper. Furthermore, the macrobeads' injectability was evaluated by injecting them into both agarose and ultrapure water. This assessment aimed to establish the practicality of delivering the macrobeads via injection.

4.2.3 Small and wide-angle X-ray scattering (SAXS and WAXS)

SAXS measurements were used to determine the phase identity and symmetry of the produced LMPs. Measurements were performed on a Bruker AXS Micro, with a microfocused X-ray source, operating at voltage and filament current of 50 kV and 1000 μA, respectively. The Cu Kα radiation (λCu Kα = 1.5418 Å) was collimated by a 2D Kratky collimator, and the data were collected by a 2D Pilatus 100K detector (or 1D VÅNTEC-1 detector in case of WAXS). The scattering vector $Q = (4\pi/\lambda) \sin\theta$, with 2θ being the scattering angle, was calibrated using silver behenate. Data were collected and azimuthally averaged using the Saxsgui software to yield 1D intensity vs. scattering vector Q, with a Q range from 0.001 to 0.5 Å–1 (and from 13 to 20 nm−1 for WAXS). For all measurements, the samples were placed inside a stainless-steel cell between two thin replaceable mica sheets and sealed by an O-ring, with a sample volume of 10 μL and a thickness of ∼1 mm. Samples were equilibrated for 30 min before measurement, whereas scattered intensity was collected over 30 min. To determine the structural parameters such as the size of the water channels, SAXS data about the lattice were combined with the composition of the samples [203]. SAXS was used to evaluate the mesophase structures

with different RAPA contents before and after the *in vitro* release experiments in 10 % EtOH with and without lipases. Additionally, the kinetics of the phase change was measured with periodic SAXS measurements.

4.2.4 Rheology

A stress-controlled rheometer (Modular Compact Rheometer MCR 72 from Anton Paar, Graz, Austria) was used in cone-plate geometry, 0.993° angle, and 49.942 mm diameter. The temperature control was set either at 25 or 38 °C. First, a strain sweep was performed at 1 Hz between 0.002 and 100% strain to determine the linear range to determine the linear viscoelastic regime (LVR), the yield and flow points. Then, oscillatory frequency sweeps were performed at 0.1% strain between 0.1 and 100 rad/s. Frequency sweep measurements were performed at a constant strain in the linear viscoelastic regime (LVR), as determined by the oscillation strain sweep (amplitude sweep) measurement performed for each sample. Within the linear viscoelastic region, in fact, the material response is independent of the magnitude of the deformation and the material structure is maintained intact; this is a necessary condition to accurately determine the mechanical properties of the material.

4.2.5 *In vitro* drug release

For this experiment, we utilized 250 mL bottles, each equipped with a custom-made metal baskets adapted from a previous report [204] and prepared by workshop of the Department of Chemistry, Biochemistry, and Pharmaceutical sciences at University of Bern, as illustrated in **Figure 22**. Each metal basket contained 25 mg of the RAPA-LMP sample. The release medium was composed of 10% EtOH in ultrapure water to maintain sink conditions and RAPA stability. The bottles were placed in an incubator at 37 °C with a shaking speed of 10 rpm. Throughout the 30 days of the study, the release medium was collected, replaced with fresh medium at each time point, and aliquots were stored for further analysis. The aliquots were frozen in liquid nitrogen, lyophilized, and resuspended with the internal standard solution for subsequent RAPA content determination using high-performance liquid chromatography (HPLC) as described in the Chapters 2 and 3.

Figure 22: Release study setup for bulk RAPA-LMPs.

A second in vitro drug release test was conducted to mimic inflammatory conditions by incorporating lipases in the release medium. In this experiment, 50 mL tubes were used, each containing 100 mg of the formulation. The release medium, containing 10% EtOH, was added to the tubes, and sampling was performed daily. The tubes were centrifuged at 1000 rcf for 5 min, after which aliquots were collected and the entire release medium was replaced with fresh medium. On day 5, for a subset of samples, the release medium was substituted with a medium containing 5000 U/mL of lipases from *Candida rugosa*. The test proceeded until day 10, with aliquots being analyzed for RAPA content using HPLC.

4.2.6 Nano-tribology

Nanotribology measurements were performed on silica sliding against silicon with colloidal probe lateral force microscopy (CP-LFM) using a Bruker Dimension Icon AFM with tipless Au-coated cantilevers (CSC-38, Mikromash, Bulgaria). Silica particles, roughly 8 µm in diameter (EKA Chemicals AB, Kromasil R), were affixed to the cantilever's end utilizing two-component epoxy adhesive with the assistance of a custom

micromanipulator. Preparation and treatment of four separate colloidal probes involved exposure to UV/ozone for 30 min before the experiment. Four silicon wafer substrates, each approximately 1x1 cm, also underwent UV/ozone treatment. Each measurement involved preliminary treatment of the silicon substrates, excluding the silica colloid probe. Treatments included either immersion in a PBS solution or application of 1 mL of a monoolein melt. In order to measure the friction of the lamellar phase, the system was brought down to room temperature and promptly supplemented with buffer just prior to the assessment. In contrast, the Pn3m sample was allowed to cool to room temperature and left to incubate with buffer for a minimum of 2 h preceding the friction measurements to ensure a complete phase transition. The process of recording friction loops involved scanning the cantilever laterally across the surface. At least five friction loops were acquired for each applied load, from which the average friction values were derived from trace and retrace curves. Coefficient of friction (COF) values were deduced from the slope of the friction force versus normal force graphs. For lateral-force calibration, the "test-probe method" as described by Cannara *et al* [152] was utilized. This involved moving a reference cantilever, affixed with a silica particle of approximately 40 μm in diameter (a test probe), laterally into contact with a pre-treated silicon wafer (1x1 cm) that acted as a "hard wall." This allowed for the acquisition of lateral sensitivity values.

4.2.7 Macro-tribology

UMT-2 tribometer (Bruker, USA) operating in linear reciprocating mode was used to measure the macroscopic friction behavior of cartilage sliding against cartilage. under various conditions. These included the presence of PBS, injected beads, Pn3m cubic LMP that was spread over the bottom cartilage surface, and melted cubic as well as lamellar LMPs, which were prepared following the same protocol as in nano-tribological measurements. Irrespective of the condition, care was taken to apply an adequate amount of material, ensuring complete coverage of the cartilage surface during each experiment. After harvesting the cartilage, the samples were preserved at -20 °C in a PBS solution containing 10% DMSO. These samples were then thawed less than 24 h before the experiment and washed with PBS to prepare them for the study, when they were affixed to the superior and inferior surfaces of the tribometer, immediately prior to testing. In each experiment, a load of 1 N was applied to the superior specimen, measuring 5x5 mm, which reciprocated over a stroke length of 2 mm at a

frequency of 1 Hz for a duration of 10 min. The specimens remained fully immersed in the buffer solution, introduced to the inferior cartilage surface along with additional lubricants, for the entirety of the experiment. All experiments were conducted under stable thermal conditions of 20 °C with a data acquisition rate of 500 Hz. For each experiment, the representative COF was calculated from the raw data of lateral and normal forces, by averaging the middle 90% of each friction loop, excluding transients associated with the ends of the stroke length. Furthermore, the initial 20% of the loops were discarded from the data analysis, ensuring the processing of steady-state friction and excluding the running-in phase.

4.2.8 Statistical analysis

Every experiment was conducted in a minimum of three repetitions, except for SAXS and rheology data, where a single replicate was measured. The presented figures represent averages accompanied by ± standard deviations, unless otherwise stated. General calculations utilized Microsoft Excel, while GraphPad Prism 9.5 was employed for generating graphs.

4.3 Results and discussion

4.3.1 Preparation and characterization of LMPs and macrobeads

RAPA is a drug that recently showed promise in pre-clinics for the treatment of OA, but its systemic side effects are calling for the development of delivery systems for IA administration, which limits the systemic concentration. On the other hand, frequent IA injections are connected with an increased risk of infections and therefore long-acting [41]. Our goal in this study was to develop a long-acting formulation of RAPA, which recognizes disease-related cues, such as increased lipase presence, and delivers the drug on demand. To do this, we encapsulated RAPA in MO-based LMPs, which based on the results in **Figure 23**, is homogenously distributed in the bulk formulation. This result is important for the use of the formulation in the clinics, as each dose should contain equal amount of the active pharmaceutical ingredient.

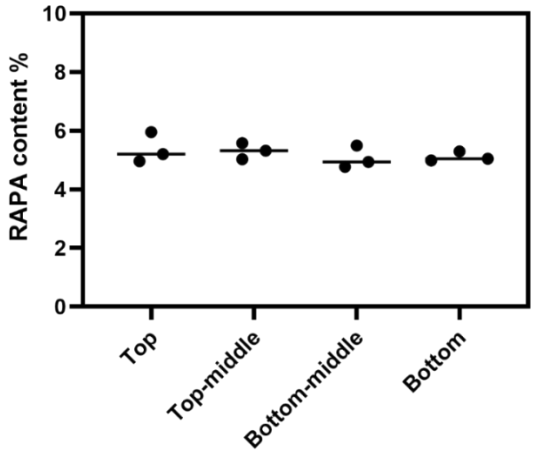

Figure 23: Homogeneity of RAPA (5 w/w%) in bulk LMP. The mean value is represented with a line.

Next, macrobeads were formed by adding molten MO with RAPA in cold water dropwise. To evaluate the impact of RAPA on their size, several concentrations of RAPA were used in this test and the results presented in **Figure 24** show that the size of beads slightly decreases at 5 % RAPA compared with 0.1 % RAPA and 1 % RAPA.

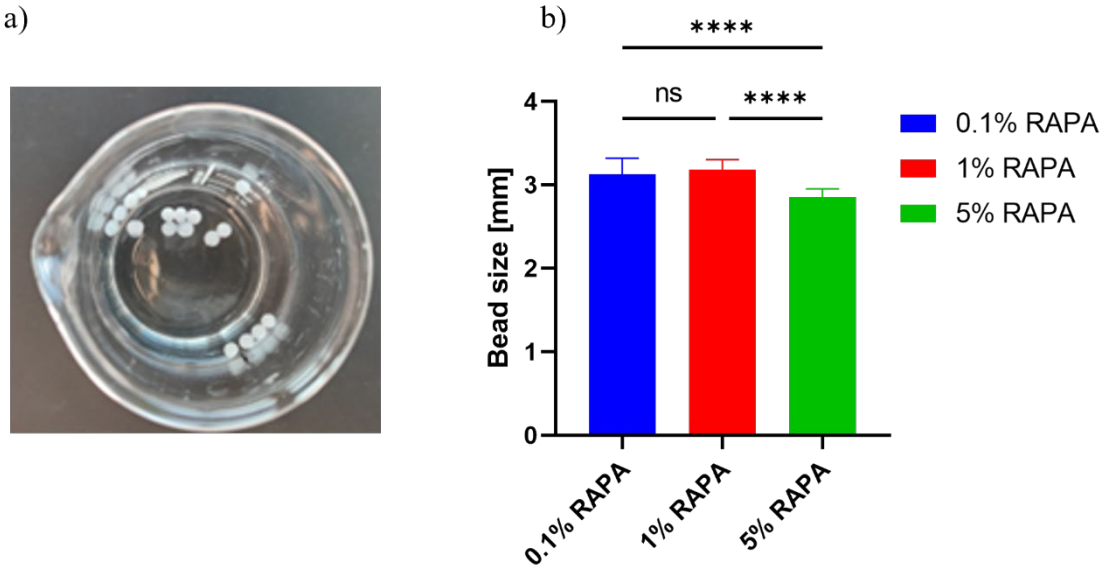

*Figure 24:a) Macrobeads. b) Size of macrobeads as measured with caliper with 0.1 m/m% (n=30), 1 m/m% (n=20), 5 m/m% (n=20) RAPA content. Statistical significance is designated as ***-p<0.0001 and ns-p>0.05.*

To investigate this phenomenon, LMPs with different RAPA content were assessed with SAXS and WAXS. The measurements were performed at RT and 37 °C to mimic the conditions before and after IA injection *in vivo* and the results are shown in **Figure 25**. SAXS data demonstrated that there are no differences between RT and 37 °C in terms of the liquid crystal structure. However, in the SAXS and WAXS curves for LMPs with varying RAPA content, small Bragg's peaks were observed at q = 0.5 $Å^{-1}$ and q = 14 $Å^{-1}$ when the RAPA concentration was increased to 5%. These peaks are likely a manifestation of the precipitated RAPA and suggest that the drug may not be completely solubilized within the LMPs at this concentration. Nonetheless, the limited impact of these peaks on the overall structure and bead size suggests that the LMPs can still tolerate higher RAPA concentrations.

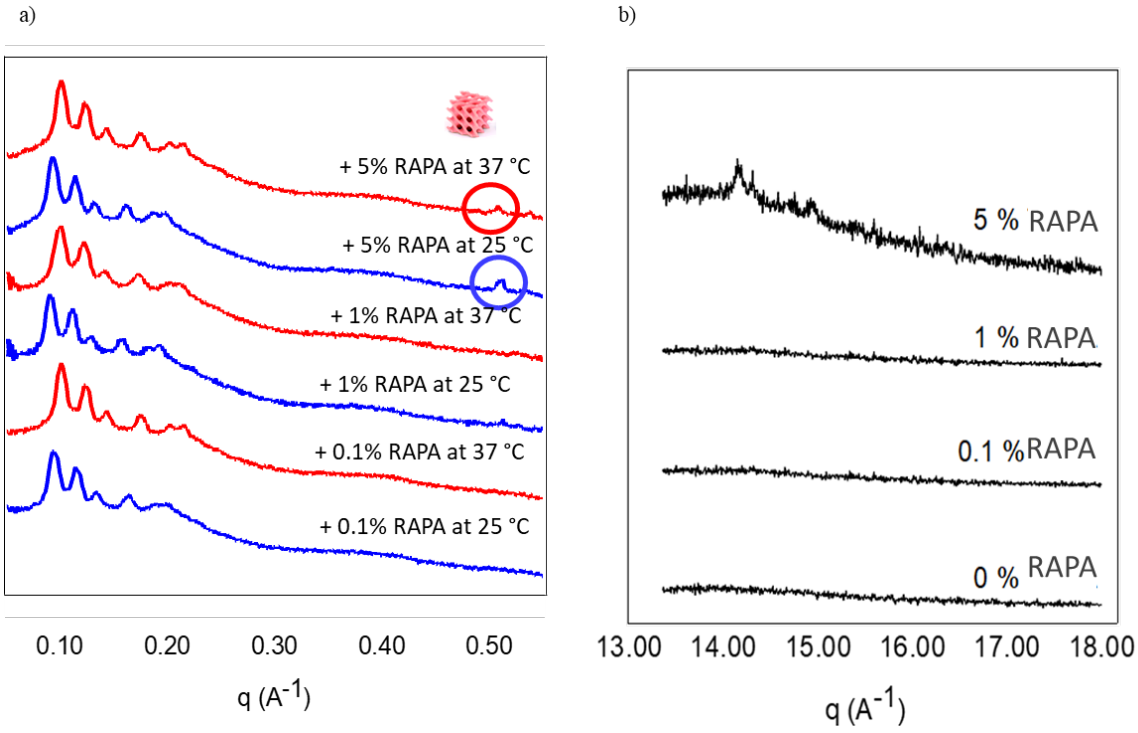

Figure 25: a) SAXS spectra of LMPs with 0.1 %, 1 % and 5 % RAPA in LMPs at room temperature (RT = 25 °C) and body temperature (37 °C). b) WAXS at RT of different RAPA concentrations.

To investigate the LMPs' phase transition kinetics, we conducted SAXS measurements at various time points during incubation in buffer. This analysis is crucial for understanding the rate at which phase transitions occur following injection into the human body. Initially, we prepared beads having a lamellar phase containing 10%

water. These beads were then placed in a buffer solution to trigger a conversion into other mesophases, which were then measured. As shown in **Figure 26**, no phase transition occurred during the first 20 min of incubation. However, after 30 min, the internal structure of the LMP shifted to an Ia3d inverse cubic phase. Following 2 h incubation, a transition to a Pn3m inverse cubic phase was observed, which is known to form when monoolein is exposed to 25% of water content as well as in excess of water, as indicated by previously published phase diagrams [110].

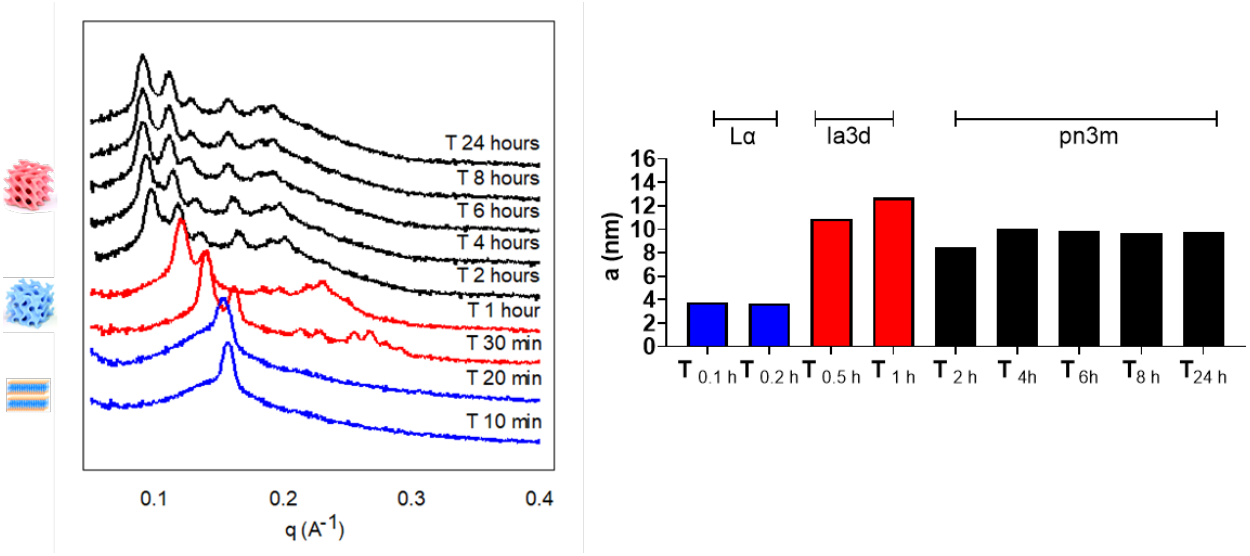

Figure 26: Phase transition kinetics of MO in water. The mesophases were analyzed with SAXS.

4.3.2 Injectability of LMPs and macrobeads

To evaluate the injectability of the macrobeads, we tested whether they could pass through an 18G needle, which is the largest gauge needle commonly used. We assessed the injectability in both agarose gel, to mimic more viscous tissue, and water. In both cases, the results were comparable, as shown in **Figure 27a** and **b**, where it is evident that the macrobeads were extruded through the needle in rod-like structure and did not retain their shape. Furthermore, we investigated the actual injected mass of the bulk LMP when administered through a more commonly used 20G needle, as LMPs are viscoelastic and some dead mass is expected. **Figure 27c** presents the linear correlation between the loaded mass and the injected mass of the formulation. To obtain 100 mg of the formulation containing 5 mg rapamycin, 174 mg need to be loaded into the syringe.

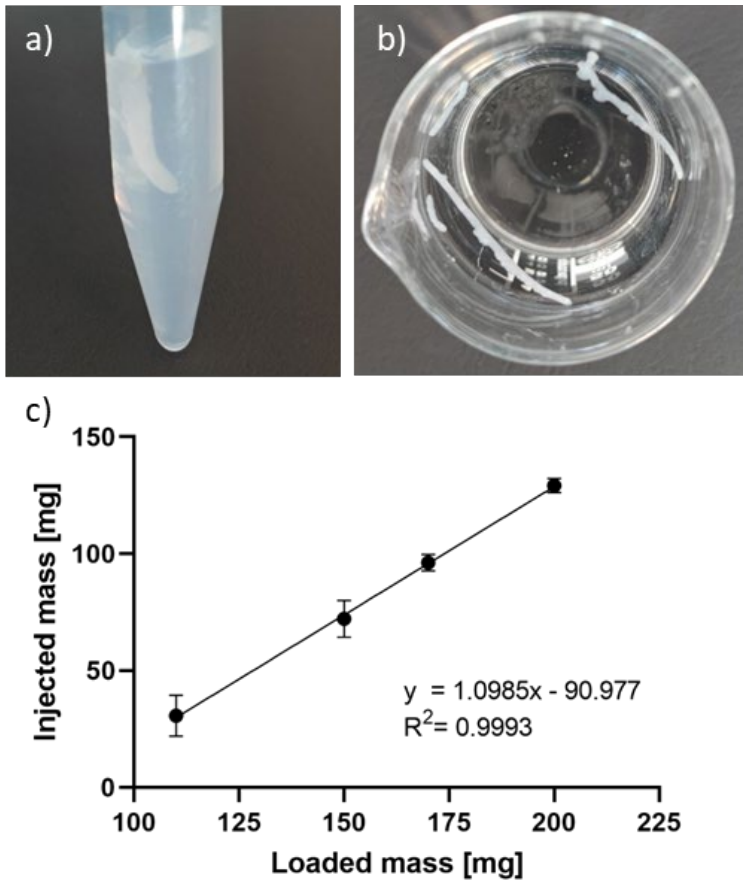

Figure 27: a) Macrobeads injected through 18G needle into agarose gel and b) water. c) Injectability of LMPs through 20G needle.

To better understand the rheological behaviour of lipidic mesophases (LMPs), both amplitude and frequency sweep measurements were performed on lamellar and Pn3m inverse cubic phases. The amplitude sweep measurements were conducted first to determine the linear viscoelastic region (LVR), which is the range of strain within which the material response remains linear and its structure is maintained intact, allowing for accurate determination of mechanical properties during frequency sweep measurements. From the amplitude sweep results presented in **Figure 28a**, the lamellar phase exhibited lower elasticity compared to the Pn3m phase, as evidenced by the lower G' value. This lower G' value is associated with the superior injectability of the lamellar phase [110], which is crucial for IA delivery. Upon hydration, the depot system forms, where the G' of the Pn3m phase becomes considerably higher, indicating a more elastic-like structure. With the LVR established, frequency sweep measurements were performed, as shown in **Figure 28b**. For the Pn3m phase, a visible rubbery

plateau region was observed, where the elastic modulus (G′) dominates over the loss modulus (G″). This phase's behaviour can be identified with a Maxwell fluid, characterized by a long relaxation time needed for the water-monoglyceride interface to return to its unperturbed state. In contrast, the lamellar phase exhibited a leathery transition behaviour, suggesting it behaves as a plastic fluid material. These results confirm the previous reports of superior injectability of the lamellar phase and demonstrate the formation of an elastic depot system upon injection into tissue, where water is abundant [110,203,205].

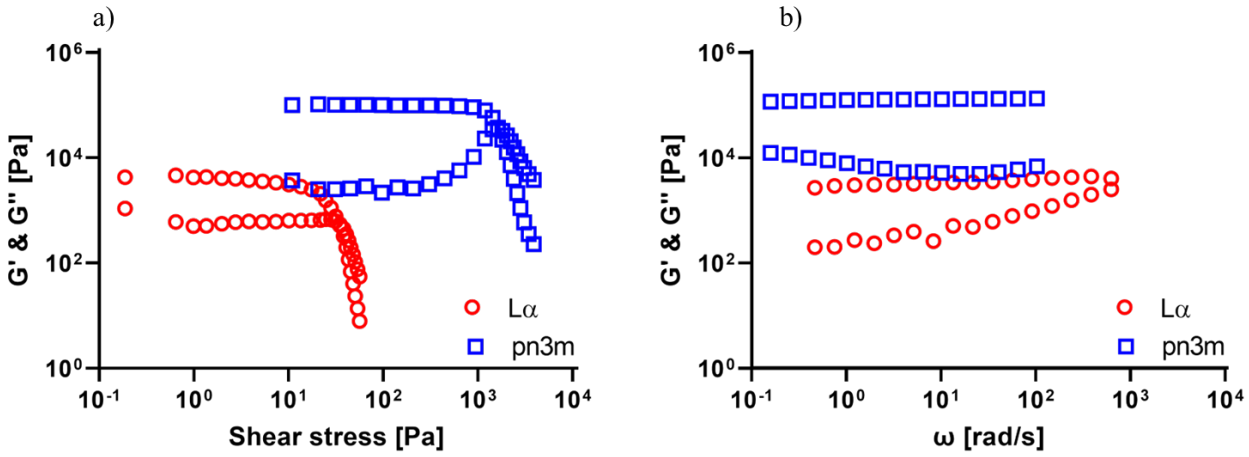

Figure 28: a) Amplitude sweeps of lamellar (Lα) phase with 10% water and fully hydrated Pn3m inverse cubic phase. b) Frequency sweep in the linear viscoelastic region – determined with amplitude sweep.

4.3.3 Drug release from LMPs

Given the chronic nature of OA, developing long-acting drug delivery systems is crucial. Therefore, we investigated the release properties of LMPs under *in vitro* conditions. **Figure 29a** depicts the long-term release under sink conditions, indicating that the drug is released over a period of 30 days, potentially allowing for monthly injections. Figure 29b shows the release kinetics of RAPA when sink conditions are not achieved, which, according to previous studies, is more physiological [206]. To simulate an OA flare, we added lipases to one sample on day 5, which are associated with the disease, and compared it to a sample without lipases. The results reveal a significant burst release after two days of lipase addition, signifying on-demand release. This

property is easily explainable as MO consists of a glycerol molecule connected to oleic acid via an ester bond, which can be cleaved by enzymes, triggering the release of cargo from the drug delivery system.

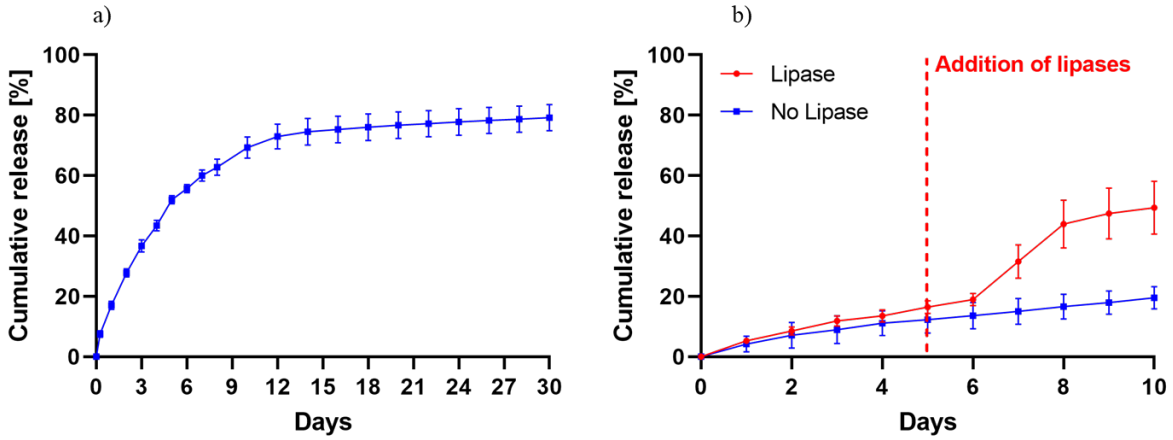

Figure 29: Release of RAPA from LMPs a) in sink conditions over 1 months and b) in OA mimicing buffer with lipases.

To better understand the effects of lipases on LMPs, we performed further investigations using SAXS. After the release study, we used the samples from conditions with and without lipases, and **Figure 30** displays the results. Our findings illustrate that lipases, likely through a process of hydrolysis, transform the Pn3m phase into an inverse hexagonal phase. This has been indicated in past studies as well [202]. Moreover, these results shed light on how the burst release of RAPA from LMPs occurs. .

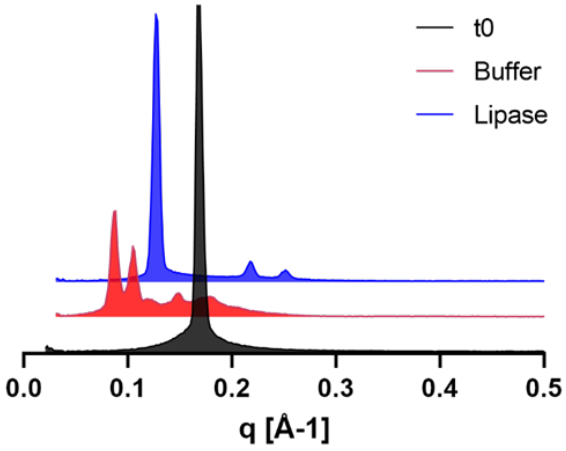

Figure 30: Phase shifts of MO as measured with SAXS, after release study in 10% EtOH in ultrapure water (buffer) and the same buffer with lipases present.

4.3.4 Tribological experiments

Healthy joints rely on natural biolubricants to prevent cartilage wear through effective lubrication. In OA, these biolubricants are notably reduced, resulting in impaired synovial fluid lubrication. This condition leads to elevated friction and subsequent cartilage degradation [20–22]. It has been proposed that combining the drug delivery with cartilage lubrication could have a synergistic effect and importantly improve the OA treatment [68,69,134]. To explore this possibility, preliminary testing was carried out on the lubrication properties of LMPs marking a first-time investigation on both nano- and macro-tribological scales. These scales were examined using techniques like colloid probe lateral force microscopy (CP-LFM) and a macro-tribometer, as illustrated in **Figure 31**. Firstly, MO was melted and applied to a silica wafer, after which it was combined with water, and friction measurements were taken. In contrast, the Pn3m sample was incubated with water for 2 h prior to measurements, ensuring a complete phase transition. A plain silicon wafer in PBS served as a control sample. In CP-LFM measurements, the coefficient of friction (COF) is inferred from the slope of the linear relationship between the applied load and the detected instrument signal, measured in millivolts. However, the results, as depicted in **Figure 31a** reveal no linear relationship between these two parameters, which can be attributed to the rough and soft surface of the applied LMP material. This circumstance rendered the measurement of nano-

tribological behaviour unachievable. To possibly overcome the challenges encountered with CP-LFM measurements, a macro-tribological study was subsequently initiated. In this study, two additional conditions were introduced: injected beads and spread bulk Pn3m LMPs. The objective was to discern whether the injection through a needle could alter the tribological behaviour of LMPs in comparison to the melt and the bulk spread of LMPs. **Figure 31b** demonstrates no significant difference between the conditions, indicating the insufficient lubricating ability of MO. It is known that the phospholipids, such as phosphatidylcholine are efficient boundary lubricants through strong hydration of the phospholipid headgroup, which forms a pressure-resistant slip-plane at the interface [21,69,175]. It is possible that MO's glycerol headgroup doesn't follow the same mechanism and therefore doesn't lead to reduced COF, as indicated in our results. An observed marginal increase in the COF with the melts could likely be due to the upper cartilage surface sinking into the thick layer of LMP, affecting the measurements, as greater force was needed for lateral movements of the upper specimen within the sample. In summary, no detectable lubricating effect was observed in the experimental setup. However, further exploration under more physiologically relevant conditions is recommended for a more comprehensive evaluation of the LMPs' impact on cartilage wear.

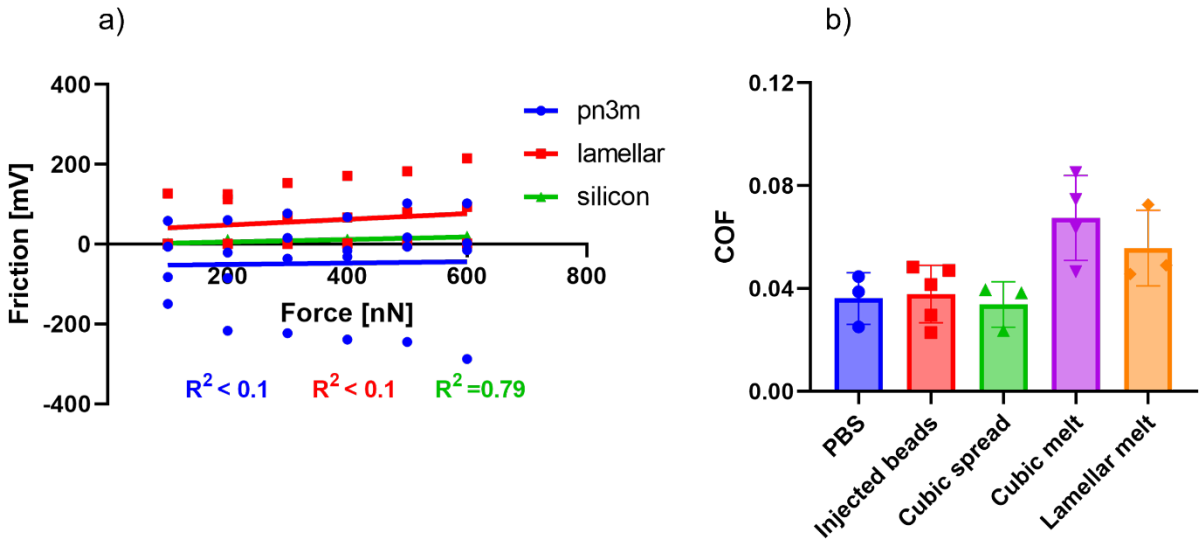

Figure 31:a) Nano-tribological results of LMPs measured with CP-LFM on silicon wafer. b) Macro-tribological results measured with UMT-2 on ex vivo cartilage.

4.4 Conclusion

In conclusion, a responsive lipidic mesophase-based drug delivery system has been successfully developed. Exhibiting a phase transition from lamellar to inverse cubic Pn3m upon exposure to buffer, the system shows increased solid-like properties and transitions to an inverse hexagonal phase in high lipase concentrations. The system, tested in macrobeads form, offers promising future development into microbeads using 3D printing technology. Effective in controlling the release of RAPA—a potential OA therapeutic agent—the system responds to lipase presence, an inflammatory marker, triggering on-demand RAPA release. This underlines the system's potential for treating inflammation-related chronic diseases, such as OA. Additionally, our research marks the first exploration of the lubrication properties of LMPs on both nano- and macro-tribological scales. The initial results did not show a significant lubrication effect, suggesting further investigation is needed under more physiologically relevant conditions to fully understand the potential role of LMPs in reducing cartilage wear.

4.5 Acknowledgments

Authors are grateful to Prof. Rafaelle Mezzenga’s laboratory for providing access to their X-ray facility and to Mohammad Alinezhadfar for providing support with the setup of macro-tribometer. We'd also like to extend our gratitude to Dr. Marianna Carone for her invaluable scientific insights, particularly with the investigation of rheological properties.

Chapter 5.

Conclusion and future perspectives

OA, a prevalent and debilitating joint condition, affects millions worldwide, posing a significant socioeconomic challenge. Current treatments primarily manage symptoms with limited potential to halt disease progression. In recent years, advances have brought forth new pharmacological strategies, such as DMOADs, aimed at slowing OA progression. As discussed in **Chapter 1**, IA drug delivery has garnered attention due to its potential to reduce systemic exposure and increase local bioavailability. Lipid-based DDSs show promise in augmenting therapeutic efficacy by improving stability, targeted delivery, and prolonged joint retention. Research is underway exploring an array of DDSs like liposomes and lipid-based nanoparticles, each leveraging different delivery mechanisms to counter OA pathology. Yet, these technologies are not yet available to patients. In our research, we aimed to advance OA DDSs, addressing multiple facets of its complex pathophysiology. We focused on innovating three distinct systems: zinc-aggregated liposomes (ZnALs), dendrimer-aggregated liposomes (DendriXALs), and lipidic mesophases (LMPs), each possessing unique properties like improved retention on the cartilage, lubrication, sustained and on-demand drug release. Our work brings novel perspectives to OA treatment, countering existing limitations and setting a trajectory for future drug delivery strategies.

Chapter 2 discusses the development and characterization of ZnALs for IA administration of a potential DMOAD – RAPA. Through encapsulation of RAPA, the liposomes demonstrated an excellent encapsulation efficiency of over 90% and exhibited stability that lasted for over four weeks. Rapid and irreversible aggregation was observed in the liposomes, with maximum aggregation reached within five minutes as confirmed by laser diffraction. The irreversible nature of this aggregation offered a significant advantage, as it facilitated further purification steps such as dialysis. This critical step proved effective in eliminating a substantial portion of excess zinc, thereby enhancing the overall safety of the formulation. Additionally, RAPA exhibited enhanced antifibrotic activity and encapsulation in ZnALs displayed a prolonged drug release compared to plain liposomes, demonstrating their potential therapeutic advantage. Moreover, the liposomal aggregates were found to form a protective layer over the cartilage, protecting it from friction. Despite these promising results, the study also uncovered a limitation: residual zinc-induced toxicity on human fibroblasts, which affected the system's potential for clinical translation. Therefore, while the chapter affirms the potential of liposomal aggregates for OA treatment, it also recognizes the necessity for further refinement of this DDS to mitigate its limitations.

Building upon the promising findings from **Chapter 2**, **Chapter 3** sets out to delve deeper into the potential of DendriXALs for intra-articular drug delivery in OA treatment. Recognizing the ideal characteristics for an aggregating agent, we sought one that would be highly biocompatible, possess anti-inflammatory and antifibrotic properties, and posses cationic properties to induce the aggregation of anionic liposomes. Dendrimers, with their unique branched structure and modifiable multivalent positive charge capacity to bind with the anionic liposomal surface, were identified as an ideal choice. These selected dendrimers demonstrated commendable biocompatibility and anti-inflammatory behaviour, and further analyses confirmed a significant antifibrotic effect on human OA synovial fibroblasts. We characterized the DendriXALs using cryoTEM and fluorescence microscopy, unveiling a structure analogous to the previously studied ZnALs. Importantly, these dendrimer-aggregated liposomes exhibited non-toxicity on human synovial cells when administered at therapeutic doses. DendriXALs presented remarkable potential for cartilage preservation, outperforming conventional liposomes and PBS control in terms of friction reduction. Moreover, they showed enhanced retention on cartilage and decreased particle uptake by macrophages, addressing the critical issue of clearance from joint space. In essence, **Chapter 3** provides compelling in vitro proof-of-concept data showing that aggregated liposomes, specifically DendriXALs, could act as an efficient drug delivery platform. They have the potential to provide sustained drug release, lubricate cartilage by improving retention on the cartilage surface, and reduce clearance via decreased macrophage uptake. This research establishes a robust foundation for the translation of aggregated liposomes to animal studies, which would then have to show the efficacy of such systems. Follow-up animal investigations can draw upon the successful *in vivo* studies from other researchers, which have exhibited the beneficial outcomes of improved joint retention, prolonged intra-articular drug residence, and better preservation of joint structures compared to plain liposomes or free drugs. To track and understand the biodistribution of these therapeutic entities, pharmacokinetic studies could be undertaken using an *in vivo* small animal imaging system. This would involve tracking the intensity of fluorescently labelled liposomes and labelled DendriXALs within rat joints over a period extending from the initial injection up to four weeks, utilizing an *In vivo* imaging system (IVIS) to perform these observations. Alongside this, the pharmacokinetic assessment should also involve the administration of DendriXALs carrying a model drug, such as an approved drug like dexamethasone or a potential DMOAD. Subsequent monitoring of the drug concentration in the synovial fluid and plasma could

demonstrate a reduced systemic exposure to the drug, thus potentially decreasing the risk of adverse effects. Subsequent pharmacodynamic studies, designed in harmony with the pharmacokinetic study timeline, would aim to evaluate gene expression within the synovium. This would involve assessing markers indicative of both fibrosis and inflammation. In addition to these molecular analyses, a histopathological examination using the Mankin scoring system would provide valuable insight into the impact of DendriXALs on the cartilage structure. These comprehensive assessments could establish an evidence base that underscores the therapeutic potential of DendriXALs for OA treatment.

Drawing on the potential of aggregated liposomes demonstrated in the previous chapters, **Chapter 4** presents a shift in focus to the development and characterization of a RAPA-loaded LMP-based DDS. The high lipid content makes this system suitable for sustained RAPA delivery, where on-demand release is enabled due to the sensitivity of monoolein-based LMPs on enzymatic degradation. Our *in vitro* studies demonstrated that OA-associated lipases stimulate RAPA release due to ester bond cleavage. Through X-ray scattering techniques, the characterization of LMPs was conducted meticulously. It was found that the precursor lamellar liquid crystal phase transitions to an inverse cubic liquid crystal phase within 2 h after the introduction of excess water, mimicking IA injection into the joint space. Preliminary experiments revealed the feasibility of macrobead formation, warranting further investigation into potential microbead creation, which would facilitate syringe-needle passage while preserving bead morphology. Tribological performance evaluations, however, did not indicate any significant lubricating properties, signposting an area for future development. Given LMPs' biocompatibility and efficacy in on-demand RAPA delivery, future investigations could test the system's capacity to minimize systemic absorption from the joint space and extend drug retention therein. Despite the lack of lubrication observed, the addition of amphiphilic lipids such as phosphatidylcholine to the mixture could potentially enhance this property. The current study was conducted at room temperature, thus, future evaluations at physiological conditions could provide more relevant insights.

Our research lays the groundwork for improving OA treatments via novel lipid-based drug delivery systems. While challenges, such as residual zinc-induced toxicity in ZnALs (**Chapter 2**), were largely addressed with DendriXALs (**Chapter 3**), further in vivo studies are needed to substantiate their capacity for enhancing joint

retention, cartilage preservation, and overall therapeutic efficacy. Concurrently, the LMP technology presented in **Chapter 4** invites additional exploration. This includes conducting experiments under physiological conditions, enriching lipid mixtures with lubricating phospholipids, and potentially developing microbeads. These prospective investigations and enhancements aim to propel the effectiveness of these innovative systems and translate them to the next developmental stage.

Appendix

Supplementary information per chapter

6.1 Chapter 2 supplementary information

6.1.1 Dialysis device for *in vitro* drug release

Figure S1: Dialysis device for drug release experiments a) dissasebled without a membrane, b) assembled with a 100 nm polycarbonate membrane and c) inside a 50 mL conical tube.

6.1.2 Stability of liposomes in release medium

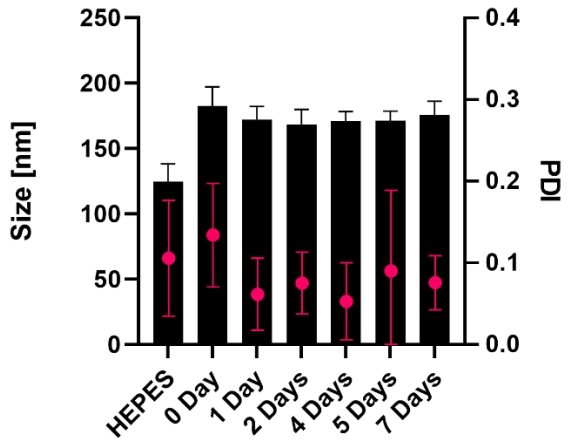

Figure S2: Stability of liposomes in 10 % EtOH throughout 7 days. Size, PDI and absolute intensity were measured with DLS.

6.1.3 Primers for gene expression studies

αSMA Fwd: 5' GAC AAT GGC TCT GGG CTC TGT AA 3', Rev: 5'ATG CCA TGT TCT ATC GGG TAC TT 3'

Col1A1 Fwd: 5' CAG CCG CTT CAC CTA CAG C 3', Rev: 5' TTT TGT ATT CAA TCA CTG TCT TGC C 3'

Col3A1 Fwd: 5' GGA CCT CCT GGT GCT ATA GGT 3', Rev: 5' CGG GTC TAC CTG ATT CTC CAT 3')

RPLP0 Fwd: 5'-GCG TCC TCG TGG AAGTGA CAT CG 3', Rev: 5'-TCA GGG ATT GCC ACG CAG GG 3'

6.1.4 DSC thermograms

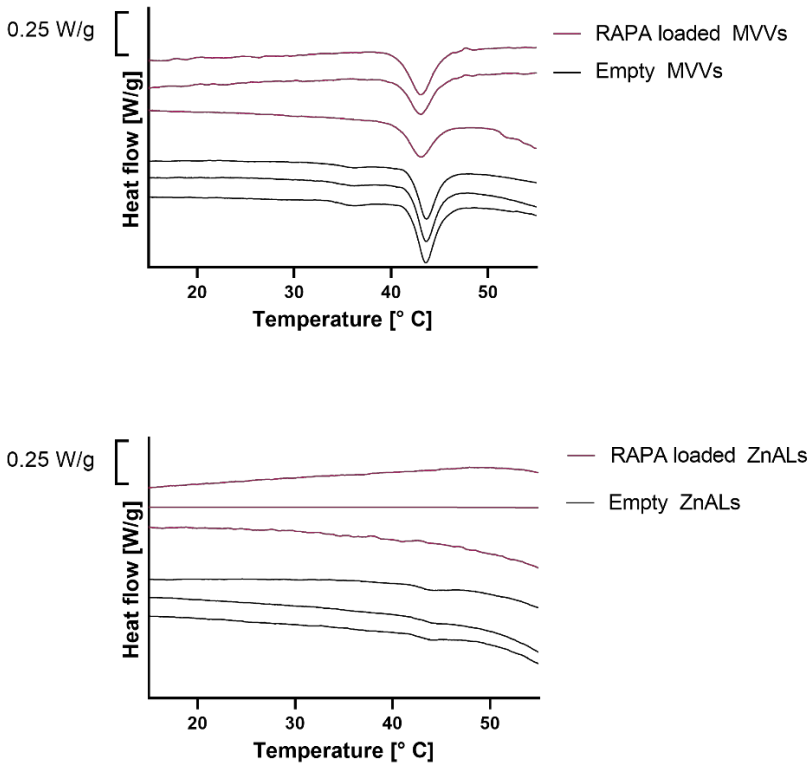

Figure S3: DSC thermograms of unextruded liposomes – multilamellar vesicles (MLVs) and of ZnALs with loaded RAPA and without (empty). Each sample included 20 mM total lipid content and ZnALs included 150 mM Zn^{2+}. Each thermogram is vertically shifted to avoid overlapping one another.

6.1.5 Fluorescence microscopy images

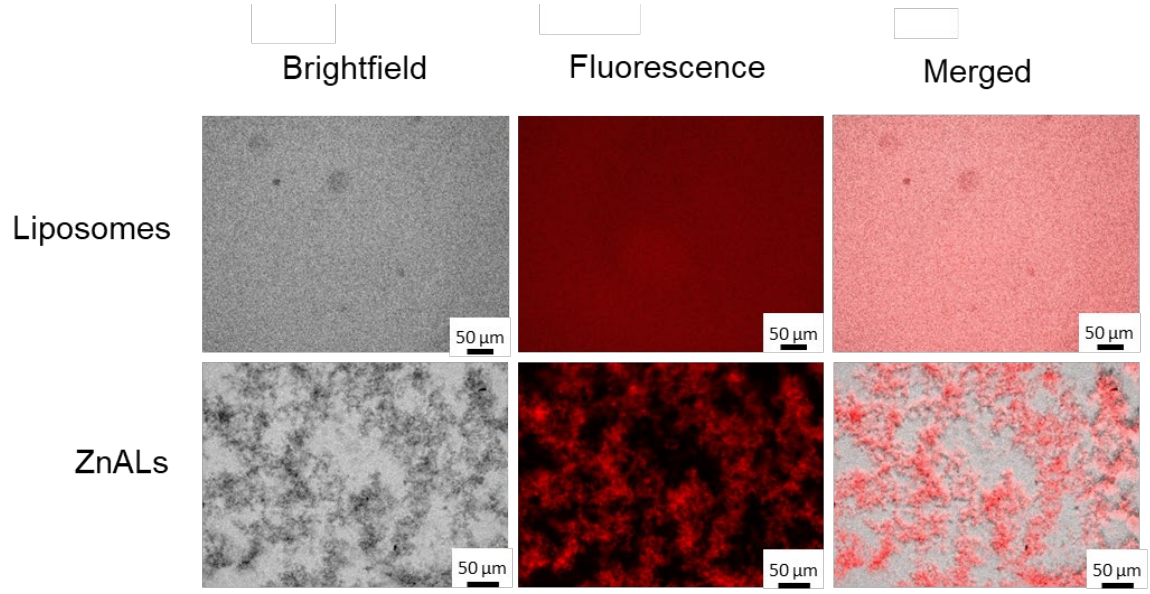

Figure S4: Fluorescence microscopy images of liposomes and ZnALs at 5 mM lipid content, 150 mM Zn^{2+} and encapsulated fluorescent DiD probe.

6.1.6 RAPA dose and Zn content in ZnALs

Table S1: Dose of RAPA and Zn^{2+} in ZnALs.

RAPA dose[μg/mL]	c(Zn^{2+}) [mM]
0.1	0.5
1	5.0
2	10

6.1.7 Supplementary videos

Supplementary videos 1, 2, and 3 are available through Zenodo online repository through the link: https://zenodo.org/record/7993495.

6.2 Chapter 3 supplementary information

6.2.1 Cell uptake of DendriXALs

A minimum of 5000 cells were measured in total for each sample before implementing our three-step gating process, which is illustrated in **Figure S5**:

a) Selection of Single Cells: The first step of the gating process involved selecting single cells from the cell suspension. This helped to eliminate cell aggregates and debris, ensuring that only individual cells were included in the analysis. The determination of single cells was based on their bright field area and aspect ratio.

b) Selection of Focused Cells: After the selection of single cells, the next step was to gate focused cells. This was achieved by disregarding out-of-focus cells and selecting the top 60% based on the Gradient RMS feature. This step ensured the high quality of acquired images and accurate measurements of fluorescence intensity.

c) Selection of Live Cells: The final step was to select live cells. This was typically done using a high Hoechst stain intensity (>10000) and low PI intensity as parameters for live cell identification. However, in one replicate where Hoechst staining encountered a technical issue, only PI staining was used for exclusion. The gating ensured that the count of live cells remained above 500 for all samples.

Detailed information about each step, along with a representative gating illustration, can be found **Figure S5**.

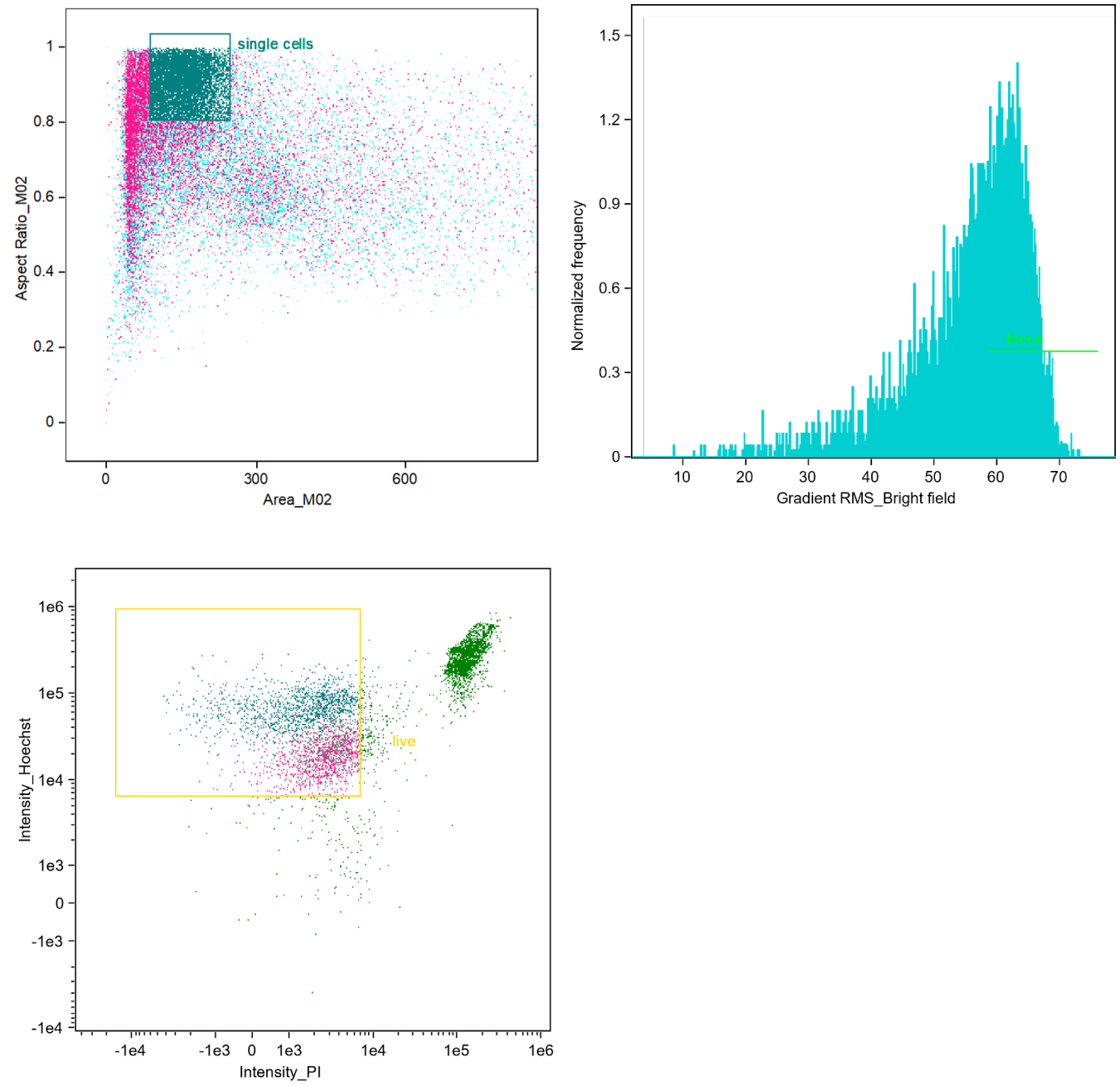

Figure S5: Representative gating illustration with Image Stream(R). a) Selection of single cells, b) Selection of focused cells, c) Selection of live cells.

6.2.2 Aggregation in presence of salts

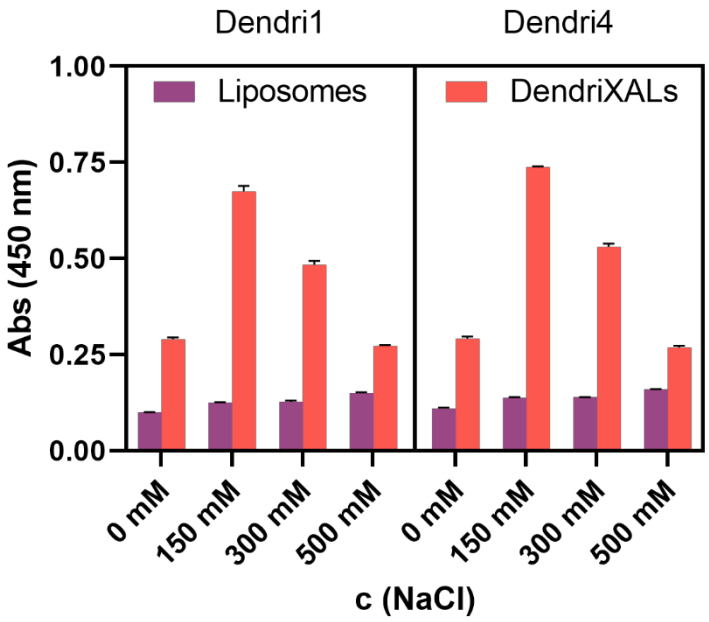

Figure S6: Aggregation in presence of NaCl at different concentrations. The optical density was measured with a plate reader at 450 nm wavelength 5 minutes after mixing DendriXs and liposomes. Concentration of DendriXs was kept constant at 50 µg/mL and lipid content was adjusted (0.66 mM for Dendri1, and 0.73 mM for Dendri4). NaCl was mixed with DendriXs before the mixing with liposomes.

6.2.3 *In vitro* drug release

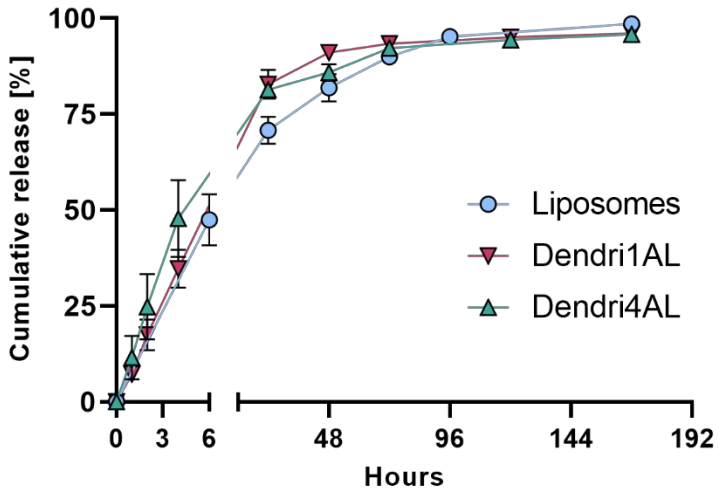

Figure S7: Release of rapamycin from customized dialysis device with 10 % ethanol in ultrapure water as release medium. The total lipid concentration in all cases was 5 mM with a 30/1 L/D ratio. The setup was previously reported [69]. Results are reported as a mean of 3 replicates with standard deviations.

6.2.4 DendriXAL retention on cartilage surface

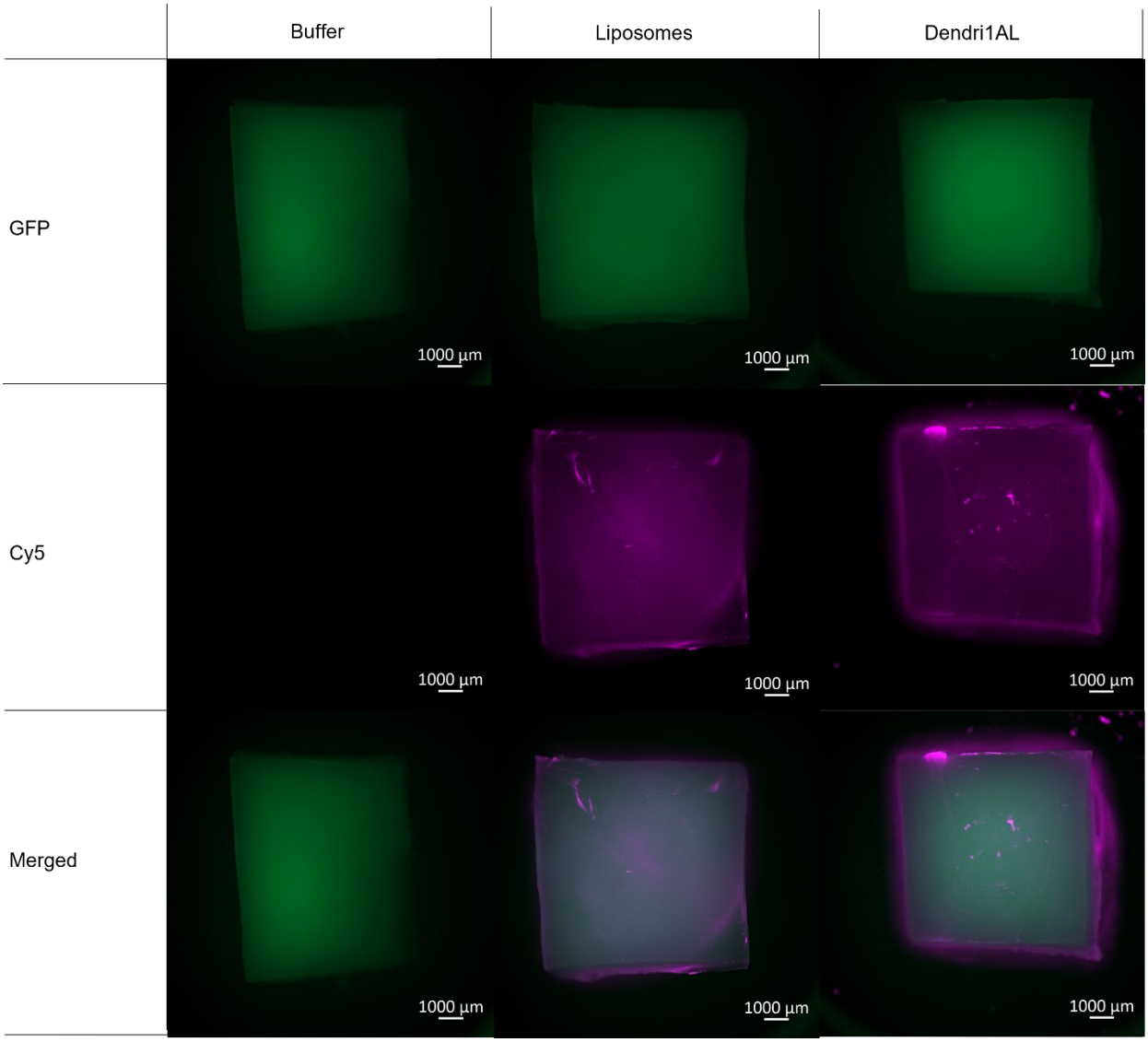

Figure S8: DiD labelled Dendri1AL and liposomes' retention on porcine cartilage surface. Images were captured at 10X magnification with fluorescence stereomicroscope. The concentration of lipids was 0.66 mM and concentration of Dendri1 was 50 µg/mL.

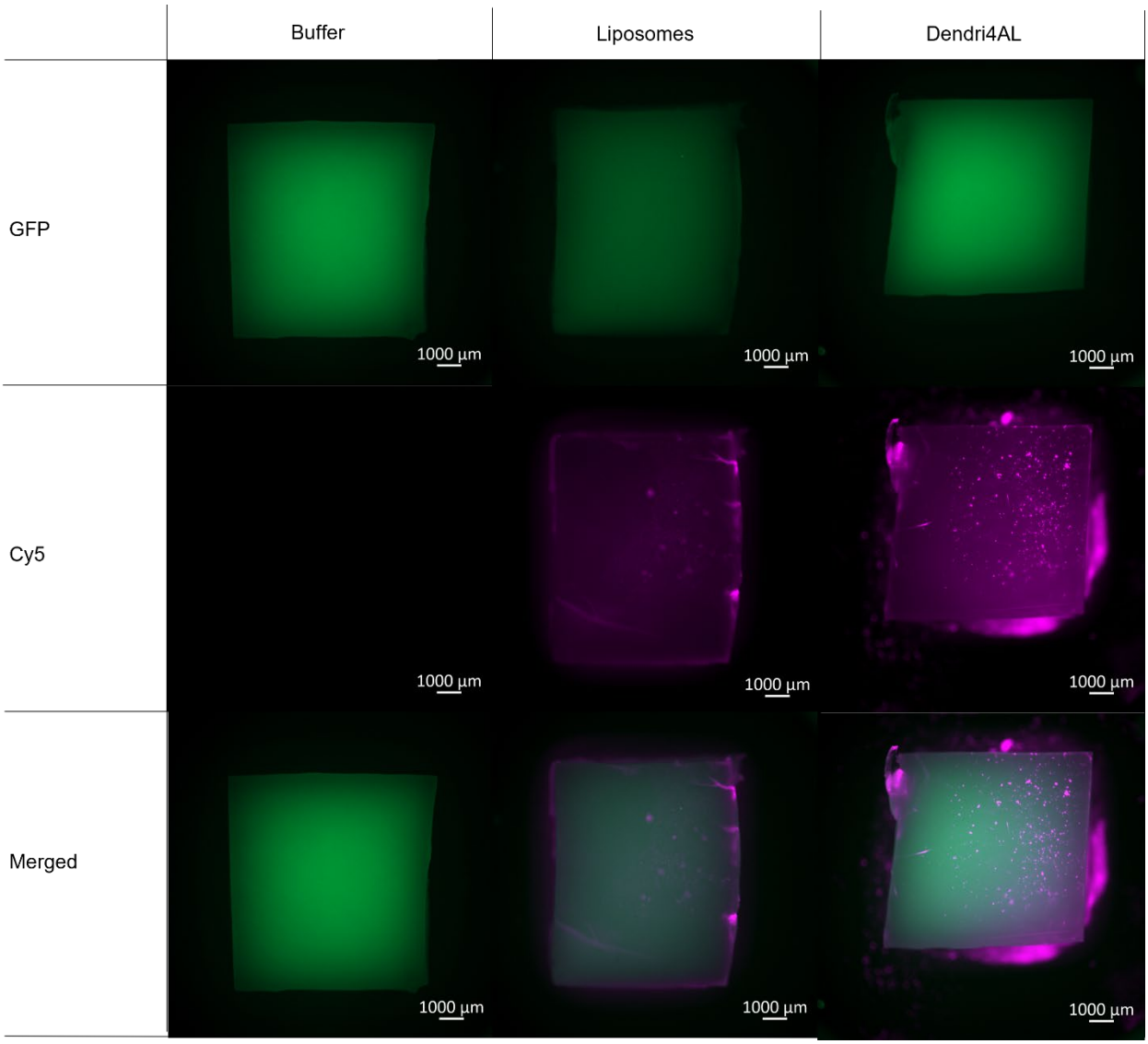

Figure S9: DiD labelled Dendri4AL and liposomes' retention on porcine cartilage surface. Images were captured at 10X magnification with fluorescence stereomicroscope. The concentration of lipids was 0.73 mM and concentration of Dendri4 was 50 µg/mL..

Abbreviations

αSMA	Alpha smooth muscle actin
AFM	Atomic force microscopy
AL	Aggregated liposome
ASOs	Antisense oligonucleotides
atRA	All-trans retinoic acid
COF	Coefficient of friction
Col1A1	Collagen type I alpha 1 chain
Col3A1	Collagen type III alpha 1 chain
COX	Cyclooxigenase
CP-LFM	Colloidal probe lateral force microscopy
cryoTEM	Cryogenic transmission electron microscopy
DDS	Drug delivery system
DendriX	Dendrimer X
DendriXAL	Dendrimer X aggregated liposome
DiD	1,1′-dioctadecyl-3,3,3′,3′- tetramethylindodicarbocyanine, 4-chlorobenzenesulfonate salt
DLin-MC3-DMA	4-(dimethylamino)-butanoic acid, (10Z,13Z)-1-(9Z,12Z)-9,12-octadecadien-1-yl-10,13-nonadecadien-1-yl ester
DLS	Dynamic light scattering

DMAOD	Disease modifying anti-osteoarthritis drug
DMEM	Dulbecco's modified Eagle's medium
DPBS	Dulbecco's phosphate-buffered saline
DPPC	1,2-Dipalmitoyl-sn-glycero-3-phosphocholine
DSC	Differential scanning calorimetry
DSPC	Distearoylphosphatidylcholine
DSPE	1,2-Distearoyl-sn-glycero-3-phosphoethanolamine
DSPG	1,2-Distearoyl-sn-glycero-3-phospho-(10-rac-glycerol)
EE%	Encapsulation efficiency
EMA	European Medicines Agency
FCS	Fetal calf serum
FDA	Food and drug administration
GRAS	Generally recognized as safe
HA	Hyaluronic acid
HPLC	High-performance liquid chromatography
HSPC	Hydrogenated soybean phosphatidylcholine
IA	Intra-articular
IGF-1	Insulin-like growth factor-1
IL	Interleukin
L/D	Lipid-to-drug ratio

LC-MS	Liquid chromatography–mass spectrometry
LIPUS	Low-intensity pulsed ultrasound
LMP	Lipidic mesophase
LNP	Lipid-based nanoparticle
miRNA	Micro RNA
MMP	Matrix metalloproteinase
MO	Monoolein
mRNA	Messenger RNA
mTOR	Mammalian target of rapamycin
ncRNAs	Non-coding RNAs
NLC	Nanostructured lipid nanoparticle
NSAID	Non-steroid anti-inflammatory drug
NTA	Nanoparticle tracking analysis
OA	Osteoarthritis
OARSI	Osteoarthritis Research Society International
PAMAM	Poly(amidoamine)
PBS	Phosphate buffer saline
PDI	Polydispersity index
PEG	Polyethylene glycol
PI	Propidium iodide

PLGA	Poly(lactic-co-glycolic acid)
RA	Rheumatoid arthritis
RAMBA	retinoic acid metabolism blocking agent
RAPA	Rapamycin
RNA	Ribonucleic acid
RNAi	RNA interference
SAXS	Small-angle X-ray scattering
SEC	Size exclusion chromatography
SF	Synovial fibroblast
siRNA	Small interfering RNA
SLN	Solid lipid nanoparticle
SUV	Small unilamellar vesicle
TFA	Trifluoroacetic acid
TGFβ	Transforming growth factor beta
TNFα	Tumor necrosis factor alpha
WAXS	Wide-angle X-ray scattering
WOMAC	Western Ontario and McMaster Universities Arthritis
ZnAL	Zinc-aggregated liposome

References

[1] Q. Yao, X. Wu, C. Tao, W. Gong, M. Chen, M. Qu, Y. Zhong, T. He, S. Chen, G. Xiao, Osteoarthritis: pathogenic signaling pathways and therapeutic targets, Signal Transduct. Target. Ther. 2023 81. 8 (2023) 1–31. https://doi.org/10.1038/s41392-023-01330-w.

[2] A. De Luna, A. Otahal, S. Nehrer, Mesenchymal Stromal Cell-Derived Extracellular Vesicles – Silver Linings for Cartilage Regeneration?, Front. Cell Dev. Biol. 8 (2020) 1548. https://doi.org/10.3389/FCELL.2020.593386.

[3] U. Nedunchezhiyan, I. Varughese, A.R.J. Sun, X. Wu, R. Crawford, I. Prasadam, Obesity, Inflammation, and Immune System in Osteoarthritis, Front. Immunol. 13 (2022) 3505. https://doi.org/10.3389/FIMMU.2022.907750.

[4] S. Safiri, A.A. Kolahi, E. Smith, C. Hill, D. Bettampadi, M.A. Mansournia, D. Hoy, A. Ashrafi-Asgarabad, M. Sepidarkish, A. Almasi-Hashiani, G. Collins, J. Kaufman, M. Qorbani, M. Moradi-Lakeh, A.D. Woolf, F. Guillemin, L. March, M. Cross, Global, regional and national burden of osteoarthritis 1990-2017: a systematic analysis of the Global Burden of Disease Study 2017, Ann. Rheum. Dis. 79 (2020) 819–828. https://doi.org/10.1136/ANNRHEUMDIS-2019-216515.

[5] H. Long, Q. Liu, H. Yin, K. Wang, N. Diao, Y. Zhang, J. Lin, A. Guo, Prevalence Trends of Site-Specific Osteoarthritis From 1990 to 2019: Findings From the Global Burden of Disease Study 2019, Arthritis Rheumatol. 74 (2022) 1172–1183. https://doi.org/10.1002/ART.42089.

[6] J. Lo, L. Chan, S. Flynn, A Systematic Review of the Incidence, Prevalence, Costs, and Activity and Work Limitations of Amputation, Osteoarthritis, Rheumatoid Arthritis, Back Pain, Multiple Sclerosis, Spinal Cord Injury, Stroke, and Traumatic Brain Injury in the United States: A 2019 Update, Arch. Phys. Med. Rehabil. 102 (2021) 115–131. https://doi.org/10.1016/J.APMR.2020.04.001.

[7] S.X. Wang, A.X. Ganguli, A. Bodhani, J.K. Medema, W.M. Reichmann, D. Macaulay, Healthcare resource utilization and costs by age and joint location among osteoarthritis patients in a privately insured population, J. Med. Econ. 20 (2017) 1299–1306. https://doi.org/10.1080/13696998.2017.1377717.

[8] Q. Liu, J. Niu, H. Li, Y. Ke, R. Li, Y. Zhang, J. Lin, Knee Symptomatic Osteoarthritis, Walking Disability, NSAIDs Use and All-cause Mortality: Population-based Wuchuan Osteoarthritis Study, Sci. Reports 2017 71. 7 (2017) 1–7. https://doi.org/10.1038/s41598-017-03110-3.

[9] M.S. O'Brien, J.J. McDougall, Age and frailty as risk factors for the development of osteoarthritis, Mech. Ageing Dev. 180 (2019) 21–28. https://doi.org/10.1016/J.MAD.2019.03.003.

[10] P.K. Sacitharan, Ageing and osteoarthritis, Subcell. Biochem. 91 (2019) 123–159. https://doi.org/10.1007/978-981-13-3681-2_6.

[11] R.F. Loeser, J.A. Collins, B.O. Diekman, Ageing and the pathogenesis of osteoarthritis, Nat. Rev. Rheumatol. 2016 127. 12 (2016) 412–420. https://doi.org/10.1038/nrrheum.2016.65.

[12] C. Reyes, K.M. Leyland, G. Peat, C. Cooper, N.K. Arden, D. Prieto-Alhambra, Association Between Overweight and Obesity and Risk of Clinically Diagnosed Knee, Hip, and Hand Osteoarthritis: A Population-Based Cohort Study, Arthritis Rheumatol. 68 (2016) 1869–1875. https://doi.org/10.1002/ART.39707.

[13] B. Raud, C. Gay, C. Guiguet-Auclair, A. Bonnin, L. Gerbaud, B. Pereira, M. Duclos, Y. Boirie, E. Coudeyre, Level of obesity is directly associated with the clinical and functional consequences of knee osteoarthritis, Sci. Reports 2020 101. 10 (2020) 1–7. https://doi.org/10.1038/s41598-020-60587-1.

[14] D.J. Hunter, S. Bierma-Zeinstra, Osteoarthritis, Lancet. 393 (2019) 1745–1759. https://doi.org/10.1016/S0140-6736(19)30417-9.

[15] A. Maglaviceanu, B. Wu, M. Kapoor, Fibroblast-like synoviocytes: Role in synovial fibrosis associated with osteoarthritis, Wound Repair Regen. 29 (2021) 642–649. https://doi.org/10.1111/WRR.12939.

[16] S. Glyn-Jones, A.J.R. Palmer, R. Agricola, A.J. Price, T.L. Vincent, H. Weinans, A.J. Carr, Osteoarthritis, Lancet. 386 (2015) 376–387. https://doi.org/10.1016/S0140-6736(14)60802-3.

[17] H. Zhang, D. Cai, X. Bai, Macrophages regulate the progression of osteoarthritis, Osteoarthr. Cartil. 28 (2020) 555–561. https://doi.org/10.1016/J.JOCA.2020.01.007.

[18] A.M. Silverstein, R.M. Stefani, E. Sobczak, E.L. Tong, M.G. Attur, R.P. Shah, J.C. Bulinski, G.A. Ateshian, C.T. Hung, Toward understanding the role of cartilage particulates in synovial inflammation, Osteoarthr. Cartil. 25 (2017) 1353–1361. https://doi.org/10.1016/J.JOCA.2017.03.015.

[19] E.G. Estell, A.M. Silverstein, R.M. Stefani, A.J. Lee, L.A. Murphy, R.P. Shah, G.A. Ateshian, C.T. Hung, Cartilage Wear Particles Induce an Inflammatory Response Similar to Cytokines in Human Fibroblast-Like Synoviocytes, J. Orthop. Res. 37 (2019) 1979–1987. https://doi.org/10.1002/JOR.24340.

[20] S. Jahn, J. Seror, J. Klein, Lubrication of Articular Cartilage, Annu. Rev. Biomed. Eng. 18 (2016) 235–258. https://doi.org/10.1146/ANNUREV-BIOENG-081514-123305.

[21] H. Yuan, L.L.E. Mears, Y. Wang, R. Su, W. Qi, Z. He, M. Valtiner, Lubricants for osteoarthritis treatment: From natural to bioinspired and alternative strategies, Adv. Colloid Interface Sci. 311 (2023) 102814. https://doi.org/10.1016/J.CIS.2022.102814.

[22] T.E. Ludwig, J.R. McAllister, V. Lun, J.P. Wiley, T.A. Schmidt, Diminished cartilage-lubricating ability of human osteoarthritic synovial fluid deficient in proteoglycan 4: Restoration through proteoglycan 4 supplementation, Arthritis Rheum. 64 (2012) 3963–3971. https://doi.org/10.1002/ART.34674.

[23] D.T. Felson, The sources of pain in knee osteoarthritis: Editorial review, Curr. Opin. Rheumatol. 17 (2005)

624–628. https://doi.org/10.1097/01.BOR.0000172800.49120.97.

[24] B. Abramoff, F.E. Caldera, Osteoarthritis: Pathology, Diagnosis, and Treatment Options, Med. Clin. North Am. 104 (2020) 293–311. https://doi.org/10.1016/J.MCNA.2019.10.007.

[25] A.J. Goff, D. De Oliveira Silva, M. Merolli, E.C. Bell, K.M. Crossley, C.J. Barton, Patient education improves pain and function in people with knee osteoarthritis with better effects when combined with exercise therapy: a systematic review, J. Physiother. 67 (2021) 177–189. https://doi.org/10.1016/J.JPHYS.2021.06.011.

[26] M. Fransen, S. McConnell, A.R. Harmer, M. Van Der Esch, M. Simic, K.L. Bennell, Exercise for osteoarthritis of the knee: a Cochrane systematic review, Br. J. Sports Med. 49 (2015) 1554–1557. https://doi.org/10.1136/BJSPORTS-2015-095424.

[27] M. Fransen, S. Mcconnell, G. Hernandez-Molina, S. Reichenbach, Exercise for osteoarthritis of the hip, Cochrane Database Syst. Rev. 2014 (2014). https://doi.org/10.1002/14651858.CD007912.PUB2.

[28] I.A. Jones, R. Togashi, M.L. Wilson, N. Heckmann, C.T. Vangsness, Intra-articular treatment options for knee osteoarthritis, Nat. Rev. Rheumatol. 2018 152. 15 (2018) 77–90. https://doi.org/10.1038/s41584-018-0123-4.

[29] Y. Song, J. Zhang, H. Xu, Z. Lin, H. Chang, W. Liu, L. Kong, Mesenchymal stem cells in knee osteoarthritis treatment: A systematic review and meta-analysis, J. Orthop. Transl. 24 (2020) 121–130. https://doi.org/10.1016/J.JOT.2020.03.015.

[30] S.T. Skou, E.M. Roos, M.B. Laursen, M.S. Rathleff, L. Arendt-Nielsen, O. Simonsen, S. Rasmussen, A Randomized, Controlled Trial of Total Knee Replacement, N. Engl. J. Med. 373 (2015) 1597–1606. https://doi.org/10.1056/NEJMOA1505467.

[31] A. Perl, Activation of mTOR (mechanistic target of rapamycin) in rheumatic diseases, Nat. Rev. Rheumatol. 2015 123. 12 (2015) 169–182. https://doi.org/10.1038/nrrheum.2015.172.

[32] H. Sasaki, K. Takayama, T. Matsushita, K. Ishida, S. Kubo, T. Matsumoto, N. Fujita, S. Oka, M. Kurosaka, R. Kuroda, Autophagy modulates osteoarthritis-related gene expression in human chondrocytes, Arthritis Rheum. 64 (2012) 1920–1928. https://doi.org/10.1002/ART.34323.

[33] K. Takayama, Y. Kawakami, M. Kobayashi, N. Greco, J.H. Cummins, T. Matsushita, R. Kuroda, M. Kurosaka, F.H. Fu, J. Huard, Local intra-articular injection of rapamycin delays articular cartilage degeneration in a murine model of osteoarthritis, Arthritis Res. Ther. 16 (2014) 1–10. https://doi.org/10.1186/S13075-014-0482-4.

[34] T. Matsuzaki, T. Matsushita, Y. Tabata, T. Saito, T. Matsumoto, K. Nagai, R. Kuroda, M. Kurosaka, Intra-articular administration of gelatin hydrogels incorporating rapamycin–micelles reduces the development of

experimental osteoarthritis in a murine model, Biomaterials. 35 (2014) 9904–9911. https://doi.org/10.1016/J.BIOMATERIALS.2014.08.041.

[35] B. Caramés, A. Hasegawa, N. Taniguchi, S. Miyaki, F.J. Blanco, M. Lotz, Autophagy activation by rapamycin reduces severity of experimental osteoarthritis, Ann. Rheum. Dis. 71 (2012) 575–581. https://doi.org/10.1136/ANNRHEUMDIS-2011-200557.

[36] L. Zhu, P. Kamalathevan, L.A. Koneva, J.M. Zarebska, A. Chanalaris, H. Ismail, A. Wiberg, M. Ng, H. Muhammad, J. Walsby-Tickle, J.S.O. McCullagh, F.E. Watt, S.N. Sansom, D. Furniss, M.D. Gardiner, T.L. Vincent, Variants in ALDH1A2 reveal an anti-inflammatory role for retinoic acid and a new class of disease-modifying drugs in osteoarthritis, Sci. Transl. Med. 14 (2022). https://doi.org/10.1126/SCITRANSLMED.ABM4054.

[37] Y. Cho, S. Jeong, H. Kim, D. Kang, J. Lee, S.-B. Kang, J.-H. Kim, Disease-modifying therapeutic strategies in osteoarthritis: current status and future directions, Exp. Mol. Med. 2021 5311. 53 (2021) 1689–1696. https://doi.org/10.1038/s12276-021-00710-y.

[38] W.M. Oo, S.P.C. Yu, M.S. Daniel, D.J. Hunter, Disease-modifying drugs in osteoarthritis: current understanding and future therapeutics, Expert Opin. Emerg. Drugs. 23 (2018) 331–347. https://doi.org/10.1080/14728214.2018.1547706.

[39] M. Di Francesco, A. Fragassi, M. Pannuzzo, M. Ferreira, S. Brahmachari, P. Decuzzi, Management of osteoarthritis: From drug molecules to nano/micromedicines, Wiley Interdiscip. Rev. Nanomedicine Nanobiotechnology. 14 (2022) e1780. https://doi.org/10.1002/WNAN.1780.

[40] X. Li, B. Dai, J. Guo, L. Zheng, Q. Guo, J. Peng, J. Xu, L. Qin, Nanoparticle–Cartilage Interaction: Pathology-Based Intra-articular Drug Delivery for Osteoarthritis Therapy, Nano-Micro Lett. 2021 131. 13 (2021) 1–48. https://doi.org/10.1007/S40820-021-00670-Y.

[41] C. Albert, O. Brocq, D. Gerard, C. Roux, L. Euller-Ziegler, Septic knee arthritis after intra-articular hyaluronate injection: Two case reports, Jt. Bone Spine. 73 (2006) 205–207. https://doi.org/10.1016/J.JBSPIN.2005.03.005.

[42] M. Cao, M.T.Y. Ong, P.S.H. Yung, R.S. Tuan, Y. Jiang, Role of synovial lymphatic function in osteoarthritis, Osteoarthr. Cartil. 30 (2022) 1186–1197. https://doi.org/10.1016/J.JOCA.2022.04.003.

[43] S. Brown, S. Kumar, B. Sharma, Intra-articular targeting of nanomaterials for the treatment of osteoarthritis, Acta Biomater. 93 (2019) 239–257. https://doi.org/10.1016/J.ACTBIO.2019.03.010.

[44] H. Derendorf, H. Möllmann, A. Grüner, D. Haack, G. Gyselby, Pharmacokinetics and pharmacodynamics of glucocorticoid suspensions after intra-articular administration, Clin. Pharmacol. Ther. 39 (1986) 313–317. https://doi.org/10.1038/CLPT.1986.45.

[45] J. Gao, Z. Xia, H.B. Mary, J. Joseph, J.N. Luo, N. Joshi, Overcoming barriers for intra-articular delivery of disease-modifying osteoarthritis drugs, Trends Pharmacol. Sci. 43 (2022) 171–187. https://doi.org/10.1016/J.TIPS.2021.12.004.

[46] H. Huang, Z. Lou, S. Zheng, J. Wu, Q. Yao, R. Chen, L. Kou, D. Chen, Intra-articular drug delivery systems for osteoarthritis therapy: shifting from sustained release to enhancing penetration into cartilage, Drug Deliv. 29 (2022) 767–791. https://doi.org/10.1080/10717544.2022.2048130.

[47] Z. Wang, S. Wang, K. Wang, X. Wu, C. Tu, C. Gao, Stimuli-Sensitive Nanotherapies for the Treatment of Osteoarthritis, Macromol. Biosci. 21 (2021) 2100280. https://doi.org/10.1002/MABI.202100280.

[48] U. Kauscher, M.N. Holme, M. Björnmalm, M.M. Stevens, Physical stimuli-responsive vesicles in drug delivery: Beyond liposomes and polymersomes, Adv. Drug Deliv. Rev. 138 (2019) 259–275. https://doi.org/10.1016/J.ADDR.2018.10.012.

[49] J. Pradal, P. Maudens, C. Gabay, C.A. Seemayer, O. Jordan, E. Allémann, Effect of particle size on the biodistribution of nano- and microparticles following intra-articular injection in mice, Int. J. Pharm. 498 (2016) 119–129. https://doi.org/10.1016/J.IJPHARM.2015.12.015.

[50] J.A. Champion, A. Walker, S. Mitragotri, Role of particle size in phagocytosis of polymeric microspheres, Pharm. Res. 25 (2008) 1815–1821. https://doi.org/10.1007/S11095-008-9562-Y.

[51] X. Lin, C.T. Tsao, M. Kyomoto, M. Zhang, Injectable Natural Polymer Hydrogels for Treatment of Knee Osteoarthritis, Adv. Healthc. Mater. 11 (2022) 2101479. https://doi.org/10.1002/ADHM.202101479.

[52] M. Rahimi, G. Charmi, K. Matyjaszewski, X. Banquy, J. Pietrasik, Recent developments in natural and synthetic polymeric drug delivery systems used for the treatment of osteoarthritis, Acta Biomater. 123 (2021) 31–50. https://doi.org/10.1016/J.ACTBIO.2021.01.003.

[53] K. He, X. Huang, R. Shan, X. Yang, R. Song, F. Xie, G. Huang, Intra-articular Injection of Lornoxicam and MicroRNA-140 Co-loaded Cationic Liposomes Enhanced the Therapeutic Treatment of Experimental Osteoarthritis, AAPS PharmSciTech. 23 (2022) 1–17. https://doi.org/10.1208/S12249-021-02149-W.

[54] Y. Zhong, Y. Zhou, R. Ding, L. Zou, H. Zhang, X. Wei, D. He, Intra-articular treatment of temporomandibular joint osteoarthritis by injecting actively-loaded meloxicam liposomes with dual-functions of anti-inflammation and lubrication, Mater. Today Bio. 19 (2023) 100573. https://doi.org/10.1016/J.MTBIO.2023.100573.

[55] V.A. Guilherme, L.N.M. Ribeiro, A.C.S. Alcântara, S.R. Castro, G.H. Rodrigues da Silva, C.G. da Silva, M.C. Breitkreitz, J. Clemente-Napimoga, C.G. Macedo, H.B. Abdalla, R. Bonfante, C.M.S. Cereda, E. de Paula, Improved efficacy of naproxen-loaded NLC for temporomandibular joint administration, Sci. Reports 2019 91. 9 (2019) 1–11. https://doi.org/10.1038/s41598-019-47486-w.

[56] R.I. El-Gogary, M.A. Khattab, H. Abd-Allah, Intra-articular multifunctional celecoxib loaded hyaluronan nanocapsules for the suppression of inflammation in an osteoarthritic rat model, Int. J. Pharm. 583 (2020) 119378. https://doi.org/10.1016/J.IJPHARM.2020.119378.

[57] Y. Lei, X. Wang, J. Liao, J. Shen, Y. Li, Z. Cai, N. Hu, X. Luo, W. Cui, W. Huang, Shear-responsive boundary-lubricated hydrogels attenuate osteoarthritis, Bioact. Mater. 16 (2022) 472–484. https://doi.org/10.1016/J.BIOACTMAT.2022.02.016.

[58] D.J. Hunter, C.C. Chang, J.C.C. Wei, H.Y. Lin, C. Brown, T.T. Tai, C.F. Wu, W.C.M. Chuang, S.F. Shih, TLC599 in patients with osteoarthritis of the knee: a phase IIa, randomized, placebo-controlled, dose-finding study, Arthritis Res. Ther. 24 (2022) 1–11. https://doi.org/10.1186/S13075-022-02739-4.

[59] E. Singh, R. Banerjee, In vivo efficacy & phantom imaging connote the theranostic potential of a drug-loaded lipid nanobubble, J. Drug Deliv. Sci. Technol. 74 (2022) 103568. https://doi.org/10.1016/J.JDDST.2022.103568.

[60] J. Yang, Y. Zhu, F. Wang, L. Deng, X. Xu, W. Cui, Microfluidic liposomes-anchored microgels as extended delivery platform for treatment of osteoarthritis, Chem. Eng. J. 400 (2020) 126004. https://doi.org/10.1016/J.CEJ.2020.126004.

[61] X. Chen, L. Zhang, X. Shao, W. Gong, T. Shi, J. Dong, Y. Shi, S. Shen, Y. He, J. Qin, J. Lu, Q. Jiang, B. Guo, X. Chen, L. Zhang, X.Y. Shao, W. Gong, T.S. Shi, J. Dong, Y. Shi, S.Y. Shen, Y. He, J.H. Qin, Q. Jiang, B.S. Guo, Specific Clearance of Senescent Synoviocytes Suppresses the Development of Osteoarthritis based on Aptamer-Functionalized Targeted Drug Delivery System, Adv. Funct. Mater. 32 (2022) 2109460. https://doi.org/10.1002/ADFM.202109460.

[62] H.M. Ebada, M.M. Nasra, R.A. Nassra, A.A. Solaiman, O.Y. Abdallah, Cationic nanocarrier of rhein based on hydrophobic ion pairing approach as intra-articular targeted regenerative therapy for osteoarthritis, Colloids Surfaces B Biointerfaces. 211 (2022) 112285. https://doi.org/10.1016/J.COLSURFB.2021.112285.

[63] H.M.K. Ebada, M.M.A. Nasra, R.A. Nassra, O.Y. Abdallah, Chondroitin sulfate-functionalized lipid nanoreservoirs: a novel cartilage-targeting approach for intra-articular delivery of cassic acid for osteoarthritis treatment, Drug Deliv. 29 (2022) 652–663. https://doi.org/10.1080/10717544.2022.2041130.

[64] X. Liang, Y. Chen, L. Wu, A. Maharjan, B. Regmi, J. Zhang, S. Gui, In situ hexagonal liquid crystal for intra-articular delivery of sinomenine hydrochloride, Biomed. Pharmacother. 117 (2019) 108993. https://doi.org/10.1016/J.BIOPHA.2019.108993.

[65] X. Ai, Y. Duan, Q. Zhang, D. Sun, R.H. Fang, R. Liu-Bryan, W. Gao, L. Zhang, Cartilage-targeting ultrasmall lipid-polymer hybrid nanoparticles for the prevention of cartilage degradation, Bioeng. Transl. Med. 6 (2021) e10187. https://doi.org/10.1002/BTM2.10187.

[66] Y. He, M. Sun, J. Wang, X. Yang, C. Lin, L. Ge, C. Ying, K. Xu, A. Liu, L. Wu, Chondroitin sulfate

microspheres anchored with drug-loaded liposomes play a dual antioxidant role in the treatment of osteoarthritis, Acta Biomater. 151 (2022) 512–527. https://doi.org/10.1016/J.ACTBIO.2022.07.052.

[67] C.H. Chen, S.M. Kuo, Y.C. Tien, P.C. Shen, Y.W. Kuo, H.H. Huang, Steady Augmentation of Anti-Osteoarthritic Actions of Rapamycin by Liposome-Encapsulation in Collaboration with Low-Intensity Pulsed Ultrasound , Int. J. Nanomedicine. 15 (2020) 3771–3790. https://doi.org/10.2147/IJN.S252223.

[68] Y. Lei, Y. Wang, J. Shen, Z. Cai, C. Zhao, H. Chen, X. Luo, N. Hu, W. Cui, W. Huang, Injectable hydrogel microspheres with self-renewable hydration layers alleviate osteoarthritis, Sci. Adv. 8 (2022). https://doi.org/10.1126/SCIADV.ABL6449.

[69] G. Bordon, S.N. Ramakrishna, S.G. Edalat, R. Eugster, A. Arcifa, S. Aleandri, M.F. Bertoncelj, L. Isa, R. Crockett, O. Distler, P. Luciani, Liposomal aggregates sustain the release of rapamycin and protect cartilage from friction, BioRxiv. (2023) 2023.03.23.533793. https://doi.org/10.1101/2023.03.23.533793.

[70] Y. Liang, X. Xu, X. Li, J. Xiong, B. Li, L. Duan, D. Wang, J. Xia, Chondrocyte-Targeted MicroRNA Delivery by Engineered Exosomes toward a Cell-Free Osteoarthritis Therapy, ACS Appl. Mater. Interfaces. 12 (2020) 36938–36947. https://doi.org/10.1021/ACSAMI.0C10458.

[71] X. Yu, T. Xu, H. Shi, J. Hong, X. Jin, L. Cao, J. Wang, Y. Lin, Z. Pan, S. Wang, J. Fang, K. Xu, H. Song, Z. Zhou, S. Zhu, J. Yin, Y. Qi, X. Dai, Cartilage-targeting mRNA-lipid nanoparticles rescue perifocal apoptotic chondrocytes for integrative cartilage repair, Chem. Eng. J. 465 (2023) 142841. https://doi.org/10.1016/J.CEJ.2023.142841.

[72] M.J. Richard, J.B. Driban, T.E. McAlindon, Pharmaceutical treatment of osteoarthritis, Osteoarthr. Cartil. 31 (2023) 458–466. https://doi.org/10.1016/J.JOCA.2022.11.005.

[73] R.R. Bannuru, M.C. Osani, E.E. Vaysbrot, N.K. Arden, K. Bennell, S.M.A. Bierma-Zeinstra, V.B. Kraus, L.S. Lohmander, J.H. Abbott, M. Bhandari, F.J. Blanco, R. Espinosa, I.K. Haugen, J. Lin, L.A. Mandl, E. Moilanen, N. Nakamura, L. Snyder-Mackler, T. Trojian, M. Underwood, T.E. McAlindon, OARSI guidelines for the non-surgical management of knee, hip, and polyarticular osteoarthritis, Osteoarthr. Cartil. 27 (2019) 1578–1589. https://doi.org/10.1016/J.JOCA.2019.06.011.

[74] S.L. Kolasinski, T. Neogi, M.C. Hochberg, C. Oatis, G. Guyatt, J. Block, L. Callahan, C. Copenhaver, C. Dodge, D. Felson, K. Gellar, W.F. Harvey, G. Hawker, E. Herzig, C.K. Kwoh, A.E. Nelson, J. Samuels, C. Scanzello, D. White, B. Wise, R.D. Altman, D. DiRenzo, J. Fontanarosa, G. Giradi, M. Ishimori, D. Misra, A.A. Shah, A.K. Shmagel, L.M. Thoma, M. Turgunbaev, A.S. Turner, J. Reston, 2019 American College of Rheumatology/Arthritis Foundation Guideline for the Management of Osteoarthritis of the Hand, Hip, and Knee, Arthritis Care Res. 72 (2020) 149–162. https://doi.org/10.1002/ACR.24131.

[75] R.H. Quinn, J. Murray, R. Pezold, Q. Hall, Management of Osteoarthritis of the Hip, J. Am. Acad. Orthop. Surg. 26 (2018) E434–E436. https://doi.org/10.5435/JAAOS-D-18-00351.

[76] O. Bruyère, G. Honvo, N. Veronese, N.K. Arden, J. Branco, E.M. Curtis, N.M. Al-Daghri, G. Herrero-Beaumont, J. Martel-Pelletier, J.P. Pelletier, F. Rannou, R. Rizzoli, R. Roth, D. Uebelhart, C. Cooper, J.Y. Reginster, An updated algorithm recommendation for the management of knee osteoarthritis from the European Society for Clinical and Economic Aspects of Osteoporosis, Osteoarthritis and Musculoskeletal Diseases (ESCEO), Semin. Arthritis Rheum. 49 (2019) 337–350. https://doi.org/10.1016/J.SEMARTHRIT.2019.04.008.

[77] C. Cooper, R. Chapurlat, N. Al-Daghri, G. Herrero-Beaumont, O. Bruyère, F. Rannou, R. Roth, D. Uebelhart, J.Y. Reginster, Safety of Oral Non-Selective Non-Steroidal Anti-Inflammatory Drugs in Osteoarthritis: What Does the Literature Say?, Drugs and Aging. 36 (2019) 15–24. https://doi.org/10.1007/S40266-019-00660-1.

[78] A.M. Schjerning, P. McGettigan, G. Gislason, Cardiovascular effects and safety of (non-aspirin) NSAIDs, Nat. Rev. Cardiol. 2020 179. 17 (2020) 574–584. https://doi.org/10.1038/s41569-020-0366-z.

[79] L.J. Hunter, D.M. Wood, P.I. Dargan, The patterns of toxicity and management of acute nonsteroidal anti-inflammatory drug (NSAID) overdose, Open Access Emerg. Med. 3 (2011) 39–48. https://doi.org/10.2147/OAEM.S22795.

[80] T. Subongkot, Combined effect of sonophoresis and a microemulsion on the dermal delivery of celecoxib, Drug Deliv. 27 (2020) 1087–1093. https://doi.org/10.1080/10717544.2020.1797244.

[81] G. Singh, J.G. Fort, J.L. Goldstein, R.A. Levy, P.S. Hanrahan, A.E. Bello, L. Andrade-Ortega, C. Wallemark, N.M. Agrawal, G.M. Eisen, W.F. Stenson, G. Triadafilopoulos, Celecoxib Versus Naproxen and Diclofenac in Osteoarthritis Patients: SUCCESS-I Study, Am. J. Med. 119 (2006) 255–266. https://doi.org/10.1016/J.AMJMED.2005.09.054.

[82] L.N.M. Ribeiro, M.C. Breitkreitz, V.A. Guilherme, G.H.R. da Silva, V.M. Couto, S.R. Castro, B.O. de Paula, D. Machado, E. de Paula, Natural lipids-based NLC containing lidocaine: from pre-formulation to in vivo studies, Eur. J. Pharm. Sci. 106 (2017) 102–112. https://doi.org/10.1016/J.EJPS.2017.05.060.

[83] R. Tenchov, R. Bird, A.E. Curtze, Q. Zhou, Lipid Nanoparticles from Liposomes to mRNA Vaccine Delivery, a Landscape of Research Diversity and Advancement, ACS Nano. 15 (2021) 16982–17015. https://doi.org/10.1021/ACSNANO.1C04996.

[84] H. Berry, H.A. Bird, C. Black, D.R. Blake, A.M. Freeman, D.N. Golding, E.B.D. Hamilton, M.I.V. Jayson, B. Kidd, H. Kohn, R. Million, S. Ollier, I. Smith, B.D. Williams, A.D. Woolf, A double blind, multicentre, placebo controlled trial of lornoxicam in patients with osteoarthritis of the hip and knee., Ann. Rheum. Dis. 51 (1992) 238–242. https://doi.org/10.1136/ARD.51.2.238.

[85] K. Pavelka, A comparison of the therapeutic efficacy of diclofenac in osteoarthritis: a systematic review of randomised controlled trials, Curr. Med. Res. Opin. 28 (2011) 163–178.

https://doi.org/10.1185/03007995.2011.649848.

[86] R. Newton, Molecular mechanisms of glucocorticoid action: what is important?, Thorax. 55 (2000) 603–613. https://doi.org/10.1136/THORAX.55.7.603.

[87] R. Kijowski, Risks and Benefits of Intra-articular Corticosteroid Injection for Treatment of Osteoarthritis: What radiologists and patients need to know, Radiology. 293 (2019) 664–665. https://doi.org/10.1148/RADIOL.2019192034.

[88] A. Stout, J. Friedly, C.J. Standaert, Systemic Absorption and Side Effects of Locally Injected Glucocorticoids, PM&R. 11 (2019) 409–419. https://doi.org/10.1002/PMRJ.12042.

[89] A. de Leon, R. Perera, P. Nittayacharn, M. Cooley, O. Jung, A.A. Exner, Ultrasound Contrast Agents and Delivery Systems in Cancer Detection and Therapy, Adv. Cancer Res. 139 (2018) 57–84. https://doi.org/10.1016/BS.ACR.2018.04.002.

[90] H.P. Marti, F.J. Frey, Nephrotoxicity of rapamycin: an emerging problem in clinical medicine, Nephrol. Dial. Transplant. 20 (2005) 13–15. https://doi.org/10.1093/NDT/GFH639.

[91] S. Merkel, N. Mogilevskaja, M. Mengel, H. Haller, A. Schwarz, Side Effects of Sirolimus, Transplant. Proc. 38 (2006) 714–715. https://doi.org/10.1016/j.transproceed.2006.01.044.

[92] N. Pallet, C. Legendre, Adverse events associated with mTOR inhibitors, Expert Opin. Drug Saf. 12 (2013) 177–186. https://doi.org/10.1517/14740338.2013.752814.

[93] M. Raish, A. Ahmad, M. Shahid, Y.A.B. Jardan, A. Ahad, M.A. Kalam, M.A. Ansari, M. Iqbal, N. Ali, K.M. Alkharfy, F.I. Al-Jenoobi, Effects of Apigenin on Pharmacokinetics of Dasatinib and Probable Interaction Mechanism, Mol. 2023, Vol. 28, Page 1602. 28 (2023) 1602. https://doi.org/10.3390/MOLECULES28041602.

[94] C. Lee, H. Guo, W. Klinngam, S.R. Janga, F. Yarber, S. Peddi, M.C. Edman, N. Tiwari, S. Liu, S.G. Louie, S.F. Hamm-Alvarez, J.A. Mackay, Berunda Polypeptides: Biheaded Rapamycin Carriers for Subcutaneous Treatment of Autoimmune Dry Eye Disease, Mol. Pharm. (2019). https://doi.org/10.1021/ACS.MOLPHARMACEUT.9B00263.

[95] P.R. Coryell, B.O. Diekman, R.F. Loeser, Mechanisms and therapeutic implications of cellular senescence in osteoarthritis, Nat. Rev. Rheumatol. 2020 171. 17 (2020) 47–57. https://doi.org/10.1038/s41584-020-00533-7.

[96] J.N. Justice, A.M. Nambiar, T. Tchkonia, N.K. LeBrasseur, R. Pascual, S.K. Hashmi, L. Prata, M.M. Masternak, S.B. Kritchevsky, N. Musi, J.L. Kirkland, Senolytics in idiopathic pulmonary fibrosis: Results from a first-in-human, open-label, pilot study, EBioMedicine. 40 (2019) 554–563. https://doi.org/10.1016/J.EBIOM.2018.12.052.

[97] A. Nambiar, D. Kellogg, J. Justice, M. Goros, J. Gelfond, R. Pascual, S. Hashmi, M. Masternak, L. Prata, N. LeBrasseur, A. Limper, S. Kritchevsky, N. Musi, T. Tchkonia, J. Kirkland, Senolytics dasatinib and quercetin in idiopathic pulmonary fibrosis: results of a phase I, single-blind, single-center, randomized, placebo-controlled pilot trial on feasibility and tolerability, EBioMedicine. 90 (2023) 104481. https://doi.org/10.1016/j.ebiom.2023.104481.

[98] G. Zhu, X. Chen, Aptamer-based targeted therapy, Adv. Drug Deliv. Rev. 134 (2018) 65–78. https://doi.org/10.1016/J.ADDR.2018.08.005.

[99] G. Cai, G. Jones, F.M. Cicuttini, A.E. Wluka, Y. Wang, C. Hill, H. Keen, B. Antony, X. Wang, B. de Graaff, M. Thompson, T. Winzenberg, K. Buttigieg, D. Aitken, Study protocol for a randomised controlled trial of diacerein versus placebo to treat knee osteoarthritis with effusion-synovitis (DICKENS), Trials. 23 (2022) 1–16. https://doi.org/10.1186/S13063-022-06715-W.

[100] G.N. Smith, S.L. Myers, K.D. Brandt, E.A. Mickler, M.E. Albrecht, Diacerhein treatment reduces the severity of osteoarthritis in the canine cruciate-deficiency model of osteoarthritis, Arthritis Rheum. 42 (1999) 545–554. https://doi.org/10.1002/1529-0131.

[101] PRAC re-examines diacerein and recommends that it remain available with restrictions | European Medicines Agency, (n.d.). https://www.ema.europa.eu/en/news/prac-re-examines-diacerein-recommends-it-remain-available-restrictions (accessed May 7, 2023).

[102] R. Paliwal, S.R. Paliwal, R. Kenwat, B. Das Kurmi, M.K. Sahu, Solid lipid nanoparticles: a review on recent perspectives and patents, Expert Opin. Ther. Pat. 30 (2020) 179–194. https://doi.org/10.1080/13543776.2020.1720649.

[103] Y.X. Gao, B.F. Cheng, J.J. Lian, D.D. Guo, J.W. Qin, Y.B. Zhang, H.J. Yang, M. Wang, L. Wang, Z.W. Feng, Liquiritin, a flavone compound from licorice, inhibits IL-1β-induced inflammatory responses in SW982 human synovial cells, J. Funct. Foods. 33 (2017) 142–148. https://doi.org/10.1016/J.JFF.2017.03.039.

[104] C. Yu, H. Zang, C. Yang, D. Liang, S. Quan, D. Li, Y. Li, Q. Dong, F. Wang, L. Li, Study of chondroitin sulfate E oligosaccharide as a promising complement C5 inhibitor for osteoarthritis alleviation, Mater. Sci. Eng. C. 127 (2021) 112234. https://doi.org/10.1016/J.MSEC.2021.112234.

[105] S. Zhou, W. Lu, L. Chen, Q. Ge, D. Chen, Z. Xu, D. Shi, J. Dai, J. Li, H. Ju, Y. Cao, J. Qin, S. Chen, H. Teng, Q. Jiang, AMPK deficiency in chondrocytes accelerated the progression of instability-induced and ageing-associated osteoarthritis in adult mice, Sci. Reports 2017 71. 7 (2017) 1–14. https://doi.org/10.1038/srep43245.

[106] L.Y. Chen, Y. Wang, R. Terkeltaub, R. Liu-Bryan, Activation of AMPK-SIRT3 signaling is chondroprotective by preserving mitochondrial DNA integrity and function, Osteoarthr. Cartil. 26 (2018)

1539–1550. https://doi.org/10.1016/J.JOCA.2018.07.004.

[107] P. Xia, S. Shen, Q. Lin, K. Cheng, S. Ren, M. Gao, X. Li, Low-Intensity Pulsed Ultrasound Treatment at an Early Osteoarthritis Stage Protects Rabbit Cartilage From Damage via the Integrin/Focal Adhesion Kinase/Mitogen-Activated Protein Kinase Signaling Pathway, J. Ultrasound Med. 34 (2015) 1991–1999. https://doi.org/10.7863/ULTRA.14.10016.

[108] P. Chen, C. Xia, S. Mei, J. Wang, Z. Shan, X. Lin, S. Fan, Intra-articular delivery of sinomenium encapsulated by chitosan microspheres and photo-crosslinked GelMA hydrogel ameliorates osteoarthritis by effectively regulating autophagy, Biomaterials. 81 (2016) 1–13. https://doi.org/10.1016/J.BIOMATERIALS.2015.12.006.

[109] Y. Jiang, M. Gao, W. Wang, Y. Lang, Z. Tong, K. Wang, H. Zhang, G. Chen, M. Liu, Y. Yao, X. Xiao, Sinomenine Hydrochloride Protects against Polymicrobial Sepsis via Autophagy, Int. J. Mol. Sci. 2015, Vol. 16, Pages 2559-2573. 16 (2015) 2559–2573. https://doi.org/10.3390/IJMS16022559.

[110] S. Aleandri, R. Mezzenga, The physics of lipidic mesophase delivery systems, Phys. Today. 73 (2020) 38. https://doi.org/10.1063/PT.3.4522.

[111] L. Zhou, L.E. Rubin, C. Liu, Y. Chen, Short Interfering RNA (siRNA)-Based Therapeutics for Cartilage Diseases, Regen. Eng. Transl. Med. 7 (2021) 283–290. https://doi.org/10.1007/S40883-020-00149-Z.

[112] C. Rinaldi, M.J.A. Wood, Antisense oligonucleotides: the next frontier for treatment of neurological disorders, Nat. Rev. Neurol. 2017 141. 14 (2017) 9–21. https://doi.org/10.1038/nrneurol.2017.148.

[113] J.K.W. Lam, M.Y.T. Chow, Y. Zhang, S.W.S. Leung, siRNA Versus miRNA as Therapeutics for Gene Silencing, Mol. Ther. - Nucleic Acids. 4 (2015) e252. https://doi.org/10.1038/MTNA.2015.23.

[114] R. Kole, A.R. Krainer, S. Altman, RNA therapeutics: beyond RNA interference and antisense oligonucleotides, Nat. Rev. Drug Discov. 2012 112. 11 (2012) 125–140. https://doi.org/10.1038/nrd3625.

[115] C. Pauli, R. Whiteside, F.L. Heras, D. Nesic, J. Koziol, S.P. Grogan, J. Matyas, K.P.H. Pritzker, D.D. D'Lima, M.K. Lotz, Comparison of cartilage histopathology assessment systems on human knee joints at all stages of osteoarthritis development, Osteoarthr. Cartil. 20 (2012) 476. https://doi.org/10.1016/J.JOCA.2011.12.018.

[116] S. EL Andaloussi, S. Lakhal, I. Mäger, M.J.A. Wood, Exosomes for targeted siRNA delivery across biological barriers, Adv. Drug Deliv. Rev. 65 (2013) 391–397. https://doi.org/10.1016/J.ADDR.2012.08.008.

[117] H. Aini, K. Itaka, A. Fujisawa, H. Uchida, S. Uchida, S. Fukushima, K. Kataoka, T. Saito, U. Il Chung, S. Ohba, Messenger RNA delivery of a cartilage-anabolic transcription factor as a disease-modifying strategy for osteoarthritis treatment, Sci. Reports 2016 61. 6 (2016) 1–12. https://doi.org/10.1038/srep18743.

[118] C. V. Pecot, G.A. Calin, R.L. Coleman, G. Lopez-Berestein, A.K. Sood, RNA interference in the clinic: challenges and future directions, Nat. Rev. Cancer 2011 111. 11 (2010) 59–67. https://doi.org/10.1038/nrc2966.

[119] D.J. Hunter, L. March, M. Chew, Osteoarthritis in 2020 and beyond: a Lancet Commission, Lancet. 396 (2020) 1711–1712. https://doi.org/10.1016/S0140-6736(20)32230-3.

[120] J. Camardo, The Rapamune era of immunosuppression 2003: the journey from the laboratory to clinical transplantation, Transplant. Proc. 35 (2003) S18–S24. https://doi.org/10.1016/S0041-1345(03)00356-7.

[121] L.H. Meng, X.S. Zheng, Toward rapamycin analog (rapalog)-based precision cancer therapy, Acta Pharmacol. Sin. 2015 3610. 36 (2015) 1163–1169. https://doi.org/10.1038/aps.2015.68.

[122] W. Wu, Z. He, Z. Zhang, X. Yu, Z. Song, X. Li, Intravitreal injection of rapamycin-loaded polymeric micelles for inhibition of ocular inflammation in rat model, Int. J. Pharm. 513 (2016) 238–246. https://doi.org/10.1016/j.ijpharm.2016.09.013.

[123] S. Chen, M.N. van Tok, V.L. Knaup, L. Kraal, D. Pots, L. Bartels, E.M. Gravallese, J.D. Taurog, M. van de Sande, L.M. van Duivenvoorde, D.L. Baeten, mTOR Blockade by Rapamycin in Spondyloarthritis: Impact on Inflammation and New Bone Formation in vitro and in vivo, Front. Immunol. 10 (2020) 2344. https://doi.org/10.3389/FIMMU.2019.02344.

[124] Z.W. Lai, R. Kelly, T. Winans, I. Marchena, A. Shadakshari, J. Yu, M. Dawood, R. Garcia, H. Tily, L. Francis, S. V. Faraone, P.E. Phillips, A. Perl, Sirolimus in patients with clinically active systemic lupus erythematosus resistant to, or intolerant of, conventional medications: a single-arm, open-label, phase 1/2 trial, Lancet. 391 (2018) 1186–1196. https://doi.org/10.1016/S0140-6736(18)30485-9.

[125] T. Weichhart, mTOR as Regulator of Lifespan, Aging, and Cellular Senescence: A Mini-Review, Gerontology. 64 (2018) 127–134. https://doi.org/10.1159/000484629.

[126] J.E. Wilkinson, L. Burmeister, S. V. Brooks, C.C. Chan, S. Friedline, D.E. Harrison, J.F. Hejtmancik, N. Nadon, R. Strong, L.K. Wood, M.A. Woodward, R.A. Miller, Rapamycin slows aging in mice, Aging Cell. 11 (2012) 675–682. https://doi.org/10.1111/J.1474-9726.2012.00832.X.

[127] H. Sasaki, K. Takayama, T. Matsushita, K. Ishida, S. Kubo, T. Matsumoto, N. Fujita, S. Oka, M. Kurosaka, R. Kuroda, Autophagy modulates osteoarthritis-related gene expression in human chondrocytes, Arthritis Rheum. 64 (2012) 1920–1928. https://doi.org/10.1002/ART.34323.

[128] B. Caramés, A. Hasegawa, N. Taniguchi, S. Miyaki, F.J. Blanco, M. Lotz, Autophagy Activation by Rapamycin Reduces Severity of Experimental Osteoarthritis, Ann. Rheum. Dis. 71 (2012) 575. https://doi.org/10.1136/ANNRHEUMDIS-2011-200557.

[129] Y. Zhang, F. Vasheghani, Y.H. Li, M. Blati, K. Simeone, H. Fahmi, B. Lussier, P. Roughley, D. Lagares,

J.P. Pelletier, J. Martel-Pelletier, M. Kapoor, Cartilage-specific deletion of mTOR upregulates autophagy and protects mice from osteoarthritis, Ann. Rheum. Dis. 74 (2015) 1432–1440. https://doi.org/10.1136/ANNRHEUMDIS-2013-204599.

[130] J. Shen, S. Li, D. Chen, TGF-β signaling and the development of osteoarthritis, Bone Res. 2014 21. 2 (2014) 1–7. https://doi.org/10.1038/boneres.2014.2.

[131] J. Friščić, M. Böttcher, C. Reinwald, H. Bruns, B. Wirth, S.J. Popp, K.I. Walker, J.A. Ackermann, X. Chen, J. Turner, H. Zhu, L. Seyler, M. Euler, P. Kirchner, R. Krüger, A.B. Ekici, T. Major, O. Aust, D. Weidner, A. Fischer, F.T. Andes, Z. Stanojevic, V. Trajkovic, M. Herrmann, A. Korb-Pap, I. Wank, A. Hess, J. Winter, V. Wixler, J. Distler, G. Steiner, H.P. Kiener, B. Frey, L. Kling, K. Raza, S. Frey, A. Kleyer, T. Bäuerle, T.R. Hughes, A. Grüneboom, U. Steffen, G. Krönke, A.P. Croft, A. Filer, J. Köhl, K. Klein, C.D. Buckley, G. Schett, D. Mougiakakos, M.H. Hoffmann, The complement system drives local inflammatory tissue priming by metabolic reprogramming of synovial fibroblasts, Immunity. 54 (2021) 1002-1021.e10. https://doi.org/10.1016/J.IMMUNI.2021.03.003.

[132] W.C. Chen, S.W. Wang, C.Y. Lin, C.H. Tsai, Y.C. Fong, T.Y. Lin, S.L. Weng, H. Da Huang, K.W. Liao, C.H. Tang, Resistin enhances monocyte chemoattractant protein-1 production in human synovial fibroblasts and facilitates monocyte migration, Cell. Physiol. Biochem. 52 (2019) 408–420. https://doi.org/10.33594/000000029.

[133] T. Karonitsch, R.K. Kandasamy, F. Kartnig, B. Herdy, K. Dalwigk, B. Niederreiter, J. Holinka, F. Sevelda, R. Windhager, M. Bilban, T. Weichhart, M. Säemann, T. Pap, G. Steiner, J.S. Smolen, H.P. Kiener, G. Superti-Furga, mTOR Senses Environmental Cues to Shape the Fibroblast-like Synoviocyte Response to Inflammation, Cell Rep. 23 (2018) 2157–2167. https://doi.org/10.1016/J.CELREP.2018.04.044.

[134] X. Ji, Y. Yan, T. Sun, Q. Zhang, Y. Wang, M. Zhang, H. Zhang, X. Zhao, Glucosamine sulphate-loaded distearoyl phosphocholine liposomes for osteoarthritis treatment: combination of sustained drug release and improved lubrication, Biomater. Sci. 7 (2019) 2716–2728. https://doi.org/10.1039/C9BM00201D.

[135] B.A. Hills, B.D. Butler, Surfactants identified in synovial fluid and their ability to act as boundary lubricants, Ann. Rheum. Dis. 43 (1984) 641–648. https://doi.org/10.1136/ard.43.4.641.

[136] W. Lin, J. Klein, W. Lin, J. Klein, Recent Progress in Cartilage Lubrication, Adv. Mater. 33 (2021) 2005513. https://doi.org/10.1002/ADMA.202005513.

[137] R. Goldberg, J. Klein, Liposomes as lubricants: beyond drug delivery, Chem. Phys. Lipids. 165 (2012) 374–381. https://doi.org/10.1016/J.CHEMPHYSLIP.2011.11.007.

[138] G. Verberne, A. Schroeder, G. Halperin, Y. Barenholz, I. Etsion, Liposomes as potential biolubricant additives for wear reduction in human synovial joints, Wear. 268 (2010) 1037–1042. https://doi.org/10.1016/J.WEAR.2009.12.037.

[139] S. Sivan, A. Schroeder, G. Verberne, Y. Merkher, D. Diminsky, A. Priev, A. Maroudas, G. Halperin, D. Nitzan, I. Etsion, Y. Barenholz, Liposomes act as effective biolubricants for friction reduction in human synovial joints, Langmuir. 26 (2010) 1107–1116. https://doi.org/10.1021/LA9024712.

[140] J. Dong, D. Jiang, Z. Wang, G. Wu, L. Miao, L. Huang, Intra-articular delivery of liposomal celecoxib–hyaluronate combination for the treatment of osteoarthritis in rabbit model, Int. J. Pharm. 441 (2013) 285–290. https://doi.org/10.1016/J.IJPHARM.2012.11.031.

[141] L. Rahnfeld, J. Thamm, F. Steiniger, P. van Hoogevest, P. Luciani, Study on the in situ aggregation of liposomes with negatively charged phospholipids for use as injectable depot formulation, Colloids Surfaces B Biointerfaces. 168 (2018) 10–17. https://doi.org/10.1016/j.colsurfb.2018.02.023.

[142] S. Aleandri, L. Rahnfeld, D. Chatzikleanthous, A. Bergadano, C. Bühr, C. Detotto, S. Fuochi, K. Weber-Wilk, S. Schürch, P. van Hoogevest, P. Luciani, Development and in vivo validation of phospholipid-based depots for the sustained release of bupivacaine, Eur. J. Pharm. Biopharm. 181 (2022) 300–309. https://doi.org/10.1016/j.ejpb.2022.11.019.

[143] A.S. Prasad, Clinical, immunological, anti-inflammatory and antioxidant roles of zinc, Exp. Gerontol. 43 (2008) 370–377. https://doi.org/10.1016/J.EXGER.2007.10.013.

[144] A.S. Prasad, Zinc is an Antioxidant and Anti-Inflammatory Agent: Its Role in Human Health, Front. Nutr. 1 (2014) 14. https://doi.org/10.3389/FNUT.2014.00014.

[145] M. Jarosz, M. Olbert, G. Wyszogrodzka, K. Młyniec, T. Librowski, Antioxidant and anti-inflammatory effects of zinc. Zinc-dependent NF-κB signaling, Inflammopharmacology 2017 251. 25 (2017) 11–24. https://doi.org/10.1007/S10787-017-0309-4.

[146] M. Ricciutelli, P. Di Martino, L. Barboni, S. Martelli, Evaluation of rapamycin chemical stability in volatile-organic solvents by HPLC, J. Pharm. Biomed. Anal. 41 (2006) 1070–1074. https://doi.org/10.1016/J.JPBA.2006.02.009.

[147] F. Alexis, S.S. Venkatraman, S.K. Rath, F. Boey, In vitro study of release mechanisms of paclitaxel and rapamycin from drug-incorporated biodegradable stent matrices, J. Control. Release. 98 (2004) 67–74. https://doi.org/10.1016/J.JCONREL.2004.04.011.

[148] X. Ge, M. Frank-Bertoncelj, K. Klein, A. McGovern, T. Kuret, M. Houtman, B. Burja, R. Micheroli, C. Shi, M. Marks, A. Filer, C.D. Buckley, G. Orozco, O. Distler, A.P. Morris, P. Martin, S. Eyre, C. Ospelt, Functional genomics atlas of synovial fibroblasts defining rheumatoid arthritis heritability, Genome Biol. 22 (2021) 1–39. https://doi.org/10.1186/S13059-021-02460-6.

[149] T.D. Schmittgen, E.J. Lee, J. Jiang, A. Sarkar, L. Yang, T.S. Elton, C. Chen, Real-time PCR quantification of precursor and mature microRNA, Methods. 44 (2008) 31–38. https://doi.org/10.1016/J.YMETH.2007.09.006.

[150] J.L. Hutter, J. Bechhoefer, Calibration of atomic-force microscope tips, Rev. Sci. Instrum. 64 (1998) 1868. https://doi.org/10.1063/1.1143970.

[151] C.P. Green, H. Lioe, J.P. Cleveland, R. Proksch, P. Mulvaney, J.E. Sader, Normal and torsional spring constants of atomic force microscope cantilevers, Rev. Sci. Instrum. 75 (2004) 1988. https://doi.org/10.1063/1.1753100.

[152] R.J. Cannara, M. Eglin, R.W. Carpick, Lateral force calibration in atomic force microscopy: A new lateral force calibration method and general guidelines for optimization, Rev. Sci. Instrum. 77 (2006) 053701. https://doi.org/10.1063/1.2198768.

[153] J. Gubernator, Active methods of drug loading into liposomes: recent strategies for stable drug entrapment and increased in vivo activity, Expert Opin Drug Deliv. 8 (2011) 565–580. https://doi.org/10.1517/17425247.2011.566552.

[154] M. Chountoulesi, N. Naziris, N. Pippa, C. Demetzos, The significance of drug-to-lipid ratio to the development of optimized liposomal formulation, J Liposome Res. 28 (2017) 249–258. https://doi.org/10.1080/08982104.2017.1343836.

[155] A. Haeri, S. Sadeghian, S. Rabbani, M.S. Anvari, M.A. Boroumand, S. Dadashzadeh, Use of remote film loading methodology to entrap sirolimus into liposomes: Preparation, characterization and in vivo efficacy for treatment of restenosis, Int. J. Pharm. 414 (2011) 16–27. https://doi.org/10.1016/j.ijpharm.2011.04.055.

[156] M.A. Rouf, I. Vural, J.M. Renoir, A.A. Hincal, Development and characterization of liposomal formulations for rapamycin delivery and investigation of their antiproliferative effect on MCF7 cells, J Liposome Res . 19 (2009) 322–331. https://doi.org/10.3109/08982100902963043.

[157] B. Sylvester, A. Porfire, D.M. Muntean, L. Vlase, L. Lupuţ, E. Licarete, A. Sesarman, M.C. Alupei, M. Banciu, M. Achim, I. Tomuţă, Optimization of prednisolone-loaded long-circulating liposomes via application of Quality by Design (QbD) approach, J. Liposome Res. 28 (2016) 49–61. https://doi.org/10.1080/08982104.2016.1254242.

[158] J.A. Zhang, G. Anyarambhatla, L. Ma, S. Ugwu, T. Xuan, T. Sardone, I. Ahmad, Development and characterization of a novel Cremophor® EL free liposome-based paclitaxel (LEP-ETU) formulation, Eur. J. Pharm. Biopharm. 59 (2005) 177–187. https://doi.org/10.1016/J.EJPB.2004.06.009.

[159] F. Lin, Z. Wang, L. Xiang, L. Deng, W. Cui, F. Lin, Z. Wang, L. Xiang, L. Deng, W. Cui, Charge-Guided Micro/Nano-Hydrogel Microsphere for Penetrating Cartilage Matrix, Adv. Funct. Mater. 31 (2021) 2107678. https://doi.org/10.1002/ADFM.202107678.

[160] X.L. Xu, Y. Xue, J.Y. Ding, Z.H. Zhu, X.C. Wu, Y.J. Song, Y.L. Cao, L.G. Tang, D.F. Ding, J.G. Xu, Nanodevices for deep cartilage penetration, Acta Biomater. 154 (2022) 23–48. https://doi.org/10.1016/J.ACTBIO.2022.10.007.

[161] C.T. Inglut, A.J. Sorrin, T. Kuruppu, S. Vig, J. Cicalo, H. Ahmad, H.C. Huang, Immunological and Toxicological Considerations for the Design of Liposomes, Nanomater. 2020, Vol. 10, Page 190. 10 (2020) 190. https://doi.org/10.3390/NANO10020190.

[162] M.C. Filion, N.C. Phillips, Toxicity and immunomodulatory activity of liposomal vectors formulated with cationic lipids toward immune effector cells, Biochim. Biophys. Acta - Biomembr. 1329 (1997) 345–356. https://doi.org/10.1016/S0005-2736(97)00126-0.

[163] D. Volodkin, V. Ball, P. Schaaf, J.C. Voegel, H. Mohwald, Complexation of phosphocholine liposomes with polylysine. Stabilization by surface coverage versus aggregation, Biochim. Biophys. Acta - Biomembr. 1768 (2007) 280–290. https://doi.org/10.1016/J.BBAMEM.2006.09.015.

[164] A. Gorman, K.R. Hossain, F. Cornelius, R.J. Clarke, Penetration of phospholipid membranes by poly-l-lysine depends on cholesterol and phospholipid composition, Biochim. Biophys. Acta - Biomembr. 1862 (2020) 183128. https://doi.org/10.1016/J.BBAMEM.2019.183128.

[165] I.M. Le-Deygen, A.S. Safronova, P. V. Mamaeva, I.M. Kolmogorov, A.A. Skuredina, E. V. Kudryashova, Drug–Membrane Interaction as Revealed by Spectroscopic Methods: The Role of Drug Structure in the Example of Rifampicin, Levofloxacin and Rapamycin, Biophys. 2022, Vol. 2, Pages 353-365. 2 (2022) 353–365. https://doi.org/10.3390/BIOPHYSICA2040032.

[166] I. Onyesom, D.A. Lamprou, L. Sygellou, S.K. Owusu-Ware, M. Antonijevic, B.Z. Chowdhry, D. Douroumis, Sirolimus encapsulated liposomes for cancer therapy: Physicochemical and mechanical characterization of sirolimus distribution within liposome bilayers, Mol. Pharm. 10 (2013) 4281–4293. https://doi.org/10.1021/MP400362V.

[167] E. Freire, C.F. Schmidt, P.L. Feigner, T.E. Thompson, D. Lichtenberg, Y. Barenholz, Effect of Surface Curvature on Stability, Thermodynamic Behavior, and Osmotic Activity of Dipalmitoylphosphatidylcholine Single Lamellar Vesicles, Biochemistry. 20 (1981) 3462–3467. https://doi.org/10.1021/BI00515A024/ASSET/BI00515A024.FP.PNG_V03.

[168] J. Kuntsche, I. Freisleben, F. Steiniger, A. Fahr, Temoporfin-loaded liposomes: Physicochemical characterization, Eur. J. Pharm. Sci. 40 (2010) 305–315. https://doi.org/10.1016/J.EJPS.2010.04.005.

[169] K.M. Dhanabalan, V.K. Gupta, R. Agarwal, Rapamycin–PLGA microparticles prevent senescence, sustain cartilage matrix production under stress and exhibit prolonged retention in mouse joints, Biomater. Sci. 8 (2020) 4308–4321. https://doi.org/10.1039/D0BM00596G.

[170] A. Gaisinskaya-Kipnis, J. Klein, Normal and Frictional Interactions between Liposome-Bearing Biomacromolecular Bilayers, Biomacromolecules. 17 (2016) 2591–2602. https://doi.org/10.1021/ACS.BIOMAC.6B00614.

[171] R. Sapra, R.P. Verma, G.P. Maurya, S. Dhawan, J. Babu, V. Haridas, Designer Peptide and Protein

Dendrimers: A Cross-Sectional Analysis, Chem. Rev. 119 (2019) 11391–11441. https://doi.org/10.1021/ACS.CHEMREV.9B00153.

[172] M. Carone, S. Moreno, M. Cangiotti, M.F. Ottaviani, P. Wang, R. Carloni, D. Appelhans, DOTA Glycodendrimers as Cu(II) Complexing Agents and Their Dynamic Interaction Characteristics toward Liposomes, Langmuir. 36 (2020) 12816–12829. https://doi.org/10.1021/ACS.LANGMUIR.0C01776.

[173] D. Erzina, A. Capecchi, S. Javor, J.L. Reymond, An Immunomodulatory Peptide Dendrimer Inspired from Glatiramer Acetate, Angew. Chemie Int. Ed. 60 (2021) 26403–26408. https://doi.org/10.1002/ANIE.202113562.

[174] F. Weber, D.C. Ivan, S.T. Proulx, G. Locatelli, S. Aleandri, P. Luciani, Beyond Trial and Error: A Systematic Development of Liposomes Targeting Primary Macrophages, Adv. NanoBiomed Res. 1 (2021) 2000098. https://doi.org/10.1002/ANBR.202000098.

[175] R. Goldberg, A. Schroeder, G. Silbert, K. Turjeman, Y. Barenholz, J. Klein, Boundary Lubricants with Exceptionally Low Friction Coefficients Based on 2D Close-Packed Phosphatidylcholine Liposomes, Adv. Mater. 23 (2011) 3517–3521. https://doi.org/10.1002/ADMA.201101053.

[176] B. Roy, A.K. Panda, S. Parimi, I. Ametov, T. Barnes, C.A. Prestidge, Physico-chemical Studies on the Interaction of Dendrimers with Lipid Bilayers. 1. Effect of Dendrimer Generation and Liposome Surface Charge, J. Oleo Sci. 63 (2014) 1185–1193. https://doi.org/10.5650/JOS.ESS14081.

[177] B. Roy, P. Guha, P. Nahak, G. Karmakar, S. Maiti, A.K. Mandal, A.G. Bykov, A. V. Akentiev, B.A. Noskov, K. Tsuchiya, K. Torigoe, A.K. Panda, Biophysical Correlates on the Composition, Functionality, and Structure of Dendrimer-Liposome Aggregates, ACS Omega. 3 (2018) 12235–12245. https://doi.org/10.1021/ACSOMEGA.8B01187.

[178] K.S. Trosheva, S.A. Sorokina, Efimova, P.I. Semenyuk, A.K. Berkovich, A.A. Yaroslavov, Z.B. Shifrina, Interaction of multicomponent anionic liposomes with cationic pyridylphenylene dendrimer: Does the complex behavior depend on the liposome composition?, Biochim. Biophys. Acta - Biomembr. 1863 (2021) 183761. https://doi.org/10.1016/J.BBAMEM.2021.183761.

[179] W. Lin, R. Goldberg, J. Klein, Poly-phosphocholination of liposomes leads to highly-extended retention time in mice joints, J. Mater. Chem. B. 10 (2022) 2820–2827. https://doi.org/10.1039/D1TB02346B.

[180] N. Onishchenko, D. Tretiakova, E. Vodovozova, Spotlight on the protein corona of liposomes, Acta Biomater. 134 (2021) 57–78. https://doi.org/10.1016/J.ACTBIO.2021.07.074.

[181] S.C. Semple, A. Chonn, P.R. Cullis, Interactions of liposomes and lipid-based carrier systems with blood proteins: Relation to clearance behaviour in vivo, Adv. Drug Deliv. Rev. 32 (1998) 3–17. https://doi.org/10.1016/S0169-409X(97)00128-2.

[182] W.H. Lee, C.Y. Loo, D. Traini, P.M. Young, Nano- and micro-based inhaled drug delivery systems for targeting alveolar macrophages, Expert Opin. Drug Deliv. 12 (2015) 1009–1026. https://doi.org/10.1517/17425247.2015.1039509.

[183] E. Mathew, G.E. Hardee, C.F. Bennett, K.D. Lee, Cytosolic delivery of antisense oligonucleotides by listeriolysin O-containing liposomes, Gene Ther. 2003 1013. 10 (2003) 1105–1115. https://doi.org/10.1038/sj.gt.3301966.

[184] P.C. Peng, R.L. Hong, Y.J. Tsai, P.T. Li, T. Tsai, C.T. Chen, Dual-effect liposomes encapsulated with doxorubicin and chlorin e6 augment the therapeutic effect of tumor treatment, Lasers Surg. Med. 47 (2015) 77–87. https://doi.org/10.1002/LSM.22312.

[185] K. Makino, N. Yamamoto, K. Higuchi, N. Harada, H. Ohshima, H. Terada, Phagocytic uptake of polystyrene microspheres by alveolar macrophages: effects of the size and surface properties of the microspheres, Colloids Surfaces B Biointerfaces. 27 (2003) 33–39. https://doi.org/10.1016/S0927-7765(02)00042-5.

[186] A. Petit, E.M. Redout, C.H. van de Lest, J.C. de Grauw, B. Müller, R. Meyboom, P. van Midwoud, T. Vermonden, W.E. Hennink, P. René van Weeren, Sustained intra-articular release of celecoxib from in situ forming gels made of acetyl-capped PCLA-PEG-PCLA triblock copolymers in horses, Biomaterials. 53 (2015) 426–436. https://doi.org/10.1016/J.BIOMATERIALS.2015.02.109.

[187] B. Sterner, M. Harms, S. Wöll, M. Weigandt, M. Windbergs, C.M. Lehr, The effect of polymer size and charge of molecules on permeation through synovial membrane and accumulation in hyaline articular cartilage, Eur. J. Pharm. Biopharm. 101 (2016) 126–136. https://doi.org/10.1016/J.EJPB.2016.02.004.

[188] N. Yin, X. Guo, R. Sun, H. Liu, L. Tang, J. Gou, T. Yin, H. He, Y. Zhang, X. Tang, Intra-articular injection of indomethacin–methotrexate in situ hydrogel for the synergistic treatment of rheumatoid arthritis, J. Mater. Chem. B. 8 (2020) 993–1007. https://doi.org/10.1039/C9TB01795J.

[189] C.H. Evans, V.B. Kraus, L.A. Setton, Progress in intra-articular therapy, Nat. Rev. Rheumatol. 2013 101. 10 (2013) 11–22. https://doi.org/10.1038/nrrheum.2013.159.

[190] S.N.R. Shiadeh, E. Khodaverdi, M.F. Maleki, F. Eisvand, A. Nazari, J. Zarqi, F. Hadizadeh, H. Kamali, A sustain-release lipid-liquid crystal containing risperidone based on glycerol monooleate, glycerol dioleate, and glycerol trioleate: In-vitro evaluation and pharmacokinetics in rabbits, J. Drug Deliv. Sci. Technol. 70 (2022) 103257. https://doi.org/10.1016/J.JDDST.2022.103257.

[191] N. Joshi, J. Yan, S. Levy, S. Bhagchandani, K. V. Slaughter, N.E. Sherman, J. Amirault, Y. Wang, L. Riegel, X. He, T.S. Rui, M. Valic, P.K. Vemula, O.R. Miranda, O. Levy, E.M. Gravallese, A.O. Aliprantis, J. Ermann, J.M. Karp, Towards an arthritis flare-responsive drug delivery system, Nat. Commun. 2018 91. 9 (2018) 1–11. https://doi.org/10.1038/s41467-018-03691-1.

[192] R. Mezzenga, J.M. Seddon, C.J. Drummond, B.J. Boyd, G.E. Schröder-Turk, L. Sagalowicz, R. Mezzenga, M. Seddon, C.J. Drummond, B.J. Boyd, G.E. Schröder-Turk, L. Sagalowicz, Nature-Inspired Design and Application of Lipidic Lyotropic Liquid Crystals, Adv. Mater. 31 (2019) 1900818. https://doi.org/10.1002/ADMA.201900818.

[193] N. Rahanyan-Kägi, S. Aleandri, C. Speziale, R. Mezzenga, E.M. Landau, Stimuli-Responsive Lipidic Cubic Phase: Triggered Release and Sequestration of Guest Molecules, Chem. – A Eur. J. 21 (2015) 1873–1877. https://doi.org/10.1002/CHEM.201405580.

[194] I. Martiel, N. Baumann, J.J. Vallooran, J. Bergfreund, L. Sagalowicz, R. Mezzenga, Oil and drug control the release rate from lyotropic liquid crystals, J. Control. Release. 204 (2015) 78–84. https://doi.org/10.1016/J.JCONREL.2015.02.034.

[195] R. Negrini, R. Mezzenga, PH-responsive lyotropic liquid crystals for controlled drug delivery, Langmuir. 27 (2011) 5296–5303. https://doi.org/10.1021/LA200591U.

[196] R. Negrini, W.K. Fong, B.J. Boyd, R. Mezzenga, pH-responsive lyotropic liquid crystals and their potential therapeutic role in cancer treatment, Chem. Commun. 51 (2015) 6671–6674. https://doi.org/10.1039/C4CC10274F.

[197] M. Carone, M.R. Spalinger, R.A. Gaultney, R. Mezzenga, A. Mookhoek, P. Krebs, G. Rogler, P. Luciani, S. Aleandri, Temperature-triggered in situ forming lipid mesophase gel for local treatment of ulcerative colitis, BioRxiv. (2022) 2022.09.28.509483. https://doi.org/10.1101/2022.09.28.509483.

[198] H. Wang, T. Peng, H. Wu, J. Chen, M. Chen, L. Mei, F. Li, W. Wang, C. Wu, X. Pan, In situ biomimetic lyotropic liquid crystal gel for full-thickness cartilage defect regeneration, J. Control. Release. 338 (2021) 623–632. https://doi.org/10.1016/J.JCONREL.2021.08.062.

[199] J. Li, S.G. Kim, J. Blenis, Rapamycin: One drug, many effects, Cell Metab. 19 (2014) 373–379. https://doi.org/10.1016/j.cmet.2014.01.001.

[200] O. Elzenaty, P. Luciani, S. Aleandri, A lipidic mesophase with tunable release properties for the local delivery of macromolecules: the apoferritin nanocage, a case study, J. Mater. Chem. B. 10 (2022) 3876–3885. https://doi.org/10.1039/D2TB00403H.

[201] W.K. Fong, T. Hanley, B.J. Boyd, Stimuli responsive liquid crystals provide 'on-demand' drug delivery in vitro and in vivo, J. Control. Release. 135 (2009) 218–226. https://doi.org/10.1016/J.JCONREL.2009.01.009.

[202] Q. Liu, Y. Xiao, A. Hawley, B.J. Boyd, Lipid-based lyotropic liquid crystalline phase transitions as a novel assay platform using birefringence as the visual signal output, J. Mater. Chem. B. 8 (2020) 6277–6285. https://doi.org/10.1039/D0TB00355G.

[203] R. Mezzenga, C. Meyer, C. Servais, A.I. Romoscanu, L. Sagalowicz, R.C. Hayward, Shear Rheology of Lyotropic Liquid Crystals: A Case Study, Langmuir. 21 (2005) 3322–3333. https://doi.org/10.1021/LA046964B.

[204] L.S. Karfeld-Sulzer, C. Ghayor, B. Siegenthaler, M. De Wild, J.C. Leroux, F.E. Weber, N-methyl pyrrolidone/bone morphogenetic protein-2 double delivery with in situ forming implants, J. Control. Release. 203 (2015) 181–188. https://doi.org/10.1016/J.JCONREL.2015.02.019.

[205] C. Speziale, R. Ghanbari, R. Mezzenga, Rheology of Ultraswollen Bicontinuous Lipidic Cubic Phases, Langmuir. 34 (2018) 5052–5059. https://doi.org/10.1021/ACS.LANGMUIR.8B00737.

[206] D.J. Burgess, A.S. Hussain, T.S. Ingallinera, M.L. Chen, Assuring quality and performance of sustained and controlled release parenterals: Workshop report, AAPS PharmSci. 4 (2002) 1–11. https://doi.org/10.1208/PS040205.

Acknowledgements

Firstly, I would like to express my gratitude to Prof. Jean-Louis Reymond and Prof. Jörg Huwyler for dedicating their valuable time to review my doctoral thesis and for agreeing to serve as my internal and external examiner. Secondly, I want to convey my deep appreciation to Prof. Paola Luciani for welcoming me into her research group. The experience in her lab not only fostered my growth as a scientist, but also as a communicator and a self-starter. Although it wasn't always smooth sailing, our relationship and collaboration helped me identify my strengths and areas for improvement, which will undoubtedly benefit my future endeavours. I would also like to acknowledge her for providing me with opportunities such as access to various courses and supporting my ambition to visit another lab during my PhD.

My sincere thanks go to Prof. Oliver Distler, who graciously hosted me in his lab during my research visit to Zürich. His support during this period proved crucial for my PhD project and provided me with the opportunity to delve deeper into the field of molecular biology and enhance my knowledge of cell culture. I wish to extend my special thanks to Dr. Mojca Frank Bertoncelj, who arrived during a significant shift in my project towards rheumatology and osteoarthritis. Her guidance and network proved invaluable in securing a grant for my research visit, which played a pivotal role in the success of my PhD project. In the same breath, I would like to acknowledge Sam Edalat for his patient assistance in the lab at University Hospital Zürich and for our thought-provoking discussions. I extend this gratitude to everyone at EMPA and ETH Zürich, particularly Dr. Rowena Crockett, Dr. Andrea Arcifa and Dr. Shivaprakash Narve Ramakrishna. The success of my PhD project is largely attributable to your invaluable contributions.

I am very grateful to both former and current members of the Luciani group, especially Despo, Ivo, Aymar, Remo, Rafaela, Assumpta, Sarah, Simone, and Cristina. Our scientific discussions spurred me to think outside the box and further developed my skills as a scientist. I thank you for the inspiring brainstorming sessions and camaraderie. Special thanks go to Marianna for being both by my side and on my side, regardless of the circumstances. When faced with disappointing results, she offered encouragement, and in times of success, we celebrated together. Her unwavering support made the PhD experience more manageable and enabled the

realization of projects like PharmaCamp. Lastly, I want to thank my parents, who have supported me through thick and thin and offered emotional support when needed.

Thank you all, hvala vsem!

Declaration of consent

on the basis of Article 18 of the PromR Phil.-nat. 19

Name, First Name: Bordon, Gregor

Registration Number: 19-130-277

Study program: Dissertation

Title of the thesis: Next-generation lipidic drug delivery systems for osteoarthritis treatment

Supervisor: Prof. Dr. Paola Luciani

I declare herewith that this thesis is my own work and that I have not used any sources other than those stated. I have indicated the adoption of quotations as well as thoughts taken from other authors as such in the thesis. I am aware that the Senate pursuant to Article 36 paragraph 1 litera r of the University Act of September 5th, 1996 and Article 69 of the University Statute of June 7th, 2011 is authorized to revoke the doctoral degree awarded on the basis of this thesis.
For the purposes of evaluation and verification of compliance with the declaration of originality and the regulations governing plagiarism, I hereby grant the University of Bern the right to process my personal data and to perform the acts of use this requires, in particular, to reproduce the written thesis and to store it permanently in a database, and to use said database, or to make said database available, to enable comparison with theses submitted by others.

Bern, June 1st 2023

Signature
Gregor Bordon